UNIVERSIDAD DE GRANADA

PROGRAMA DE DOCTORADO EN QUÍMICA

FACULTAD DE CIENCIAS

DEPARTAMENTO DE QUÍMICA INORGÁNICA

TESIS DOCTORAL / Ph.D. THESIS

Geles de carbón para electro-reducción de CO_2 a hidrocarburos, electro-reducción de oxígeno, y almacenamiento de energía

Carbon gels for the electro-reduction of CO_2 to hydrocarbons, electro-reduction of oxygen, and energy storage

ABDALLA ABDELWAHAB ABDELSALAM

Granada, Marzo 2017

Editor: Universidad de Granada. Tesis Doctorales
Autor: Abdalla Abdelwahab
ISBN: 978-84-9163-184-2
URI: http://hdl.handle.net/10481/46039

Geles de carbón para electro-reducción de CO_2 a hidrocarburos, electro-reducción de oxígeno, y almacenamiento de energía

Carbon gels for the electro-reduction of CO_2 to hydrocarbons, electro-reduction of oxygen, and energy storage

por / by

ABDALLA ABDELWAHAB ABDELSALAM

Memoria presentada para aspirar al grado de Doctor
por la Universidad de Granada

Fdo.: **Abdalla Abdelwahab Abdelsalam**

Directores de la Tesis / Supervisors

Prof. Dr. Francisco Carrasco Marín, Catedrático del Departamento de Química Inorgánica, Universidad de Granada.

Prof. Dr. Agustín Francisco Pérez Cadenas, Profesor Titular del Departamento de Química Inorgánica, Universidad de Granada.

Prof. Dra. María Pérez Cadenas, Profesora Ayudante Doctor del Departamento de Química Inorgánica y Técnica, Universidad Nacional de Educación a Distancia**.**

GELES DE CARBÓN PARA ELECTRO-REDUCCIÓN DE CO_2 A HIDROCARBUROS, ELECTRO-REDUCCIÓN DE OXÍGENO, Y ALMACENAMIENTO DE ENERGÍA

Tesis presentada para aspirar al grado de Doctor por

ABDALLA ABDELWAHAB ABDELSALAM

Realizada bajo la dirección del Catedrático de Química Inorgánica Prof. Dr. Francisco Carrasco Marín, y de los Profesores Dr. Agustín F. Pérez Cadenas y Dra. María Pérez Cadenas, en la Facultad de Ciencias de la Universidad de Granada, y juzgada el día 27 de marzo de 2017, en dicha Facultad, por el siguiente Tribunal:

PRESIDENTE:

Prof. Dr. María Ángeles Ferro García, Catedrática de Química Inorgánica, Universidad de Granada.

VOCALES:

Prof. Dr. Antonio José López Peinado, Catedrático de Química Inorgánica, Universidad Nacional de Educación a Distancia, Madrid.
Prof. Dra. María de la Luz Godino Salido, Profesora Titular de Química Inorgánica, Universidad de Jaén.
Dra. Esther Bailón García, Investigadora Contratada, Instituto Superior Técnico, Lisboa.

SECRETARIO:

Prof. Dra. María Isidora Bautista Toledo, Profesora Titular de Química Inorgánica, Universidad de Granada.

Francisco Carrasco Marín, Agustín F. Pérez Cadenas y María Pérez Cadenas como directores de la presente Tesis Doctoral, y el doctorando Abdalla Abdelwahab Abdelsalam

GARANTIZAN QUE

el trabajo ha sido realizado por el doctorando respetando los derechos de otros autores a ser citados cuando se han utilizado sus resultados o publicaciones.

Y para que conste a los efectos oportunos, en el cumplimiento de la legislación vigente, firmamos el presente certificado en Granada a 23 de febrero del 2017.

Prof. Dr. Francisco Carrasco Marín, Catedrático del Departamento de Química Inorgánica, Universidad de Granada.

Prof. Dr. Agustín Francisco Pérez Cadenas, Profesor Titular del Departamento de Química Inorgánica, Universidad de Granada.

Prof. Dra. María Pérez Cadenas, Profesora Ayudante Doctor del Departamento de Química Inorgánica y Técnica, Universidad Nacional de Educación a Distancia**.**

Abdalla Abdelwahab Abdelsalam, B.Sc. In Applied Chemistry.

Acknowledgements

This thesis would have not been possible without the support of my supervisors, colleagues, family and friends who in different ways encouraged me and shared this long way. To all of you, I express my grateful acknowledgment and sincerely thank for bringing this thesis to a successful end.

I would like to acknowledge my professor **Agustín Francisco Pérez Cadenas** for giving me the opportunity to come to Spain to work in an interesting project and to have this amazing life experience and taught me the basis for my Ph. D project. I also thank Professor **Francisco Carrasco Marín** and Professor **María Pérez Cadenas** for all the discussions we have had together and the good guidance they have given me throughout this project. I appreciate Professor **Francisco J. Maldonado Hódar** for his useful discussions and instructions. I also appreciate a lot the opportunity they have given me to present my work in international conferences.

I feel very lucky for having had the opportunity to work in a highly cooperative group. It has been a pleasure to work with all of you. I want to acknowledge **Esther Bailón García** who helped me from my first experimental day in preparations of carbon gels and during the whole Ph.D. I also thank **Abdelhakim Elmouwahidi** who helped me in designing the set up I have been working on and taught me how to work with it. I also acknowledge the good work of **Jesica Castelo Quibén**, who has made great effort in the electrochemical CO_2 reduction

experiments, and **Jose Vivo Vilches** for his help with the oxygen reduction reaction.

Acknowledgements are also owed to our head department professor **Carlos Moreno Castilla** and everyone in the Inorganic Chemistry Department, Faculty of Science, Granada University. I also thank all of my colleagues who support me and helped me throughout my work **María Helena, David.**

I dedicate this work to my family father, mother and my brothers. A special thanks goes to my wife for helping me throughout my life.

Finally, I would like to thank everybody who was important to the successful realization of my thesis, as well as expressing my apology for every one that I unfortunately forgot to mention.

Abdalla Abdelwahab

March 2017

This research has been supported by the Spanish projects CTQ2013-44789-R (MINECO) and P12-RNM-2892 (Junta de Andalucía), and FEDER. Acknowledgement is also goes to ERASMUS MUNDUS Program for the ELEMENT scholarship.

Resumen / Abstract

En la presente Tesis Doctoral se han desarrollado diferentes series de geles de carbón dopados con metales de transición, tales como níquel, hierro y cobalto. Se han preparado tanto aerogeles, como xerogeles de carbon dopados, utilizando tres contenidos de metal dopante distintos. Todos los materiales se han caracterizado exhaustivamente, y se ha estudiado su comportamiento en tres aplicaciones electro-químicas de máxima actualidad, como son: la electro-reducción de dióxido de carbono a hidrocarburos, la electro-reducción de oxígeno, y como electrodos para super-condensadores. Todos los resultados electro-químicos obtenidos se han correlacionado con las propiedades químicas y texturales de los materiales de carbón dopados desarrollados. Los geles de carbón dopados con hierro y cobalto se han comportado muy bien como electro-catalizadores para la reducción de CO_2, detectándose hidrocarburos ligeros de 1 a 4 átomos de carbono, con una alta selectividad a hidrocarburos tipo C3. En el caso de los geles de carbón dopados con hierro, se ha determinado una clara dependencia de la eficiencia faradaica con el tamaño de partícula de hierro: a menor tamaño de partícula, mayor eficiencia y actividad. Por otro lado, lo aerogeles de carbón dopados con Ni desarrollados son especialmente interesantes como catalizadores para la electro-reducción de oxígeno, y también como electrodos para super-condensadores; y en ambas aplicaciones el aumento del contenido en Ni produce una clara mejora del comportamiento electro-químico. En términos generales, la capacidad de grafitización que tienen estos metales de transición durante el tratamiento térmico de carbonización,

catalizando en todos los casos la formación de clústeres grafíticos alrededor de las partículas metálicas, junto con un buen desarrollo de la mesoporosidad y microporosidad, hace de estos geles de carbón dopados unos materiales muy prometedores para poder ser implementados en las aplicaciones electo-químicas estudiadas.

Several series of carbon gels, aerogels and xerogels, doped with nickel, cobalt or iron, and with three different metal loadings, have been prepared, exhaustively characterized and tested in three electro-chemical applications such as, carbon dioxide reduction to hydrocarbons, oxygen reduction reaction, and as electrodes for supercapacitors. All the obtained electro-chemical results have been correlated with the textural and chemical properties of the developed doped carbon materials and these have been structured in the following Chapters:

Chapter I: **Introduction and objectives**. This Chapter collects the state of the art of environmental and energetic problems related with the studied electro-chemical applications, as well as the type of developed materials. Finally the objectives of the work are described.

Chapter II: **Synthesis of the materials and characterization techniques**. This Chapter describes in detail the preparation of all the developed materials, and the experimental conditions of the common characterization techniques used in the Chapters III, IV, V and VI.

Chapter III: **Cobalt-Doped Carbon Gels as Electro-Catalysts for the Reduction of CO_2 to Hydrocarbons**. This Chapter contains the article published in *Catalysts* journal with its publishing format, in which two original series of carbon gels doped with different cobalt loadings and well-developed mesoporosity, aerogels and xerogels, were prepared, exhaustively characterized, and tested as cathodes for the electro-catalytic reduction of CO_2 to hydrocarbons at atmospheric pressure. Commercial cobalt and graphite sheets have also were tested as cathodes for comparison. All of the doped carbon gels catalysed the formation of hydrocarbons, at least from type C1 to C4. The catalytic activity depends mainly on the metal loading, nevertheless, the adsorption of a part of the products in the porous structure of the carbon gel cannot be ruled out. Apparent faradaic efficiencies calculated with these developed materials were better that those obtained with a commercial cobalt sheet as a cathode, especially considering the much lower amount of cobalt contained in the Co-doped carbon gels. The cobalt-carbon phases formed in these types of doped carbon gels improve the selectivity to C3-C4 hydrocarbons formation, obtaining even more C3 hydrocarbons than CH_4 in some cases.

Chapter IV: **Carbon gels doped with iron for the electro-reduction of CO_2 to hydrocarbons: the role of the iron particle size.** This Chapter describes the development of different types of carbon gels doped with iron, in particular an aerogel, three xerogels with different iron contents, and a carbon xerogel – carbon nanofiber composite were prepared, exhaustively characterized, and tested as cathodes for the electro-catalytic reduction of CO_2 to hydrocarbons at atmospheric pressure. Commercial iron and graphite sheets have also been tested as cathodes

for comparison. All electro-catalysts promoted the formation of C1 to C4 hydrocarbons showing a high selectivity to C3 hydrocarbons. The carbon xerogel – carbon nanofiber composite was the most selective to C4 hydrocarbons, even over long reaction times. The iron particle size is a very important parameter involved in the hydrocarbon formation. A linear correlation between mean iron particle sizes and the faradaic efficiency of the materials has been found: the smaller the iron particle size, the higher the faradaic efficiency. Iron nano-particles smaller than 4 nm seem to increase significantly the formation of hydrocarbons.

Chapter V: **Carbon aerogels doped with transition metals for oxygen reduction reaction catalysts**. In this Chapter a series of carbon aerogels doped with iron, cobalt and nickel were prepared. Samples with different Ni content were also obtained in order to test the influence of the metal proportion. Samples were characterized to analyse their textural properties, surface chemistry and crystal structures. These metal doped gels are materials with a very well developed porosity, all of them with a remarkable mesoporosity. Ni doped carbon xerogels were the ones with the largest surface area and the smallest graphitization. They also presented larger mesopore volumes than Co and Fe doped xerogels. All these materials were tested as electro-catalysts for oxygen reduction reaction. Results showed a strong influence of carbonaceous structure on electro-catalytic behaviour of aerogels. In fact, aerogel doped with Ni was the most active one, followed by Fe and Co doped ones which presented similar results. As the Ni content was larger, E^0_{onset} was reduced and kinetic current densities were increased.

Chapter VI: **Insight of the effect of graphitic clusters in the performance of carbon aerogels doped with nickel as electrodes for supercapacitors**. In this last Chapter, carbon aerogels doped with Ni described in Chapter V were tested as electrodes for supercapacitors. For this goal, electrocapacitive properties were studied by cyclic voltammetry, chronopotentiometry, and electrochemical impedance spectroscopy in a three and two-electrode cell in acidic media and non-aqueous aprotic electrolyte. Results obtained showed that using Ni as polymerization catalysts slightly decrease the micropore volume of the carbon aerogels but a great increase in their mesopore volume were obtained by N_2 adsorption. Electrochemical characterization of the electrodes and cells show that samples present high gravimetric capacitances, ranging from 182 and 219 F g^{-1} in 1 M H_2SO_4 and 49 and 63 F g^{-1} in 1 M TEATFB. The prepared capacitors showed that the equivalent series resistance decrease as Ni content increase and the capacitance increase in the same sense.

Some of the results of this work have been already published in the following Journal, and presented in several International and National Conferences:

List of papers

- Abdalla Abdelwahab, Jesica Castelo-Quibén, María Pérez-Cadenas, Abdelhakim Elmouwahidi, Francisco J. Maldonado-Hódar, Francisco Carrasco-Marín and Agustín F. Pérez-Cadenas., *Cobalt-Doped carbon gels as electro-catalysts for the reduction of CO_2 to hydrocarbons*. Catalysts, 2017. **7**(1): p. 25.

List of conferences

- **The World Conference on Carbon**, Pennsylvania, USA, July 10-15, 2016. Cobalt doped carbon gels as electro-catalysts for the reduction of CO_2 to Hydrocarbons.
- The **39th Reunion Ibérica de Adsorción**, Baeza, Spain, September 14-17, 2014. Preparation of Ni-doped carbon aerogels and their application in supercapacitors.
- The **39th Reunion Ibérica de Adsorción**, Baeza, Spain, September 14-17, 2014. Behaviour of metal-doped carbon aerogels as electrodes for supercapacitor applications.
- The **12th Reunión del Grupo Español del Carbón**, Madrid, Spain, October 20-23, 2013. Preparation of carbon aerogels electrodes doped with transition metals for the electro-catalytic reduction of CO_2 to hydrocarbons.

CONTENTS

CHAPTER I: INTRODUCTION AND OBJECTIVES

1.1.- ENERGY CRISIS, AIR POLLUTANTS AND CO_2 EMISIONS

Energy has its great importance in our lives for individual and societal. Our daily activities have come to depend on existence of energy. Nowadays, our world is facing energy crisis due to insufficient energy resources that can meet human needs. Also, the dependence of global energy production on fossil fuels which represents about 87% of the total production in many activities like electricity production, transportation, and in industries the main reason for the energy crisis. Fossil fuels burning is not only depleting the natural resources, but also is considered as the main contributor to global warming by emitting carbon dioxide CO_2 to our atmosphere [1]. Nowadays, there are many attempts to serve the environment and control of CO_2 emissions. In previous years, many studies have been made in developing new techniques toward clean energy like biofuel, solar cells, as well as the electrochemical energy storage and conversion systems like batteries, fuel cells, and electrochemical capacitors (ECs) [2].

There are a lot of contamination sources that can cause pollution to our environment. The pollution to the environment can be classified into water, soil, and air pollution. The pollution sources may be intentional like disposal of pollutants into water and fossil fuels combustion; also it may be unintentional like the production of methane by bio-decay processes and the volcanic eruptions. Among the types of pollution, air pollution become has a great importance to control its level due to its effect on the environment and the human health. Combustion processes, industrial processes, and transport are the main sources to air pollution. The most abundant air pollutants can be summarized as below.

Sulphur oxides (SO_x)

Especially sulphur dioxide SO_2, is a chemical compound produced by volcanoes and in combustion of fossil fuels which contains sulphur. When this oxide dissolves in the rain droplets, the pH of the rain reaches value lower than 5.7, thus forming acid rain. The problem with acid rain is its ability to oxidize materials such as copper and iron, the weathering of stone buildings and statues as well as having impacts on human health.

Nitrogen oxides (NO_x)

The most nitrogen oxides that have effect to the human health are attributed to nitrogen dioxide NO_2which is also a precursor for acid rain. The main producer for $NO_2$is the gas stoves and heaters in homes. NO_2 concentration between 50-150 ppm can cause lung disease, while lower concentrations may cause eye, nose, and throat irritation.

Volatile organic compounds (VOCs)

It is categorized into methane and non-methane volatile organic compounds (NMVOC). Methane is one of greenhouse gases that has efficient role in the global warming. Toluene and xylene are examples of NMVOCs which are treated as carcinogens through prolonged exposure. VOCs can be produced by incomplete combustion processes, fugitive sources, and petroleum processing.

Carbon monoxide (CO)

Fossil fuels and biomass combustion, biogenic processes, and photochemical transformation in the atmosphere are the main sources of CO and CO_2 production.

CO is produced by the incomplete combustion processes, and the main hazard of it is its toxicity. Table 1.1, summarizes all forms of air pollution, sources, and its effects [1].

Table 1.1. Types of air pollution, sources, and effects.

Pollutant	Source	Effect
CO, (CO_2)	Fossil fuels and biomass combustion	CO, Toxic CO_2, a greenhouse gas
NO, NO_2, N_2O	Lightning, gas stoves and heaters	NO_2 a precursor of acid rain, affect human health with high conc.
SO_2, SO_3	Oxidation of sulphur containing fuels, and oxidation of H_2S	Forming acid rain
Photochemical oxidants "Ozone"	Photochemical reactions based on other primary pollutants	Constituent of smog
Particulates and aerosols	Wildfires, volcanic eruptions, incomplete combustion	PM ≤ 2.5μm consists of aerosols containing carcinogenic substances. Smog formation
Metal and metalloid compounds Pb, Hg, As, Ni, and Cu	Engine wear, lubricating oil components, lamp wastes	Toxic metals
Polycyclic aromatic hydrocarbons, PAHs pyrene	Incomplete combustion of fossil fuels and vegetable matter, petroleum refineries	React with hydroxyl radicals, ozone, and nitro radicals, generating in the last case mutagenic nitro-PAHs
Volatile organic compounds, VOCs	Incomplete combustion processes, fugitive sources, and petroleum processing	CH_4, is a greenhouse gas NMVOCs, carcinogens through prolonged exposure
Halogenated hydrocarbons and polychlorinated organic compounds, chloroform	Incineration processes and car emissions	Destruction of the ozone layer
Radionuclides	Emissions from uranium processing, nuclear reactors	Damage to the environment

The impact of the high emission concentration of carbon dioxide into the environment, its effect, and how to reduce its concentration in the atmosphere is one of the topics of this thesis. So, it will discuss in more details.

1.1.1.- Carbon dioxide emission sources

Carbon dioxide is a natural occurring chemical compound consists of a carbon atom attached to two oxygen atoms CO_2, present as a gas at standard temperature and pressure [1]. The increased concentration of carbon dioxide is of interest due to its impact on the greenhouse effect. There are many sources for CO_2 emissions like fossil fuels combustion, transport, and in the industrial scale. You can imagine that the global CO_2 emissions increased by 4.6% in 2010 and it is still in increasing till now (Figure 1.1). The atmospheric concentration of carbon dioxide is different throughout the year due to the change of seasons as appears from the annual cycle (the red line) in Figure 1.1. It is also expected that the global atmospheric concentrations of the carbon dioxide remains in increase during the near future (Figure 1.2). There are many sources for CO_2 emissions but the most two sources in CO_2 emissions are electricity production and transport which produces about two-thirds of global CO_2 emissions (Figure 1.3). As appears from Figure 3, the electricity and heat production represents about 41% from the global CO_2emissions, while the transport contributes with 22%.

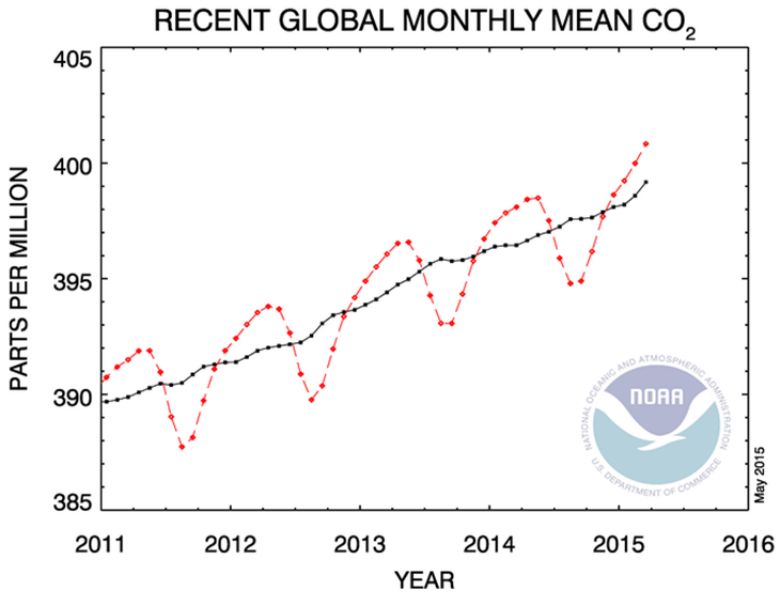

Figure 1.1. The increased amount of CO_2 emissions till 2015 [3].

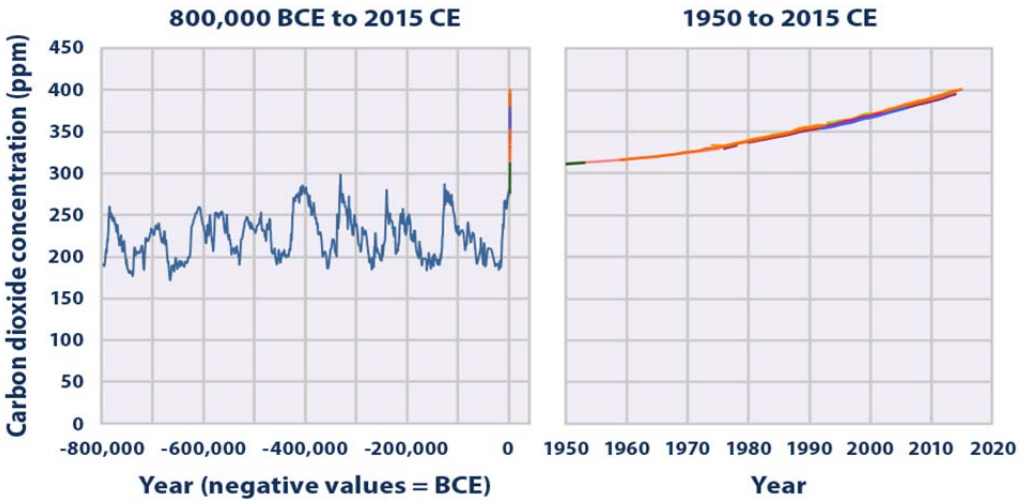

Figure 1.2. The global atmospheric concentrations of the carbon dioxide [4].

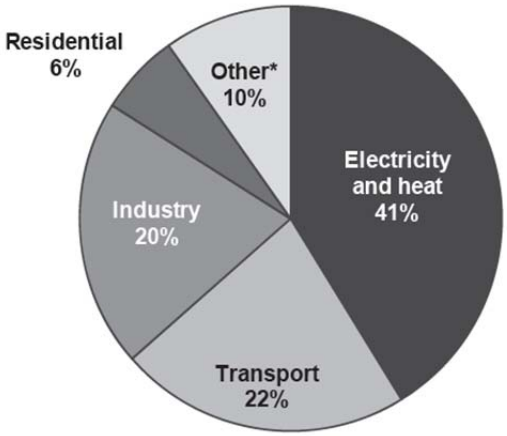

Figure 1.3. Sources of CO_2 emissions [3].

1.1.2.- CO_2 impact on the environment

This high concentration of CO_2 has its effect in human, plant production, and animals. The major problem that can cause by the high emission of CO_2 for human is the greenhouse effect or global warming [5]; in which, visible and ultraviolet radiation from the sun that passes through the stratosphere and upper atmosphere reaches the Earth surface and absorbed by the Earth then, converted to heat. This heat which is in the form of infrared radiation can be absorbed by low energy vibrational energy levels molecules like CO_2 and CH_4 thus reradiate this energy toward the Earth. Thus, this energy cannot escape from the Earth causing the atmosphere to be warmed. Since about 150 years until now, the global mean surface air temperature increased by 0.6^{o}C. The current concentration of carbon dioxide gas in the atmosphere is about 380 ppm, while it was 280 ppm in the

beginning of the 19th century [6]. Some assessments show that if the current concentration of CO_2 is doubled, the Earth's surface temperature could increase by 3.5°C. And if the temperature of the Earth increased, even as much as from 3 to 4°C, the rainfall patterns will affected dramatically, the water level in the oceans will increased, and there is a possibility to melt the polar ice caps and then every part in the Earth will be affected [1]. Figure 4, shows the human activities that produces greenhouse gases and there percentage in the atmosphere.

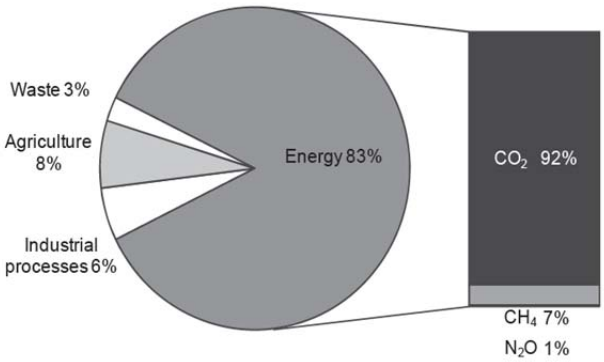

Figure 1.4. The human activities and their contribution to greenhouse gases [3].

From Figure 1.4, the energy consumption is the main contributor to the greenhouse gases which alone participate with 83% from the greenhouse gases emissions. And the dominate greenhouse gas is the carbon dioxide that contribute with about 92% of the greenhouse gases. A lot of work has been done for monitoring the effect of carbon dioxide emissions in the atmosphere on global warming in order to take actions toward reduction of its concentration in the atmosphere Figure 1.5 [4].

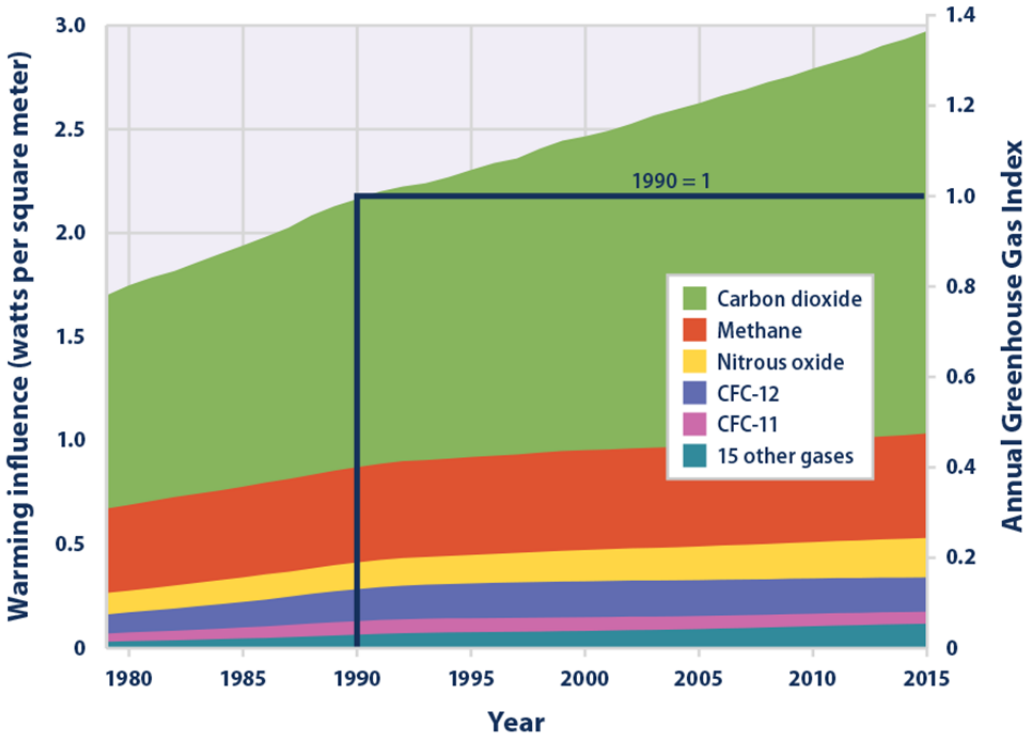

Figure 1.5. The heating effect caused by greenhouse gases in the atmosphere.

The second impact of the high concentration of the anthropogenic CO_2 in atmosphere is the ocean acidification [1,7,8], in which from about 30% to 40% of CO_2 emissions by humans dissolves into oceans, rivers, and lakes. Some of the dissolved CO_2 reacts with water to produce carbonic acid. Some of the produced carbonic acid undergoes further reaction with water to form bicarbonate ion and hydronium ion, thus increasing the ocean's acidity by increasing the H^+ ion concentration (decreasing the pH of the oceans). During the period from 1751 to 1994 the H^+ ion concentration in the oceans increased by 30%, with a decrease in the ocean's pH from 8.2 to 8.1. This decrease in the ocean's pH affects the marine

animals by inhibiting their shell growth and can also cause reproductive disorders in some fish. Figure 1.6, illustrates the mechanism of ocean acidification.

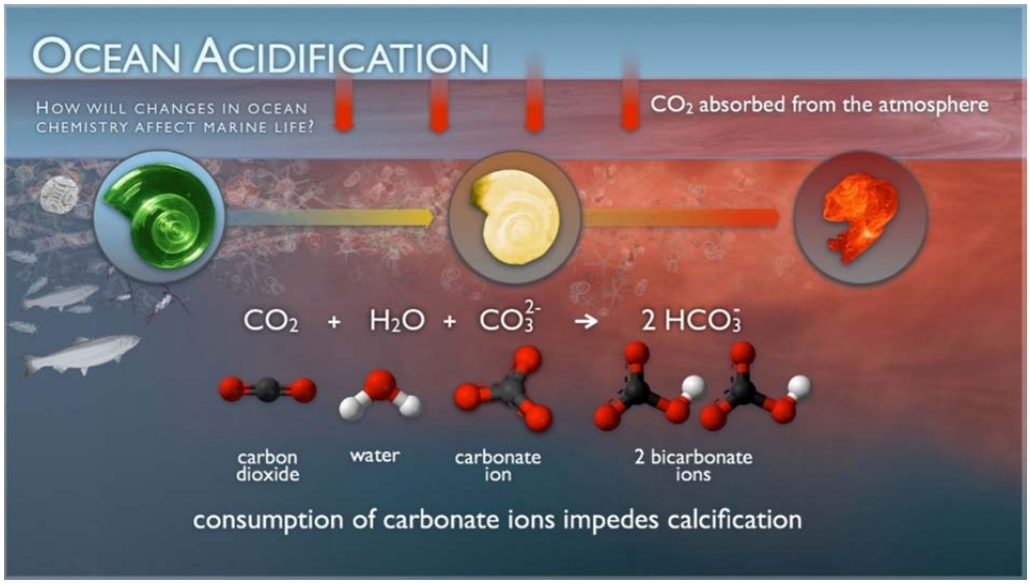

Figure 1.6. Description of ocean acidification mechanism.

On the other hand, the effect of CO_2 on plants is very different. Many studies were made to study the effect of carbon dioxide on plants such as trees, herbs, and grasses. Found that if the CO_2 concentration increased by factor 2x ambient, the plant productivity will increase by 25% to 50%.

So, we have to think how to reduce the amount of CO_2 released to the Earth. But the challenge is great due to the industrial revolution, the huge amount of fossil fuels combustion, and also due to the chemical stability of carbon dioxide. The difficulty of reducing carbon dioxide into useful products can be attributed to the high reduction over potentials or the surface of the metal catalyst can be poisoned or deactivated by the produced reduction products [9].

1.1.3.- Carbon dioxide CO_2 conversion methods

The CO_2 reduction is first discovered by Sabatier and Fischer-Tropsch since the early 1900s, in a process of conversion of CO_2 and hydrogen into hydrocarbons. There are a lot of techniques that are used to decrease the amount of CO_2 in the atmosphere some of them are discussed below.

- Radiochemical method

The first attempt to reduce CO_2 by the radiochemical method was by Getoff et al [10]. In aqueous media, CO_2 is converted into HCOOH and HCHO using γ-radiation.

$$CO_2 \xrightarrow{\gamma - radiation} HCOOH, HCHO$$

- Chemical reduction by metals method

This occurs at relatively high temperature.

$$2Mg + CO_2 \rightarrow 2MgO + C$$
$$2Na + 2CO_2 \rightarrow Na_2C_2O_4$$

- The biochemical method

By aiding of Methanobacterium thermoautotrophicum bacteria CO_2 can be converted into methane CH_4 [11].

$$CO_2 + 4H_2 \xrightarrow{bacteria} CH_4 + 2H_2O$$

- The electrochemical method

The electrochemical method for CO_2 reduction has great interest [12-15], also it is the topic of this thesis so it will be discussed in more details in the next section. In a brief, in electrochemical cell CO_2 is transformed into more reduced chemical species where, the obtained product depends on the number of electrons involved in the reduction process.

$$CO_2 + xe^- + xH^+ \xrightarrow{eV} CO, HCOOH, (COOH)_2$$

- Photo-electrochemical method

The photo-electrochemical reduction technique is a process in which in electrochemical cell CO_2 is transformed into hydrocarbon species in the presence of solar energy [16].

$$CO_2 + 2e^- + 2H^+ \xrightarrow{h\nu, eV} CO + H_2O$$

The photo-electrochemical reduction process of CO_2needs a catalyst that can be homogenous or heterogeneous [17]. Recent works aim to develop this catalyst which mainly depends on semiconductor or metal-decorated semiconductor electrodes Figure 1.7. By exposing to light, the semiconductor photo-catalyst the electrons promote from the valence band to the conduction band leaving a hole in the valence band. Generation of the electron/hole pair occurred only if the light energy is greater than or equal to the photo-catalyst band gap. The recombination

process between the negative electron and the positive hole can be done either in the bulk of the electrode or in the surface.

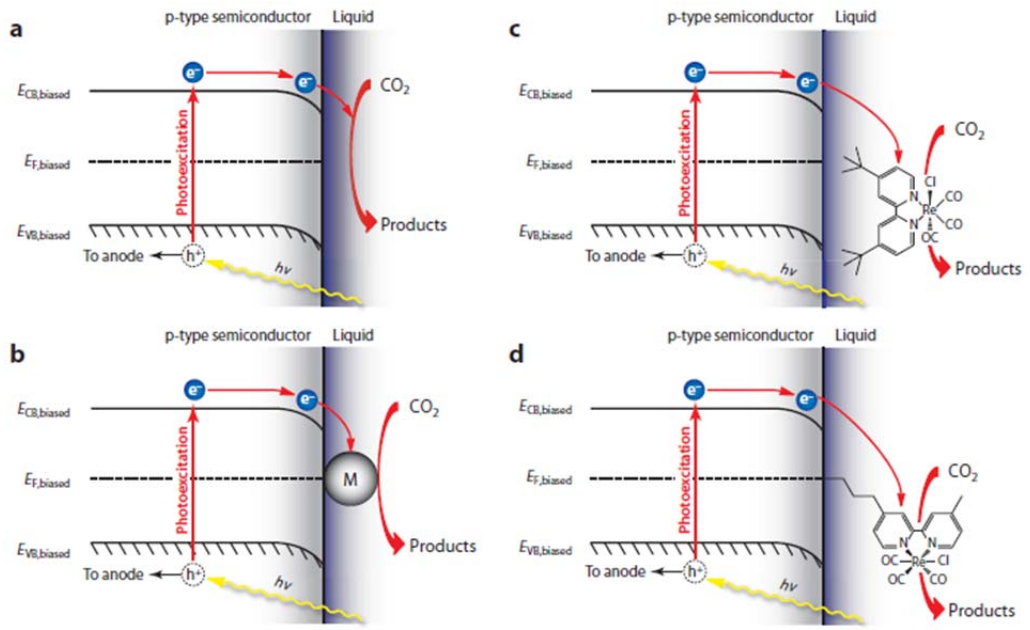

Figure 1.7. Schematic diagrams of four different schemes for light-assisted CO_2 reduction on a semiconducting photocathode [9].

(a) Heterogeneous catalysis on a semiconductor electrode, (b) heterogeneous catalysis on a metal-decorated semiconductor electrode, (c) Homogeneous catalysis through a semiconductor/molecular catalyst junction, and (d) heterogeneous catalysis through a molecular catalyst–decorated semiconductor electrode.

In the photo-electrochemical CO_2 reduction the most important parameter that must be put into account is the photochemical quantum yield that is defined as:

Photochemical quantum yield (Φ) = (moles products / absorbed photons)

X (Number of electrons needed for conversion)

1.1.4.- The electro-catalytic reduction of CO_2 into hydrocarbons

Many countries depend on fossil fuel such as petroleum and natural gas as sources of energy; however the combustion products of these energy sources are not environmentally friendly. As stated earlier, CO_2 is one of the products obtained from fossil fuel combustion and is the major contributor to the greenhouse effect. Catalysis technology, which deals with accelerating and directing chemical transformation of fossil fuel combustion products, become has a great importance in CO_2 reduction. Catalysis technology used to convert carbon dioxide into liquid fuels by aiding of solar or electrical energy, thereby CO_2 can be recycled into hydrocarbons or others useful chemical compounds, thus reducing the carbon dioxide concentration and its contribution to the atmospheric warming and in the same time become a source of liquid fuels.

The catalytic conversion of carbon dioxide into liquid fuels facing some challenges, because the conversion efficiency until now is low and it depends on expensive and rare materials like platinum [18] either at atmospheric pressure [19] or at high pressure [20,21]. So materials with new design and structure have to introduce to achieve high catalyst activity and product selectivity, and hence make the catalytic conversion of carbon dioxide commercially applicable.

The electro-catalyst can be categorized into homogeneous, like coordination complex and enzyme, or heterogeneous, like platinum surface and nanoparticles. The role of the electro-catalyst in the electrochemical reaction is to assist in

transferring of electrons between the electrode and the reactants, and/or facilitates the transformation of intermediate chemical.

Carbon dioxide is a stable and amphoteric molecule; the carbon atom is susceptible to nucleophilic attack, while the oxygen atoms are susceptible to electrophilic attacks (Figure 1.8).

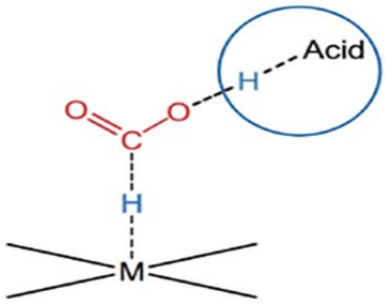

Figure 1.8. Carbon dioxide activation by nucleophilic and electrophilic attacks.

The electrochemical reduction of CO_2 is effective method by which carbon dioxide is transformed into more reduced species like hydrocarbons by aiding of the electric energy [22]. In the electrochemical reduction process, CO_2 gas reacts with H_2 gas or any other source of H^+ ion like aqueous electrolytes. Depending on the electrode material used, the electrolyte, and the experimental conditions, different products can be obtained like methane, methanol, or formic acid. The advantages of electrochemical reduction are it can be carried out at low temperature unlike Sabatier process which requires high temperature and pressure, also by using the suitable reduction method conditions reasonable Faradaic efficiency can be obtained. The Faradaic efficiency relates the moles of product obtained to the charge consumed during an electrochemical reaction.

In the electrochemical carbon dioxide reduction, electricity is required to break the C-O bond in carbon dioxide and also help in converting it to useful products. In order to produce useful products like hydrocarbons from carbon dioxide multiple-electron transfer is required for converting CO_2 to such products. The redox potentials for multi-electronic pathways are carried out at lower negative potentials than the redox potential for mono-electron reduction mechanism, so the mono-electron pathway is highly unfavourable.

The most common reactions occurred during the reduction of carbon dioxide in aqueous media at 25 ^{o}C against standard hydrogen electrode (SHE) at pH 7.0 are as follows.

$$CO_2 + H_2O + 2e^- \rightarrow CO + 2OH^- \qquad E^o = -0.52\ V$$

$$CO_2 + H_2O + 2e^- \rightarrow HCOO^- + OH^- \qquad E^o = -0.43\ V$$

$$CO_2 + 6H_2O + 8e^- \rightarrow CH_4 + 8OH^- \qquad E^o = -0.25\ V$$

$$2CO_2 + 8H_2O + 12e^- \rightarrow C_2H_4 + 12OH^- \qquad E^o = -0.34\ V$$

$$2CO_2 + 9H_2O + 12e^- \rightarrow C_2H_5OH + 12OH^- \qquad E^o = -0.33\ V$$

$$3CO_2 + 13H_2O + 18e^- \rightarrow C_3H_7OH + 18OH^- \qquad E^o = -0.32\ V$$

The expected pathways for obtaining these chemical compounds are illustrated in Figure 1.9.

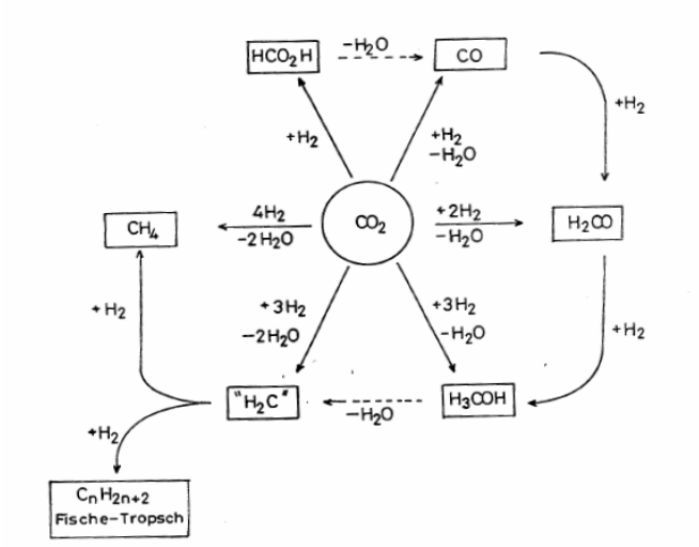

Figure 1.9. Pathways of carbon dioxide reduction.

The carbon dioxide reduction can be done by using different types of electrodes, where the flat metal based electrodes is the most used like Cu and Ag [19,23-25]. In the recent years the new research introduces new electrode materials like carbon based electrodes. Carbon gels, carbon nanotubes, and graphene oxide are examples on carbon based electrodes for CO_2 reduction [22,26].The products obtained from the carbon dioxide reduction depend greatly on the electrode materials, the applied potential, and the electrolyte used through the electrochemical reduction reaction. Carbon gels; xerogels, and aerogels, are porous nanostructured materials that recently find applications as supercapacitors, and as electro-catalyst in CO_2 conversion [22,27,28]. The solvent used in CO_2 conversion process can be aqueous or non-aqueous solution. The products obtained in aqueous and non-aqueous solutions with different electrode metals [29] can be summarized as follows.

- In aqueous media.

1. Metallic In, Sn, Hg, and Pb are selective for formic acid.
2. Metallic Zn, Au, and Ag are selective for carbon monoxide.
3. Metallic Cu is selective for hydrocarbons, aldehydes, and alcohols.
4. Metallic Al, Ga, and group VIII elements exhibit low electro-catalytic activity.

- In non-aqueous media.

1. Pb, Ti, and Hg are selective for oxalic acid.
2. Cu, Ag, Au, In, Zn, and Sn are selective for carbon monoxide and carbonate ions, while Ni, Pd, and Pt selective for carbon monoxide.
3. Al, Ga, and group VIII except (Ni, Pd, Pt) are selective for carbon monoxide and oxalic acid.

The aqueous solution has the advantage of using water as the proton source, but it is accompanied by hydrogen gas formation which competes with the carbon dioxide reduction reaction. So it is important to suppress the hydrogen formation to save the energy wasted in its evolution. The advantage of using the non-aqueous solvents is its ability to dissolve higher amount of carbon dioxide than water which results in obtaining higher concentrations of the produced chemical products. Table 1.2 summarizes the different studies made to reduce the carbon

dioxide concentration by using different electrode materials and different solvents [30,31]; it is also list the faradic efficiency obtained for each study.

Table 1.2. Different studies made to reduce the carbon dioxide concentration.

Year	Electrode	Experimental parameters (electrolyte, conditions)	Main Products (Faradaic efficiency,%)	Refs
2016	Ni_xGa_y	Aqueous $KHCO_3$ -0.48 V vs RHE	C1-C2 hydrocarbons	[32]
2015	Cu-In alloy	0.1M $KHCO_3$ -0.5 V vs RHE	CO (90)	[33]
2014	Ag foil	Ionic liquid/organic solvent	CO (90.1)	[34]
2013	Ni/Cu/Fe doped carbon xerogels	0.1 M $KHCO_3$	C1-C4 hydrocarbons	[22]
	Glassy carbon (WE), Pt wire (CE), Ag/AgCl (RE)/ $[Mn(bpy\text{-}t\ Bu)(CO)3]^+$	-2.2 V vs. SCE DMF/ 2 M H_2O	CO (100)	[35]
	Sn-powder-decorated gas diffusion layer (SnGDL) electrode	-1.6 V vs. NHE Aqueous $NaHCO_3$ solution	HCOOH/ $HCOO^-$ (70)	[36]
2012	Glassy carbon (WE); aqueous SCE electrode (RE); Pt wire (CE)	DMF + 0.1 MnBu4NPF6 + 2 M H_2O	CO (> 90)	[37]
	Sn foil with an active surface area of 1 cm^2	-1.7 V vs. SCE 0.1 M Na_2SO_4	HCOOH/ $HCOO^-$ (~ 90)	[38]
2011	Electrodeposited cuprous oxide film	0.5 M $KHCO_3$solution saturated with CO_2 -1.1 V vs. SCE	CH_3OH (38)	[25]
	$[Mn(bpy)(CO)_3]$+ $[Mn(dmbpy)(CO)_3]$+	0.1 M TBAP in MeCN -1.70 V	CO (85, 100)	[39]
2008	Illuminated p-GaPphotoelectrodes	-0.52 V vs. SCE	CH_3OH (~100)	[40]
	Polished pyrolytic graphite edge electrode (WE)	20 mM Na_2CO_3 (pH 6.5) solution	HCOOH/ $HCOO^-$ (~100)	[41]

2007	GC, Cu	$Ru(2,2'\text{-bipyridine})_2$ $(2,2'\text{ bithiazole})^{2+}$	Formate	[14]
	Granulated Sn continuous reactor	0.5 M $KHCO_3$ + 2 M KCl and 2 M KOH	Formate	[42]
2006	Cu	-	Review	[43]
	-	aqueous	Formate (86)	[44]
2005	Cu	Deactivation of Cu	CH_4 and other hydrocarbons	[45]
	Cu+Au	0.1M $KHCO_3$; 0.1M K_2SO_4	CH_4 (56.9), C_2H_4 (17.1)	[30]
	Cu polycrystalline	Sulfuric and Perchloric acid electrolytes	CH_4, C_2H_4 CH_3OH,HCHO	[46]
2004	Polypyrrole (PPy)electrode	methanol/$LiClO_4$	CH_2O(1.9)HCOOH (40.5) Acetic acid (62.2)	[47]
	Pd–Pt–Rh alloys	-	CO	[48]
	GC	MeCN-water presence of tetra azaannulene]$^{++}$	-	[49]
	Pb-granules	aqueous medium	Formic acid (94)	[50]
	Cu-mesh electrode	Neutral solution	C_2H_4 (80) ;H2 (9)	[51]
2003	Au - polycrystalline	DMSO, hexa-aza-macrocycles and its Co(II) complexes	CO and HCOOH	[52]
2002	-	methanol/$LiClO_4$	-	[53]
	Cu	aqueous $NaHCO_3$	CH_4 (46)	[54]
	Rhenium and Cu-Rh	(EQCM) with CV	CO, CH_4 (31%)	[55]
	GC	Methanol-_diphthalocyanine complexes and phthalocyanine films	CO, CH_4, $HCOO^-$	[56]
2001	Au- prepared by sputtering	KCl and KHCO3	CO and H_2	[57]
	Rhenium electrode-posited onAu	Methanol	CO (57), CH_4 (10) andH_2 (33)	[58]
	Pt porous	Perchloric acid	Formic acid, Methanol, Methane (traces)	[59]
2000	Pt - Polycrislaline	Acidic media	-	[60]
	Cu	aqueous	CH_4, C_2H_4	[13]
1999	Cu	CsOH/ methanol	Methane (8.3), Ethylene (32.3), H_2 (23)	[61]

1998	Ag	KOH-methanol	Carbon monoxide and Formic	[24]
	p-InP, p-GaAsphotocathode	Methanol	CO	[62]
	Pt, Pd supported GDE	-	Methane (38.8)	[63]
	Pb	KOH/Methanol	Formic acid, CO, Methane	[64]
	Cu/Zn oxides	at -1.30 V.	Total reduction (40.5)	[23]

1.2.- SUPERCAPACITORS

1.2.1.- Overview

Start of understanding electricity at the molecular electronic level begins with the Michael Faraday work on the electron and later the work of Thomson and Millikan [65]. Also, the development of 'Leyden jar' was has a significant effect on the discovery of the charge separation and charge storage principle on two surfaces separated by a glass layer which later become have its importance on electrical technology, electronics, and electrochemical engineering devices. The Leyden jar was referred to it in the early technological applications as the 'condenser', but later the Leyden jar is referred to it as a 'capacitor' and its charge storage per volt capability is named as 'Capacitance' *C*, given in units of farads.

The mechanisms of electrical charge storage in capacitors at the atomic physical level was poorly understood till 140 years after the development of the Leyden jar capacitor, Faraday was the first one assume correct ideas about polarization in the dielectric materials of charged condensers. The principle behind storing the electrical energy in a charged capacitor begins to be known

since 1745; when applying a voltage difference V, between two plates accommodating charges +q and –q, the stored energy [65,66].

$$G = ½ CV^2 \text{ or } ½ qV \quad (1.1)$$

Where G is the Gibbs free energy and C is the capacitance. Becker granted a patent in 1957 to be the first one using this principle in the practical point of view as in a cell or battery.

1.2.2.- Supercapacitor types

A supercapacitor is a device suited to the rapid storage and release of energy, and among all electrochemical energy storage and conversion systems, supercapacitor has great importance stated by the national science foundation (NSF) in USA; 'Supercapacitors Could Be Key to a Green Energy Future' due to its long cycle life (>100,000 cycles), high dynamics of charge propagation, and high power density [67]. Supercapacitors provide ideal solution for the increasing power demands of energy storage systems because of their high power density which is higher than that of lithium ion batteries by thousands of times and also their energy density is larger than the conventional capacitors.

So a supercapacitor is used in many applications like electronics, memory back-up systems and hybrid cars. Many researchers believe that supercapacitors will be the best alternative solution for the gas-fuelled automobiles. But the main drawback of a supercapacitor is its low specific energy density in aqueous based electrolytes compared to batteries and fuel cells [68]. So it is important to

introduce new electrodes in supercapacitors application to overcome this limitation and enhance its capacitance.

Based on their mode of energy storage, supercapacitors can be classified into two types [69,70]: (i) Pseudocapacitors, where energy storage occurs through Faradaic electrochemical storage with electron charge transfer by redox reactions. (ii) Electrochemical double layer capacitors (EDLCs), where energy storage occurs through electrostatic storage that take place by separation of charge in a Helmholtz double layer at the interface between the electrode surface and electrolyte, so the capacitance of electrochemical double layer supercapacitors depends on the surface area of the used electrode.

The capacitor electrodes can be metal, semiconductor, or colloid surfaces. Carbon is a unique element suited for the fabrication of double layer electrochemical capacitors electrodes due to its high surface area and its unreactive character that makes it has a potential voltage range of ideal polarizability; approaching 1.0 V in aqueous electrolytes and up to 3.5 V in non aqueous electrolytes [67,70-74]. Graphite, glassy carbon, activated carbon, and carbon black all are forms of carbon used in electrochemical capacitors. In the development of EDLCs, the optimum control of electrode pore size and specific surface area for an appropriate electrolyte is crucial in improving the supercapacitor performance [65,75]. Recently, carbon gels found a very good application in catalysis and electrochemical double layer capacitors due to its tuneable surface area, pore volume, and pore size distribution depending on the synthesis and processing conditions [68,76,77]. The carbon gels can be doped with transition metals to gain the advantages of both materials [78]. The large capacitances that can be derived from the RuO_2 film systems and carbon double

layer type capacitors led to the terms 'supercapacitor' or 'ultracapacitor' respectively. Recently, these two terms are combined to be 'electrochemical capacitors'.

1.2.3.- Supercapacitor structure

The supercapacitor structure (Figure 1.10) is similar to that of battery in which two porous electrodes are deposited onto a current collector, immersed in an electrolyte and the two electrodes are separated by dielectric porous separator [65].

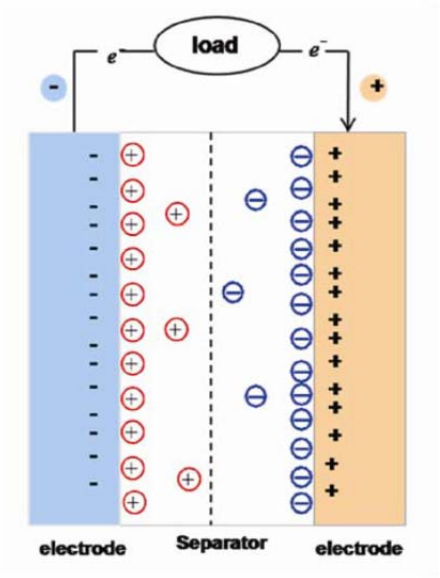

Figure 1.10. The supercapacitor structure.

With applying a voltage difference between the two electrodes, the negative ions of the electrolyte are attracted to the positive electrode while the positive ions

are attracted to the negative electrode. The components of the supercapacitor including the electrodes, electrolyte, separator thickness, as well as the current collector all have a very important effect of the supercapacitor performance and must be considered in designing a high performance supercapacitor device. Simple representation of an equivalent resistor-capacitor (RC) circuit is illustrated in Figure 1.11, in which C_a and C_c represent the capacitances of the anode and cathode respectively. R_s is the equivalent series resistance (ESR) of the cell and R_f is the resistance responsible for single electrode self dis-charging.

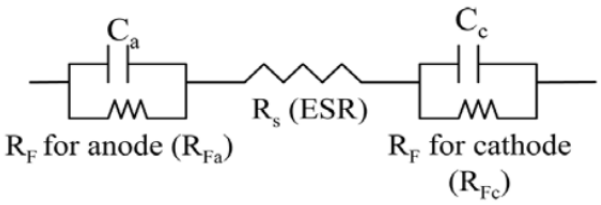

Figure 1.11. Representation of an equivalent resistor-capacitor (RC) circuit.

Then, the total supercapacitor capacitance which is a sum of the anode and cathode capacitances and can be expressed as

$$\frac{1}{C_T} = \frac{1}{C_a} + \frac{1}{C_c} \tag{1.2}$$

The maximum energy stored and maximum power obtained from such a single cell supercapacitor are given by equations:

$$E = \frac{1}{2} C_T V^2 \tag{1.3}$$

$$P = \frac{V^2}{4R_s} \tag{1.4}$$

Where V is the cell voltage (V), C_T is the total cell capacitance (farads), and R_s is the equivalent series resistance (ohms). From equations (1.3) and (1.4) for obtaining high-performance supercapacitor it must has large total capacitance, high operating cell voltage, and minimum ESR.

1.2.4.- The Electric Double Layer (EDL)

The concept of electric double layer is first described and presented by Hermann von Helmholtz in 1853. In his model, Helmholtz realizes that when a charged surface is brought in contact with an electrolyte, the co-ions are repelled away from the charged surface while the counter ions are attracted to it. Helmholtz deduced that the electrical double layer is a molecular dielectric that can store charge electrostatically. This model predicts a constant capacitance depending on the dielectric constant of the used electrolyte and the double layer thickness. In 1910 Louis Georges Gouy and in 1913 David Leonard Chapman (Gouy-Chapman Model) both of them observed that capacitance is not a constant value and it depends on the electrolyte ionic concentration and the applied potential. They also introduced the diffuse model of the double layer in which the

charge distribution of ions is a function of the distance from the charged surface; hence the electric potential drops exponentially away from the charged surface (Figure 1.12). In 1924 Stern combine both models for Helmholtz and Gouy-Chapman; he concluded that some ions adhere to the charged surface electrode as in Helmholtz model forming a so called the inner region or Stern layer, while some other ions diffuse away from the electrode forming the diffuse layer.

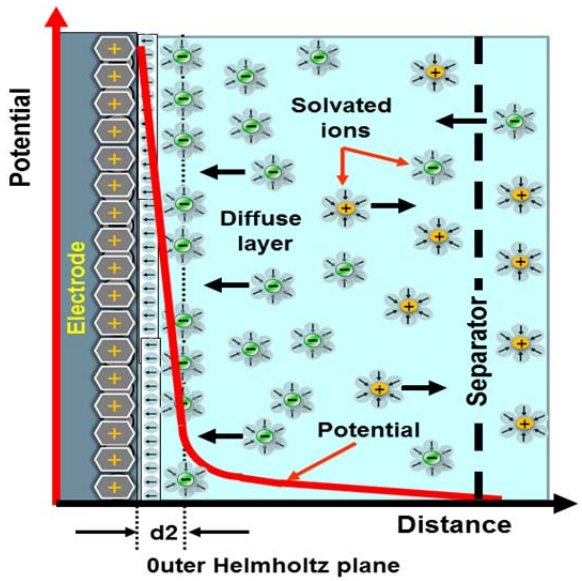

Figure 1.12. The Electric Double Layer.

The capacitance in electrochemical double layer capacitors (C_{dl}) can be expressed as a sum of capacitances from two regions, the stern layer capacitance (C_H) and the diffuse layer capacitance (C_{diff}). Thus, we can conclude that:

$$\frac{1}{C_{dl}} = \frac{1}{C_H} + \frac{1}{C_{diff}} \tag{1.5}$$

The factors that affect the behaviour of the EDL at a planar electrode and hence the capacitance can be summarized as; (i) the electrode surface area, (ii) the electrolyte type and the solvent in which the electrolyte is dissolved, (iii) the electrical filed across the electrode, (iv) the chemical affinity between the electrode surface and the electrolyte ions [79].

The specific capacitance, *C*, which is expressed in (F g^{-1}) for each electrode in the electrochemical double layer supercapacitors, is generally fellow that for parallel-plate capacitor.

$$C = \frac{\varepsilon_r \varepsilon_0}{d} A \tag{1.6}$$

Where, ε_r is the electrolyte dielectric constant, ε_0 is the permittivity of a vacuum, A is the electrode specific surface area accessible to the electrolyte ions, and d is the effective EDL thickness (the Debye length).

From equation (1.6), the specific capacitance, *C,* is directly proportional to the specific electrode surface area, *A*. But this is almost not experimentally hold, because there are some results showed that it is not necessary the capacitance increases with increasing the electrode surface area because they believe that the submicropores of the electrode do not participate in the electrochemical double layer formation. If the solvated ions of the electrolyte is larger than the submicropores of the electrode surface then, the ions do not have the accessibility to the submicropores and hence do not contribute to the capacitance. Gogotsi and

co-workers [80] observed that maximum capacitance is obtained when the electrode pores size is very close to the electrolyte ions size.

1.3.- OXYGEN REDUCTION REACTION (ORR)

1.3.1.- Fuel Cells

Fuel cells are electrochemical devices that able to convert chemical energy into electric energy when a fuel and oxidant are supplied. Fuel cells were invented in the middle of the 19th century by Sir William Grove [81]. Fuel cells faced some problems that late their introducing in the market, like economic factors, materials designing problem, and inadequacies in electrochemical devices operation. At the beginning of the 20th century fuel cells find a great attention due to increase use of electricity and increase demand of converting chemical into electrical energy. The first successful application for fuel cells was in the space technologies, where it can provide the required electrical energy, heat, and potable water for the crew.

A lot of research work focused to develop the fuel cells and its technology due to their excel advantages over the batteries. According to their working mechanism fuel cell bear similarities to both batteries and engines, however, it has a superior advantages in that it does not need recharging and generates drinking water when the used fuel is hydrogen, so, it is considered as ‘zero emission engine’ [82]. Due to its environmentally friendly, fuel cells find commercial applications in transportation, stationary power generation, and in low power portable devices. Fuel cells facing from two major limitations that affect their market availability; cost and reliability.

1.3.2.- Types of fuel cells

Fuel cells can be classified according to the employed electrolyte in the cell. The direct methanol fuel cell (DMFC) is the only exception to that classifications in which methanol is electrochemically oxidized directly in the fuel cell. Another classification for fuel cells can be performed according to the operating temperature, so we have low and high temperature fuel cells [81,82]. Fuel cells that belong to the low temperature fuel cells are Alkaline Fuel Cell (AFC), Proton Exchange Membrane Fuel Cell (PEMFC, also called polymer electrolyte fuel cell, PEFC, or Solid polymer electrolyte fuel cell, SPEFC), direct methanol fuel cell (DMFC), and Phosphoric acid fuel cell (PAFC). High temperature fuel cells have a range of operating temperature between 500-1000 ^{o}C, and have two types the Molten Carbonate Fuel Cell (MCFC) and Solid Oxide Fuel Cell (SOFC).

1.3.3.- Oxygen Reduction Reaction (ORR)

The fuel cell is a galvanic cell that consists of two electrodes anode and cathode, the overall reaction of half reactions can be described as following:

$$a_{ox1} + b_{red1} \rightarrow C_{red2} + d_{ox2}$$

The difference between the two half-cell reactions gives the cell voltage, *E*, that can be described by Nernst Equation, where n is the number of electrons and F is the Faraday constant.

$$E = E^{o} - \frac{RT}{nF}\ln Q \tag{1.7}$$

The free energy change, ΔG**,** of a chemical reaction is a thermochemical quantity that depend on temperature and on the composition of the reaction mixture. The values of ΔG and E are directly proportional and are related by the equation

$$\Delta G = -nFE \tag{1.8}$$

The anodic fuel cell reaction is either the direct the direct oxidation of hydrogen or the oxidation of methanol. The cathodic fuel cell reaction is usually oxygen reduction reaction (ORR) and in most cases the source of oxygen is air.
The two overall pathways in aqueous electrolytes for oxygen reduction reaction can be represented by the following equations:

1) Direct four-electron pathway:

   a) In alkaline electrolyte

   $$O_2 + 2H_2O + 4e^- \rightarrow 4OH^- \qquad E^o = 0.401\,\text{V}$$

   b) In acidic electrolyte

   $$O_2 + 4H^+ + 4e^- \rightarrow 2H_2O \qquad E^o = 1.229\,\text{V}$$

2) Peroxide pathway:

   a) In alkaline electrolyte

   $$O_2 + H_2O + 2e^- \rightarrow HOO^- + OH^- \qquad E^o = -0.065\,\text{V}$$

Followed by either peroxide reduction

$$HOO^- + H_2O + 2e^- \rightarrow 3OH^- \qquad E^o = 0.867\ \text{V}$$

Or peroxide decomposition

$$2HOO^- \rightarrow 2OH^- + O_2$$

b) In acidic electrolyte

$$O_2 + 2H^+ + 2e^- \rightarrow HOOH \qquad E^o = 0.670\ \text{V}$$

Followed by either

$$HOOH + 2H^+ + 2e^- \rightarrow 2H_2O \qquad E^o = 1.77\ \text{V}$$

Or

$$2HOOH \rightarrow 2H_2O + O_2$$

The direct four-electron pathway is preferable because the Faradaic efficiency of the reaction is greater, also it does not involve peroxide species in the solution. The major factor that limit the fuel cell performance is the cathodic oxygen reduction reaction (ORR) as it consists of several steps in which molecular oxygen dissociates at the catalyst surface and combines with hydrogen ions. Different factors can influence the reaction kinetics at electrode surface, but still the electro-catalyst itself has the major effect. Takasu et al., Bregoli, and Ross [83-85]. Found that the catalyst particle size have effect on the kinetics of the ORR and the produced Faradaic efficiency. Also another work [81] suggested that not only the particle size can affect the ORR, but also the number of active sites. Because by decreasing the particles size the surface area increases but this not approve for increasing the active sites.

So, great research focused on development of a new efficient electro-catalyst for the ORR. To date, Pt and its alloys are still the best known electro-catalysts for the ORR [86-88]. In order to reduce the cost of using pure Pt metal as a catalyst, alloying Pt with another metal reduces the cost but the metal leaches away gradually, resulting in loss of performance that reduces the total fuel cell efficiency and limit their market use.

The current fuel cell technology is based on development of non-precious metals and Pt-free electro-catalyst [89-91]. Carbon nanomaterials such as carbon nanotubes and graphene was applied as electro-catalysts for the ORR and exhibit a good performance but their efficiency is still not reach the acceptable level [92-95]. A new emerging class of carbon nanomaterials which is carbon gel have a very good electrochemical properties was found to be competitive for these materials in many applications and will be tested as electro-catalyst in oxygen reduction reaction (ORR) as well.

1.4.- CARBON GELS

1.4.1.- Carbon based materials as catalysts

Uses metals especially noble metals and metal oxides in catalysis technology play a major role in many applications. However, metal-based catalysts still suffer from some drawbacks that limit their use in a large scale such as their high cost, susceptibility to gas poisoning, and low selectivity [96]. Carbon-based materials have become promising alternatives catalysts for metal-based catalysts. Due to

their availability, resistance to corrosion, environmentally friendly, and unique surface area properties [67,97,98].

Carbon-based catalysts like activated carbon, carbon nanotubes, graphene sheets, and carbon gels are recently used materials in catalysis technology because of their surface active sites that are necessary for reactants adsorption, bond-breaking and new bond-formation, and products desorption. Consequently, great effort has recently been directed toward the development of carbon-based nanomaterials catalysts.

Carbon gels which is one of carbon-based nanomaterials family, offer the opportunity to be used as it is or doped with metals which find a very good catalytic performance in many applications such as environmental and fuel cell applications [97]. In the environmental applications, metal doped carbon gels have been considered to be effective catalyst either in the reactions carried out in the gas phase like volatile organic compounds (VOC) oxidation or in the liquid phase like catalytic wet air oxidation (CWAO) of aniline solutions [97]. In fuel cell applications, carbon gels have been used as supports for Pt-based electro-catalysts for proton-exchange membrane fuel cells (PEMFCs).

1.4.2.- Carbon gels overview

Carbon gels, xerogels and aerogels are nanostructured materials obtained from the carbonization of organic gels, which are prepared by the sol–gel polycondensation of certain organic monomers, typically resorcinol (R) and formaldehyde (F) [99]. The textural characteristics of these materials strongly depend on a careful control of the reactant concentrations and the experimental conditions of the different synthesis steps: gelation, curing, drying and carbonization/activation [100-102]. The addition of surfactants during the R-F

polymerization strongly affects the morphology of these materials and the final metal dispersion [103].Therefore, surface area, pore volume, and pore size distribution are tuneable properties related to the synthesis and processing conditions, enabling the preparation of a wide suite of materials with unique properties, e.g. for adsorption [104,105], catalytic [106-109], and electrochemical applications [22,110]. Moreover, carbon gels doped with transition metals show a high dispersion and homogeneous distribution of the metals throughout the carbon matrix [111-114]. The majority of metal cations will be anchored into the structure of the carbon gel, which minimizes the leaching of the metals in liquid phase applications. Nevertheless, a percentage of the metal phase of the doped carbon gels will not be accessible to the reactants, although preparation techniques are available that minimize this issue [103].

Carbon gels can be prepared in many forms like monoliths, beads, powders, electrodes, or thin films. The synthesis steps of the carbon gels are; preparing the initial solution, gelation and curing, drying, and carbonization. The carbon gels give us the ability to dope it with transition metals to gain the advantages of both materials. Depending on the drying process subcritical, supercritical, or freeze drying, the carbon gels are classified into xerogels, aerogels, and cryogel respectively [75,112,115-117].

1.4.3.- Carbon gels preparation

Carbon gels are derived from a polycondensation reaction between a hydroxybenzene and aldehyde monomers. Carbon gels are prepared in main four steps;

(i) Preparation of the initial mixture

The most widely used monomers for preparing the sol mixture (initial solution) are resorcinol (R) and formaldehyde (F) which are dissolved in water (W) in the presence of acidic or basic catalyst (C). The resorcinol and formaldehyde are mixed together with appropriate molar ratio, and any change in the R/F ratio will affect significantly on the porosity of the produced gel. Water is the most used solvent, however organic solvent (S) can be used. Polymeric gels with low surface area can be obtained by using low R/C ratio in the initial solution, while a high R/C ratio gives a higher possibility to colloidal gels [97]. Formaldehyde is added to the 2-, 4-, and/or 6- positions on the aromatic ring of resorcinol in an addition reaction to form the hydroxymethyl derivatives of resorcinol by the aid of a base which generates more reactive resorcinol anions (Figure 1.13). The hydroxymethyl derivatives of resorcinol, then undergo a condensation reaction to form methylene and methylene ether bridged compounds. During the condensation reaction, the products grow to form clusters that give rise to colloidal particles cross-linked with each other to produce the 'hydrogel'.

All parameters should be carefully controlled depending on the end use application and the required material properties, because any change in the starting parameter can lead to a totally different porosity. For example, using high concentration of alkaline catalyst reduces the gelation time and leads to the formation of polymeric gels with small particles and high surface areas. While by using low concentration of the alkaline catalyst leads to formation of colloidal gels with large particles size and low surface areas. Maldonado et al. [118]

prepared organic aerogels with different concentrations of alkaline catalyst i.e. sodium carbonate Na_2CO_3 the produced organic aerogels have different pore size and specific surface areas.

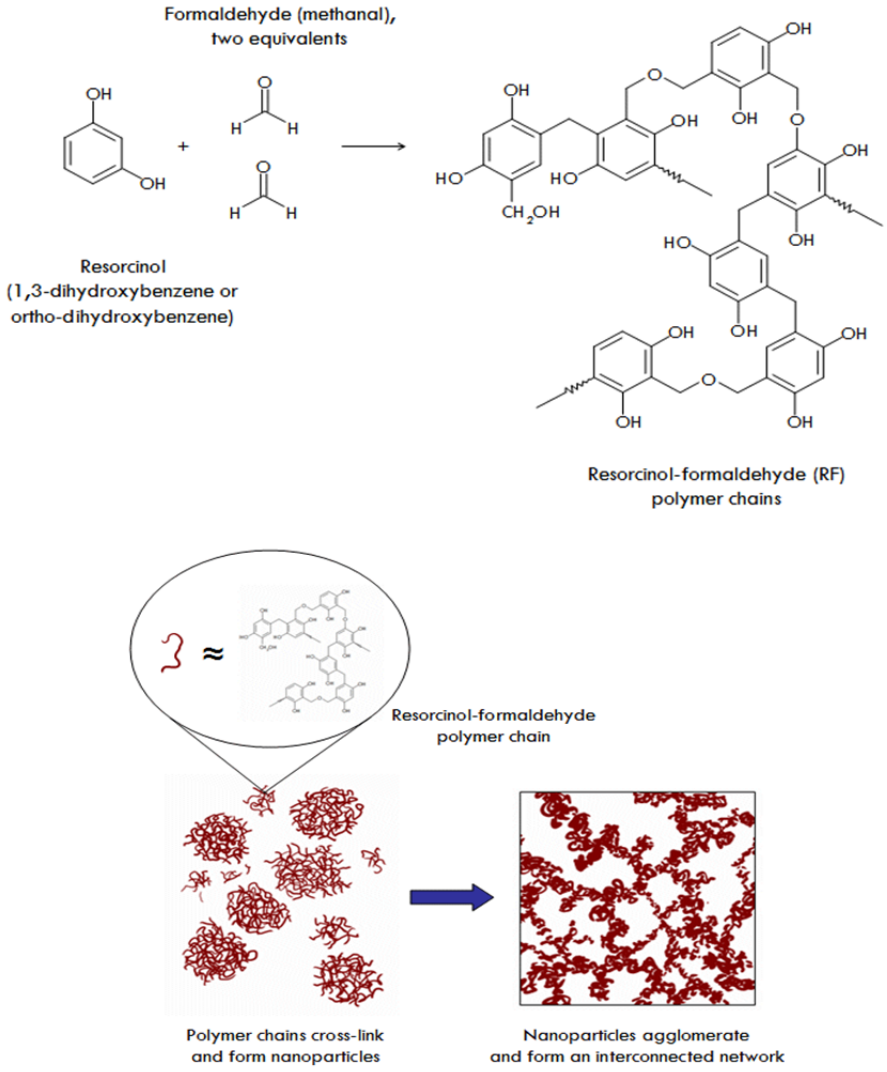

Figure 1.13. The polymerization reaction of resorcinol-formaldehyde monomers.

Also the initial pH of the solution has its effect on the produced structure, if the initial pH is high leads to high number of resorcinol anions that produces more interconnected polymeric particles and decreases the meso- and macropores.

Moreover, the molar ratios of R/F, R/W, and R/C should be carefully controlled because reducing the R/F or R/W molar ratios can produce smaller particles, less voids of gel structure, increase surface areas, and either reduce or increase pore volumes depending on the initial pH.

(ii) Gelation and curing

The colloidal solution is poured into a mold of the desired shape, then sealed to reduce solvent evaporation and, after that, heated to the desired temperature to allow the gelation and curing step to occur. In the gelation and curing step we allow for the hydrogel further cross-linking to obtain the solid organic gel. The curing time and temperature also have their effects on the produced gel structure.

(iii) Drying

In the drying step the solvent trapped inside the gel matrix is removed and the used method for removing the solvent has a great effect on the textural properties of the organic gel. The three main methods used in drying process are subcritical drying, supercritical drying, and freeze drying processes that produce the xerogels, aerogels, and cryogel respectively [102,117].

In subcritical drying the gel is dried by simple evaporation in oven or microwave. The advantages of this method are cheap, easy to perform and rapid.

However, it causes shrinkage of wide pores [116,117,119,120]. The impact of this method on the pores can be reduced by immersing the organic gels several days in acetone before drying.

Supercritical drying overcome the limitation of the subcritical method in which it preserve the porous texture and structural properties of the organic gel by removing the solvent under supercritical conditions of high pressure and temperature [78,121-123]. But this method facing some disadvantages of high cost, time consuming, and necessary to perform at least one solvent exchange with CO_2.

The third drying method is the freeze drying in which the solvent is frozen then removed from gel structure by sublimation. The advantages of this method are low shrinkage of the produced gel, produces materials with high pore diameter, and lower cost than supercritical drying method. But it is also suffer from some drawbacks like long time process, causes cracks inside gel structure, and very difficult to prepare monoliths by this method [117].

Gallegos-Suárez et al. [102] studied the effect of the drying methods applied during the synthesis processes on the micro- and mesoporosity of carbon aerogels and xerogels. They found that the microporosity development does not depend on the drying processes carried out on their corresponding organic gels. On the contrary, the mesoporous structure was affected by the applied drying method. Treatments with previous exchange of water per acetone partially prevented the mesoporosity collapse. Nevertheless, the xerogels obtained after microwave or plasmas treatments were chemically and texturally very similar to a classical thermally dried xerogel, but with the important advantage that these treatments can be carried out in very short period of times.

(iv) Carbonization and/or activation.

The organic gels is then subjected to the carbonization step to obtain their corresponding carbon gels by heating the organic gels at a temperature ranging from 773 to 2773 K under inert atmosphere of N_2 or Ar. Increasing the carbonization temperature leads to an increase in the surface area reaching a maximum then the surface area begins to decrease if the temperature exceed the critical level [124,125]. Using N_2 or Ar produces carbon gels with surface areas ranging from 600-700 m^2/g, while in case of using ammonia the surface area can be promoted to be above 1000 m^2/g [125].

In order to promote the surface area and pores volume the activation process can be carried out during or after the carbonization step. The activation process can be done chemically, or physically.

In chemical activation process, an activation agent is used such as KOH, H_3PO_4, or $ZnCl_2$ in a temperature range from 300-900 ºC. The advantages of chemical activation are its lower temperature, lower activation time, and higher porosity achieved compared to physical activation. While its disadvantages attributed to the higher cost of the activating agents and difficulty of completely removing all traces of the activating agent.

Physical activation is achieved by gasification of the gel with CO_2, steam, or combination of both in a temperature from 700-1100 ºC. It is a simple method and its cost is lower than chemical activation, while its disadvantages that it leads to more heterogeneous micropore size.

Finally, Espinosa-Iglesias et al. [126], have described that carbonization processes assisted by microwaves yield carbon gels with a different carbonaceous structure, as well as much higher oxygen contents than those obtained by conventional carbonization at a similar carbonization degree.

1.4.4.- Metal-doped carbon gels

Introducing metal species into the carbon matrix is one of the very interest research areas concerning carbon gels. That is because we take the advantages of both materials which open new applications areas for carbon gels such as adsorption and catalysis [103,108,111,114] There are three main strategies have been used to introduce metals inside the carbon framework [97]:

Dissolving the metal salts in the initial mixture changes the initial pH and hence changes the textural properties of the produced carbon gels as a result of changing the chemistry of the process. The initial pH affects the textural characteristics of the carbon gels, also the nature of the doped metal salt. Zr as a doping metal produce carbon gels with pores in the micropore range, while Ce-doped carbon aerogels have a very low microporosity. Moreno-Castilla et al, and Maldonado et al [76,113] studied the surface morphology, metal dispersion, and pore texture of transition metal-doped monolithic carbon aerogels.

Introducing a functionalized moiety with binding sites for the metal ions. Metal-doped organic gels can be prepared through the sol-gel polymerization of resorcinol derivatives that contain ion-exchange moiety with binding sites for the metal ions [97].

Depositing the metal precursor into the organic or carbon gels. Sputtering, adsorption, sublimation, and supercritical deposition are some examples on the methods used to deposit the metal precursor on both organic or carbon gel [97].

OBJECTIVES

The objectives of this work are the development of different series of carbon gels doped with transition metals and to study their behaviour and performance as electro-catalysts for carbon dioxide reduction to hydrocarbons and oxygen reduction reaction, and as electrodes for supercapacitors. In this line, carbon aerogels and xerogels, doped with three different loading of nickel, cobalt and iron will be prepared, exhaustively characterised and tested in the three above mentioned electro-chemical applications. The electro-chemical results will be correlated with the textural and chemical properties of the developed doped carbon materials.

LIST OF ACRONYMS

PCET	Proton Coupled Electron Transfer
CWAO	Catalytic Wet Air Oxidation
VOCs	Volatile Organic Compounds
NMVOC	Non-Methane Volatile Organic Compounds
GC	Glassy Carbon Electrode
RHE	Reversible Hydrogen Electrode

SCE	Saturated Calomel Electrode
NHE	Normal Hydrogen Electrode
ECs	Electrochemical Capacitors
EDLCs	Electrochemical Double Layer Capacitors
EDL	Electric Double Layer
ESR	Equivalent Series Resistance
ORR	Oxygen Reduction Reaction
DMFC	Direct Methanol Fuel Cell
AFC	Alkaline Fuel Cell
PEMFC	Proton Exchange Membrane Fuel Cell
SPEFC	Solid Polymer Electrolyte Fuel Cell
PAFC	Phosphoric Acid Fuel Cell
SOFC	Solid Oxide Fuel Cell

BIBLIOGRAPHY

[1] Aresta, M. *Carbon dioxide as chemical feedstock*. John Wiley & Sons: 2010.

[2] Winter, M.; Brodd, R.J. What are batteries, fuel cells, and supercapacitors? *Chemical reviews* **2004**, *104*, 4245-4270.

[3] Jones, C.A. National oceanic and atmospheric administration [noaa].

[4] Https://www.Epa.Gov/. United States Environmental Protection Agency (EPA): USA, Vol. 30/01/2017

[5] Amouroux, J.; Siffert, P.; Massué, J.P.; Cavadias, S.; Trujillo, B.; Hashimoto, K.; Rutberg, P.; Dresvin, S.; Wang, X. Carbon dioxide: A new material for energy storage. *Progress in Natural Science: Materials International* **2014**, *24*, 295-304.

[6] Nierenberg, W.A. *Carbon dioxide and climate*. NATIONAL ACADEMY PRESS, 2101 Constitution Avenue, N.W. : Washington, D.C. 20418, 1982; p 94.

[7] Riebesell, U.; Tortell, P.D. Effects of ocean acidification on pelagic organisms and ecosystems. *Ocean acidification* **2011**, 99-121.

[8] Doney, S.C.; Fabry, V.J.; Feely, R.A.; Kleypas, J.A. Ocean acidification: The other CO_2 problem. *Annual review of marine science* **2009**, *1*, 169-192.

[9] Kumar, B.; Llorente, M.; Froehlich, J.; Dang, T.; Sathrum, A.; Kubiak, C.P. Photochemical and photoelectrochemical reduction of CO_2. *Annual review of physical chemistry* **2012**, *63*, 541-569.

[10] Getoff, N. Radiation chemistry and the environment. *Radiation physics and chemistry* **1999**, *54*, 377-384.

[11] Zehnder, A.; Brock, T. Methane formation and methane oxidation by methanogenic bacteria. *Journal of Bacteriology* **1979**, *137*, 420-432.

[12] Hori, Y.; Wakebe, H.; Tsukamoto, T.; Koga, O. Electrocatalytic process of CO selectivity in electrochemical reduction of CO_2 at metal electrodes in aqueous media. *Electrochimica Acta* **1994**, *39*, 1833-1839.

[13] Lee, J.; Tak, Y. Electrocatalytic activity of cu electrode in electroreduction of CO_2. *Electrochimica acta* **2001**, *46*, 3015-3022.

[14] Begum, A.; Pickup, P.G. Electrocatalysis of CO_2 reduction by ruthenium benzothiazole and bithiazole complexes. *Electrochemistry Communications* **2007**, *9*, 2525-2528.

[15] Hori, Y. Electrochemical CO_2 reduction on metal electrodes. In *Modern aspects of electrochemistry*, Springer: 2008; pp 89-189.

[16] An, T.; Tang, J.; Zhang, Y.; Quan, Y.; Gong, X.; Al-Enizi, A.M.; Elzatahry, A.A.; Zhang, L.; Zheng, G. Photoelectrochemical conversion from graphitic C3N4 quantum dot decorated semiconductor nanowires. *ACS applied materials & interfaces* **2016**, *8*, 12772-12779.

[17] Li, K.; An, X.; Park, K.H.; Khraisheh, M.; Tang, J. A critical review of CO_2 photoconversion: Catalysts and reactors. *Catalysis Today* **2014**, *224*, 3-12.

[18] Gangeri, M.; Perathoner, S.; Caudo, S.; Centi, G.; Amadou, J.; Begin, D.; Pham-Huu, C.; Ledoux, M.J.; Tessonnier, J.-P.; Su, D.S. Fe and pt carbon nanotubes for the electrocatalytic conversion of carbon dioxide to oxygenates. *Catalysis Today* **2009**, *143*, 57-63.

[19] Shi, C.; Chan, K.; Yoo, J.S.; Nørskov, J.K. Barriers of electrochemical CO_2 reduction on transition metals. *Organic Process Research & Development* **2016**, *20*, 1424-1430.

[20] Kyriacou, G.; Anagnostopoulos, A. Influence co2 partial pressure and the supporting electrolyte cation on the product distribution in CO_2 electroreduction. *Journal of applied electrochemistry* **1993**, *23*, 483-486.

[21] Hara, K.; Kudo, A.; Sakata, T. Electrochemical reduction of carbon dioxide under high pressure on various electrodes in an aqueous electrolyte. *Journal of Electroanalytical Chemistry* **1995**, *391*, 141-147.

[22] Pérez-Cadenas, A.F.; Ros, C.H.; Morales-Torres, S.; Pérez-Cadenas, M.; Kooyman, P.J.; Moreno-Castilla, C.; Kapteijn, F. Metal-doped carbon xerogels for the electro-catalytic conversion of CO_2 to hydrocarbons. *Carbon* **2013**, *56*, 324-331.

[23] Ikeda, S.; Shiozaki, S.; Susuki, J.; Ito, K.; Noda, H. Electroreduction of CO_2 using cu/zn oxides loaded gas diffusion electrodes. *Studies in Surface Science and Catalysis* **1998**, *114*, 225-230.

[24] Kaneco, S.; Iiba, K.; Ohta, K.; Mizuno, T.; Saji, A. Electrochemical reduction of CO_2 at an ag electrode in KOH-Methanol at low temperature. *Electrochimica acta* **1998**, *44*, 573-578.

[25] Le, M.; Ren, M.; Zhang, Z.; Sprunger, P.T.; Kurtz, R.L.; Flake, J.C. Electrochemical reduction of CO_2 to CH_3OH at copper oxide surfaces. *Journal of the Electrochemical Society* **2011**, *158*, E45-E49.

[26] Zhao, H.-Z.; Chang, Y.-Y.; Liu, C. Electrodes modified with iron porphyrin and carbon nanotubes: Application to CO_2 reduction and mechanism of synergistic electrocatalysis. *Journal of Solid State Electrochemistry* **2013**, *17*, 1657-1664.

[27] Lee, Y.J.; Jung, J.C.; Park, S.; Seo, J.G.; Baeck, S.-H.; Yoon, J.R.; Yi, J.; Song, I.K. Preparation and characterization of metal-doped carbon aerogel for supercapacitor. *Current Applied Physics* **2010**, *10*, 947-951.

[28] Lee, Y.J.; Park, S.; Seo, J.G.; Yoon, J.R.; Yi, J.; Song, I.K. Nano-sized metal-doped carbon aerogel for pseudo-capacitive supercapacitor. *Current Applied Physics* **2011**, *11*, 631-635.

[29] Ulman, M.; Blajeni, B.; Halman, H. Electrochemical reduction of carbon dioxide on-at metallic cathodes. *Chemtech* **1984**, *14*, 235.

[30] Jitaru, M. Electrochemical carbon dioxide reduction-fundamental and applied topics. *Journal of the University of chemical Technology and Metallurgy* **2007**, *42*, 333-344.

[31] Qiao, J.; Liu, Y.; Hong, F.; Zhang, J. A review of catalysts for the electroreduction of carbon dioxide to produce low-carbon fuels. *Chemical Society Reviews* **2014**, *43*, 631-675.

[32] Torelli, D.A.; Francis, S.A.; Crompton, J.C.; Javier, A.; Thompson, J.R.; Brunschwig, B.S.; Soriaga, M.P.; Lewis, N.S. Nickel–gallium-catalyzed electrochemical reduction of CO_2 to highly reduced products at low overpotentials. *ACS Catalysis* **2016**, *6*, 2100-2104.

[33] Rasul, S.; Anjum, D.H.; Jedidi, A.; Minenkov, Y.; Cavallo, L.; Takanabe, K. A highly selective copper–indium bimetallic electrocatalyst for the electrochemical reduction of aqueous CO_2 to CO. *Angewandte Chemie International Edition* **2015**, *54*, 2146-2150.

[34] Shi, J.; Shi, F.; Song, N.; Liu, J.-X.; Yang, X.-K.; Jia, Y.-J.; Xiao, Z.-W.; Du, P. A novel electrolysis cell for CO_2 reduction to CO in ionic liquid/organic solvent electrolyte. *Journal of Power Sources* **2014**, *259*, 50-53.

[35] Smieja, J.M.; Sampson, M.D.; Grice, K.A.; Benson, E.E.; Froehlich, J.D.; Kubiak, C.P. Manganese as a substitute for rhenium in CO_2 reduction catalysts: The importance of acids. *Inorganic chemistry* **2013**, *52*, 2484-2491.

[36] Prakash, G.S.; Viva, F.A.; Olah, G.A. Electrochemical reduction of CO_2 over Sn-nafion® coated electrode for a fuel-cell-like device. *Journal of Power Sources* **2013**, *223*, 68-73.

[37] Costentin, C.; Drouet, S.; Robert, M.; Savéant, J.-M. A local proton source enhances CO_2 electroreduction to co by a molecular fe catalyst. *Science* **2012**, *338*, 90-94.

[38] Wu, J.; Risalvato, F.G.; Ke, F.-S.; Pellechia, P.; Zhou, X.-D. Electrochemical reduction of carbon dioxide i. Effects of the electrolyte on the selectivity and activity with Sn electrode. *Journal of The Electrochemical Society* **2012**, *159*, F353-F359.

[39] Bourrez, M.; Molton, F.; Chardon-Noblat, S.; Deronzier, A. [Mn (bipyridyl)(co) 3br]: An abundant metal carbonyl complex as efficient electrocatalyst for co2 reduction. *Angewandte Chemie* **2011**, *123*, 10077-10080.

[40] Barton, E.E.; Rampulla, D.M.; Bocarsly, A.B. Selective solar-driven reduction of CO_2 to methanol using a catalyzed p-gap based photoelectrochemical cell. *Journal of the American Chemical Society* **2008**, *130*, 6342-6344.

[41] Reda, T.; Plugge, C.M.; Abram, N.J.; Hirst, J. Reversible interconversion of carbon dioxide and formate by an electroactive enzyme. *Proceedings of the National Academy of Sciences* **2008**, *105*, 10654-10658.

[42] Li, H.; Oloman, C. Development of a continuous reactor for the electro-reduction of carbon dioxide to formate–part 2: Scale-up. *Journal of Applied Electrochemistry* **2007**, *37*, 1107-1117.

[43] Gattrell, M.; Gupta, N.; Co, A. A review of the aqueous electrochemical reduction of CO_2 to hydrocarbons at copper. *Journal of Electroanalytical Chemistry* **2006**, *594*, 1-19.

[44] Li, H.; Oloman, C. Development of a continuous reactor for the electro-reduction of carbon dioxide to formate–part 1: Process variables. *Journal of Applied Electrochemistry* **2006**, *36*, 1105-1115.

[45] Hori, Y.; Konishi, H.; Futamura, T.; Murata, A.; Koga, O.; Sakurai, H.; Oguma, K. "Deactivation of copper electrode" in electrochemical reduction of CO_2. *Electrochimica acta* **2005**, *50*, 5354-5369.

[46] Dubé, P.; Brisard, G. Influence of adsorption processes on the CO_2 electroreduction: An electrochemical mass spectrometry study. *Journal of Electroanalytical Chemistry* **2005**, *582*, 230-240.

[47] Jitaru, M.; Lowy, D.; Toma, M.; Toma, B.; Oniciu, L. Electrochemical reduction of carbon dioxide on flat metallic cathodes. *Journal of Applied Electrochemistry* **1997**, *27*, 875-889.

[48] Aydin, R.; Köleli, F. Electrocatalytic conversion of CO_2 on a polypyrrole electrode under high pressure in methanol. *Synthetic metals* **2004**, *144*, 75-80.

[49] Rios-Escudero, A.; Isaacs, M.; Villagrán, M.; Zagal, J.; Costamagna, J. In *Electrochemical reduction of carbon dioxide in the presence of [niii-5, 7, 12, 14-tetramethyldinaphtho [b, i][1, 4, 8, 11] tetra aza [14] annulene]++ cation*, Anales de la Asociación Química Argentina, 2004; SciELO Argentina: pp 63-71.

[50] Köleli, F.; Balun, D. Reduction of CO_2 under high pressure and high temperature on pb-granule electrodes in a fixed-bed reactor in aqueous medium. *Applied Catalysis A: General* **2004**, *274*, 237-242.

[51] Yano, H.; Tanaka, T.; Nakayama, M.; Ogura, K. Selective electrochemical reduction of CO_2 to ethylene at a three-phase interface on copper (i) halide-confined cu-mesh electrodes in acidic solutions of potassium halides. *Journal of Electroanalytical Chemistry* **2004**, *565*, 287-293.

[52] Isaacs, M.; Canales, J.C.; Riquelme, A.; Lucero, M.; Aguirre, M.J.; Costamagna, J. Contribution of the ligand to the electroreduction of CO_2

catalyzed by a cobalt (ii) macrocyclic complex. *J. Coord. Chem.* **2003**, *56*, 1193-1201.

[53] Köleli, F.; Röpke, T.; Hamann, C.H. Electrochemical impedance spectroscopic investigation of co 2 reduction on polyaniline in methanol. *Electrochimica acta* **2003**, *48*, 1595-1601.

[54] Aydin, R.; Köleli, F. Electrochemical reduction of CO_2 on a polyaniline electrode under ambient conditions and at high pressure in methanol. *Journal of Electroanalytical Chemistry* **2002**, *535*, 107-112.

[55] Kaneco, S.; Hiei, N.-h.; Xing, Y.; Katsumata, H.; Ohnishi, H.; Suzuki, T.; Ohta, K. Electrochemical conversion of carbon dioxide to methane in aqueous nahco 3 solution at less than 273 k. *Electrochimica Acta* **2002**, *48*, 51-55.

[56] Magdesieva, T.; Zhukov, I.; Kravchuk, D.; Semenikhin, O.; Tomilova, L.; Butin, K. Electrocatalytic CO_2 reduction in methanol catalyzed by mono-, di-, and electropolymerized phthalocyanine complexes. *Russian chemical bulletin* **2002**, *51*, 805-812.

[57] Schrebler, R.; Cury, P.; Suarez, C.; Munoz, E.; Gomez, H.; Cordova, R. Study of the electrochemical reduction of CO_2 on a polypyrrole electrode modified by rhenium and copper–rhenium microalloy in methanol media. *Journal of Electroanalytical Chemistry* **2002**, *533*, 167-175.

[58] Ohmori, T.; Nakayama, A.; Mametsuka, H.; Suzuki, E. Influence of sputtering parameters on electrochemical CO_2 reduction in sputtered au electrode. *Journal of Electroanalytical Chemistry* **2001**, *514*, 51-55.

[59] Schrebler, R.; Cury, P.; Herrera, F.; Gomez, H.; Cordova, R. Study of the electrochemical reduction of CO_2 on electrodeposited rhenium electrodes in methanol media. *Journal of Electroanalytical Chemistry* **2001**, *516*, 23-30.

[60] Brisard, G.; Camargo, A.; Nart, F.; Iwasita, T. On-line mass spectrometry investigation of the reduction of carbon dioxide in acidic media on polycrystalline pt. *Electrochemistry communications* **2001**, *3*, 603-607.

[61] Kaneco, S.; Iiba, K.; Ohta, K.; Mizuno, T. Electrochemical reduction of carbon dioxide on copper in methanol with various potassium supporting electrolytes at low temperature. *Journal of Solid State Electrochemistry* **1999**, *3*, 424-428.

[62] Hirota, K.; Tryk, D.; Hashimoto, K.; Okawa, M.; Fujishima, A. Photoelectrochemical reduction of highly concentrated CO_2 in methanol solution. *Studies in Surface Science and Catalysis* **1998**, *114*, 589-592.

[63] Ikeda, S.; Takagi, T.; Ito, K. Selective formation of formic acid, oxalic acid, and carbon monoxide by electrochemical reduction of carbon dioxide. *Bulletin of the Chemical Society of Japan* **1987**, *60*, 2517-2522.

[64] Kaneco, S.; Iwao, R.; Iiba, K.; Ohta, K.; Mizuno, T. Electrochemical conversion of carbon dioxide to formic acid on pb in KOH/Methanol electrolyte at ambient temperature and pressure. *Energy* **1998**, *23*, 1107-1112.

[65] Conway, B.E. *Electrochemical supercapacitors scientific fundamentals and technological applications*. Kluwer Academic/ Plenum Publishers: New York, 1999; p 366.

[66] Kang, K.Y.; Hong, S.J.; Lee, B.I.; Lee, J.S. Enhanced electrochemical capacitance of nitrogen-doped carbon gels synthesized by microwave-assisted polymerization of resorcinol and formaldehyde. *Electrochemistry Communications* **2008**, *10*, 1105-1108.

[67] Frackowiak, E.; Beguin, F. Carbon materials for the electrochemical storage of energy in capacitors. *Carbon* **2001**, *39*, 937-950.

[68] Wu, X.-L.; Xu, A.-W. Carbonaceous hydrogels and aerogels for supercapacitors. *Journal of Materials Chemistry A* **2014**, *2*, 4852-4864.

[69] Wang, G.; Zhang, L.; Zhang, J. A review of electrode materials for electrochemical supercapacitors. *Chemical Society Reviews* **2012**, *41*, 797-828.

[70] Zhao, Q.; Wang, X.; Wu, C.; Liu, J.; Wang, H.; Gao, J.; Zhang, Y.; Shu, H. Supercapacitive performance of hierarchical porous carbon microspheres prepared by simple one-pot method. *Journal of Power Sources* **2014**, *254*, 10-17.

[71] Qu, D. Studies of the activated carbons used in double-layer supercapacitors. *Journal of power sources* **2002**, *109*, 403-411.

[72] Balducci, A.; Bardi, U.; Caporali, S.; Mastragostino, M.; Soavi, F. Ionic liquids for hybrid supercapacitors. *Electrochemistry communications* **2004**, *6*, 566-570.

[73] Sato, T.; Masuda, G.; Takagi, K. Electrochemical properties of novel ionic liquids for electric double layer capacitor applications. *Electrochimica Acta* **2004**, *49*, 3603-3611.

[74] Ma, J.; Guo, Q.; Gao, H.-L.; Qin, X. Synthesis of c60/graphene composite as electrode in supercapacitors. *Fullerenes, Nanotubes and Carbon Nanostructures* **2015**, *23*, 477-482.

[75] Zapata-Benabithe, Z.; Carrasco-Marín, F.; de Vicente, J.; Moreno-Castilla, C. Carbon xerogel microspheres and monoliths from resorcinol–

formaldehyde mixtures with varying dilution ratios: Preparation, surface characteristics, and electrochemical double-layer capacitances. *Langmuir* **2013**, *29*, 6166-6173.

[76] Moreno-Castilla, C.; Maldonado-Hódar, F. Carbon aerogels for catalysis applications: An overview. *Carbon* **2005**, *43*, 455-465.

[77] Pérez-Cadenas, M.a.; Moreno-Castilla, C.; Carrasco-Marín, F.; Pérez-Cadenas, A.n.F. Surface chemistry, porous texture, and morphology of n-doped carbon xerogels. *Langmuir* **2008**, *25*, 466-470.

[78] Steiner, S.A.; Baumann, T.F.; Kong, J.; Satcher, J.H.; Dresselhaus, M.S. Iron-doped carbon aerogels: Novel porous substrates for direct growth of carbon nanotubes. *Langmuir* **2007**, *23*, 5161-5166.

[79] Decaux, C.; Ghimbeu, C.M.; Dahbi, M.; Anouti, M.; Lemordant, D.; Béguin, F.; Vix-Guterl, C.; Raymundo-Pinero, E. Influence of electrolyte ion–solvent interactions on the performances of supercapacitors porous carbon electrodes. *Journal of Power Sources* **2014**, *263*, 130-140.

[80] Simon, P.; Gogotsi, Y. Materials for electrochemical capacitors. *Nature materials* **2008**, *7*, 845-854.

[81] Carrette, L.; Friedrich, K.A.; Stimming, U. Fuel cells: Principles, types, fuels, and applications. *ChemPhysChem* **2000**, *1*, 162-193.

[82] Hoogers, G. *Fuel cell technology handbook*. CRC Press: 2003; p P. 4-23.

[83] Bregoli, L. The influence of platinum crystallite size on the electrochemical reduction of oxygen in phosphoric acid. *Electrochimica Acta* **1978**, *23*, 489-492.

[84] Sattler, M.; Ross, P. The surface structure of pt crystallites supported on carbon black. *Ultramicroscopy* **1986**, *20*, 21-28.

[85] Takasu, Y.; Ohashi, N.; Zhang, X.-G.; Murakami, Y.; Minagawa, H.; Sato, S.; Yahikozawa, K. Size effects of platinum particles on the electroreduction of oxygen. *Electrochimica Acta* **1996**, *41*, 2595-2600.

[86] Paulus, U.; Wokaun, A.; Scherer, G.; Schmidt, T.; Stamenkovic, V.; Radmilovic, V.; Markovic, N.; Ross, P. Oxygen reduction on carbon-supported Pt-Ni and Pt-Co alloy catalysts. *The Journal of Physical Chemistry B* **2002**, *106*, 4181-4191.

[87] Jayasayee, K.; Van Veen, J.R.; Manivasagam, T.G.; Celebi, S.; Hensen, E.J.; De Bruijn, F.A. Oxygen reduction reaction (ORR) activity and durability of carbon supported PtM (Co, Ni, Cu) alloys: Influence of particle size and non-noble metals. *Applied Catalysis B: Environmental* **2012**, *111*, 515-526.

[88] Wang, Y.-J.; Zhao, N.; Fang, B.; Li, H.; Bi, X.T.; Wang, H. Carbon-supported pt-based alloy electrocatalysts for the oxygen reduction reaction in polymer electrolyte membrane fuel cells: Particle size, shape, and composition manipulation and their impact to activity. *Chemical reviews* **2015**, *115*, 3433-3467.

[89] Daems, N.; Sheng, X.; Vankelecom, I.F.; Pescarmona, P.P. Metal-free doped carbon materials as electrocatalysts for the oxygen reduction reaction. *Journal of Materials Chemistry A* **2014**, *2*, 4085-4110.

[90] Shin, D.; An, X.; Choun, M.; Lee, J. Effect of transition metal induced pore structure on oxygen reduction reaction of electrospun fibrous carbon. *Catalysis Today* **2016**, *260*, 82-88.

[91] Yu, H.; Fisher, A.; Cheng, D.; Cao, D. Cu,n-codoped hierarchical porous carbons as electrocatalysts for oxygen reduction reaction. *ACS Applied Materials and Interfaces* **2016**, *8*, 21431-21439.

[92] Liang, Y.; Li, Y.; Wang, H.; Zhou, J.; Wang, J.; Regier, T.; Dai, H. Co_3O_4 nanocrystals on graphene as a synergistic catalyst for oxygen reduction reaction. *Nature materials* **2011**, *10*, 780-786.

[93] Zhang, G.; Xia, B.Y.; Wang, X. Strongly coupled $NiCo_2O_4$-rGO hybrid nanosheets as a methanol-tolerant electrocatalyst for the oxygen reduction reaction. *Advanced Materials* **2014**, *26*, 2408-2412.

[94] Liu, Y.; Jiang, H.; Zhu, Y.; Yang, X.; Li, C. Transition metals (Fe, Co, and Ni) encapsulated in nitrogen-doped carbon nanotubes as bi-functional catalysts for oxygen electrode reactions. *Journal of Materials Chemistry A* **2016**, *4*, 1694-1701.

[95] Shao, M.; Chang, Q.; Dodelet, J.-P.; Chenitz, R. Recent advances in electrocatalysts for oxygen reduction reaction. *Chemical reviews* **2016**, *116*, 3594-3657.

[96] Yu, D.; Nagelli, E.; Du, F.; Dai, L. Metal-free carbon nanomaterials become more active than metal catalysts and last longer. *The journal of physical chemistry letters* **2010**, *1*, 2165-2173.

[97] Moreno-Castilla, C. *Carbon materials for catalysis*. WILEY: 2009; p 590.

[98] Pekala, R.; Farmer, J.; Alviso, C.; Tran, T.; Mayer, S.; Miller, J.; Dunn, B. Carbon aerogels for electrochemical applications. *Journal of non-crystalline solids* **1998**, *225*, 74-80.

[99] Pekala, R.; Alviso, C.; Kong, F.; Hulsey, S. Aerogels derived from multifunctional organic monomers. *Journal of Non-Crystalline Solids* **1992**, *145*, 90-98.

[100] Morales-Torres, S.; Maldonado-Hódar, F.J.; Pérez-Cadenas, A.F.; Carrasco-Marín, F. Textural and mechanical characteristics of carbon aerogels synthesized by polymerization of resorcinol and formaldehyde using alkali carbonates as basification agents. *Physical Chemistry Chemical Physics* **2010**, *12*, 10365-10372.

[101] ElKhatat, A.M.; Al-Muhtaseb, S.A. Advances in tailoring resorcinol-formaldehyde organic and carbon gels. *Advanced materials* **2011**, *23*, 2887-2903.

[102] Gallegos-Suárez, E.; Pérez-Cadenas, A.F.; Maldonado-Hódar, F.J.; Carrasco-Marín, F. On the micro-and mesoporosity of carbon aerogels and xerogels. The role of the drying conditions during the synthesis processes. *Chemical Engineering Journal* **2012**, *181*, 851-855.

[103] Maldonado-Hódar, F.J.; Jirglova, H.; Pérez-Cadenas, A.F.; Morales-Torres, S. Chemical control of the characteristics of mo-doped carbon xerogels by surfactant-mediated synthesis. *Carbon* **2013**, *51*, 213-223.

[104] Maldonado-Hódar, F.J.; Moreno-Castilla, C.; Carrasco-Marín, F.; Pérez-Cadenas, A.F. Reversible toluene adsorption on monolithic carbon aerogels. *Journal of hazardous materials* **2007**, *148*, 548-552.

[105] Vivo-Vilches, J.; Carrasco-Marín, F.; Pérez-Cadenas, A.; Maldonado-Hódar, F. Fitting the porosity of carbon xerogel by CO_2 activation to improve the tmp/n-octane separation. *Microporous and Mesoporous Materials* **2015**, *209*, 10-17.

[106] Bailon-Garcia, E.; Carrasco-Marin, F.; Perez-Cadenas, A.; Maldonado-Hodar, F. Microspheres of carbon xerogel: An alternative pt-support for the selective hydrogenation of citral. *Applied Catalysis A: General* **2014**, *482*, 318-326.

[107] Bailón-García, E.; Elmouwahidi, A.; Álvarez, M.A.; Carrasco-Marín, F.; Pérez-Cadenas, A.F.; Maldonado-Hódar, F.J. New carbon xerogel-TiO_2 composites with high performance as visible-light photocatalysts for dye mineralization. *Applied Catalysis B: Environmental* **2017**, *201*, 29-40.

[108] Maldonado-Hódar, F.; Moreno-Castilla, C.; Pérez-Cadenas, A. Catalytic combustion of toluene on platinum-containing monolithic carbon aerogels. *Applied Catalysis B: Environmental* **2004**, *54*, 217-224.

[109] Duarte, F.; Maldonado-Hódar, F.; Pérez-Cadenas, A.; Madeira, L.M. Fenton-like degradation of azo-dye orange ii catalyzed by transition metals on carbon aerogels. *Applied Catalysis B: Environmental* **2009**, *85*, 139-147.

[110] Moreno-Castilla, C.; Dawidziuk, M.B.; Carrasco-Marín, F.; Morallon, E. Electrochemical performance of carbon gels with variable surface chemistry and physics. *Carbon* **2012**, *50*, 3324-3332.
[111] Maldonado-Hódar, F.; Pérez-Cadenas, A.; Moreno-Castilla, C. Morphology of heat-treated tunsgten doped monolithic carbon aerogels. *Carbon* **2003**, *41*, 1291-1299.
[112] Moreno-Castilla, C.; Maldonado-Hódar, F.; Pérez-Cadenas, A. Physicochemical surface properties of Fe, Co, Ni, and Cu-doped monolithic organic aerogels. *Langmuir* **2003**, *19*, 5650-5655.
[113] Maldonado-Hódar, F.; Moreno-Castilla, C.; Pérez-Cadenas, A. Surface morphology, metal dispersion, and pore texture of transition metal-doped monolithic carbon aerogels and steam-activated derivatives. *Microporous and mesoporous materials* **2004**, *69*, 119-125.
[114] Pérez-Cadenas, A.; Maldonado-Hódar, F.; Moreno-Castilla, C. Molybdenum carbide formation in molybdenum-doped organic and carbon aerogels. *Langmuir* **2005**, *21*, 10850-10855.
[115] Moreno-Castilla, C.; Maldonado-Hódar, F.J.; Rivera-Utrilla, J.; Rodríguez-Castellón, E. Group 6 metal oxide-carbon aerogels. Their synthesis, characterization and catalytic activity in the skeletal isomerization of 1-butene. *Applied Catalysis A: General* **1999**, *183*, 345-356.
[116] Bailón-García, E.; Carrasco-Marín, F.; Pérez-Cadenas, A.F.; Maldonado-Hódar, F.J. Development of carbon xerogels as alternative Pt-supports for the selective hydrogenation of citral. *Catalysis Communications* **2015**, *58*, 64-69.
[117] Job, N.; Théry, A.; Pirard, R.; Marien, J.; Kocon, L.; Rouzaud, J.-N.; Béguin, F.; Pirard, J.-P. Carbon aerogels, cryogels and xerogels: Influence of the drying method on the textural properties of porous carbon materials. *Carbon* **2005**, *43*, 2481-2494.
[118] Maldonado-Hódar, F.; Ferro-Garcıa, M.; Rivera-Utrilla, J.; Moreno-Castilla, C. Synthesis and textural characteristics of organic aerogels, transition-metal-containing organic aerogels and their carbonized derivatives. *Carbon* **1999**, *37*, 1199-1205.
[119] Zubizarreta, L.; Arenillas, A.; Domínguez, A.; Menéndez, J.; Pis, J. Development of microporous carbon xerogels by controlling synthesis conditions. *Journal of Non-Crystalline Solids* **2008**, *354*, 817-825.
[120] Moreno, A.; Arenillas, A.; Calvo, E.; Bermúdez, J.; Menéndez, J. Carbonisation of resorcinol–formaldehyde organic xerogels: Effect of

temperature, particle size and heating rate on the porosity of carbon xerogels. *Journal of Analytical and Applied Pyrolysis* **2013**, *100*, 111-116.

[121] Bozbag, S.; Zhang, L.; Aindow, M.; Erkey, C. Carbon aerogel supported nickel nanoparticles and nanorods using supercritical deposition. *The Journal of Supercritical Fluids* **2012**, *66*, 265-273.

[122] Chaichanawong, J.; Kongcharoen, K.; Areerat, S. Preparation of carbon aerogel microspheres by a simple-injection emulsification method. *Advanced Powder Technology* **2013**, *24*, 891-896.

[123] Fort, C.I.; Cotet, L.C.; Danciu, V.; Turdean, G.L.; Popescu, I.C. Iron doped carbon aerogel–new electrode material for electrocatalytic reduction of H_2O_2. *Materials Chemistry and Physics* **2013**, *138*, 893-898.

[124] Maldonado-Hodar, F.; Moreno-Castilla, C.; Rivera-Utrilla, J.; Hanzawa, Y.; Yamada, Y. Catalytic graphitization of carbon aerogels by transition metals. *Langmuir* **2000**, *16*, 4367-4373.

[125] Al-Muhtaseb, S.A.; Ritter, J.A. Preparation and properties of resorcinol–formaldehyde organic and carbon gels. *Advanced Materials* **2003**, *15*, 101-114.

[126] Espinosa-Iglesias, D.; Valverde-Sarmiento, C.; Pérez-Cadenas, A.F.; Bautista-Toledo, M.I.; Maldonado-Hódar, F.J.; Carrasco-Marín, F. Mesoporous carbon-xerogels films obtained by microwave assisted carbonization. *Materials Letters* **2015**, *141*, 135-137.

CHAPTER II: SYNTHESIS OF THE MATERIALS AND CHARACTERIZATION TECHNIQUES

2.1.- SYNTHESIS OF THE CARBON MATERIALS DOPED WITH COBALT, IRON AND NICKEL

Metal-doped carbon gels were prepared by dissolving resorcinol (R) and formaldehyde (F) in water (W) and using the corresponding metal acetate as a catalyst precursor (C). The used (R/F) and molar ratio (R/W) were 1:2 and 1:17, respectively. Different amounts of C were used in order to obtain three different Co loadings (1, 4, and 6 wt %, approx.) among the final carbon aerogels and xerogels. The mixture was stirred to obtain homogeneous solutions that were cast into glass molds and cured for one day at 40 °C, and for five days at 80 °C, obtaining the corresponding organic gels. Then, the organic gels were immersed in acetone to exchange the solvent media [1]. Two different drying processes, supercritical CO_2 or thermal oven, were carried out in order to obtain the aerogel (A) or xerogel (X) series, respectively. Finally, the organic gels were carbonized in a N_2 flow at 900 °C during 5 h, and using a heating rate of 1 °C/min. The names of the obtained carbon gels were the following: ACo1, ACo4, ACo6, XCo1, XCo4, XCo6, ANi1, ANi4, ANi6, AFe1, AFe6, XFe1 and XFe6 indicating the numbers the approximate percentage of metal content.

On the other hand, a second type carbon xerogel, hereafter as XFe6b, was obtained avoiding the exchange with acetone before the thermal drying. An additional material was prepared by heating sample XFe6b at 700 ºC in H_2 flow during 1 h, and after that, the H_2 flow was changed *in situ* by a mixture of $He:C_2H_4:H_2$ with a volumetric ratio of 90:10:20, respectively, keeping the same

temperature during 2 h. In these conditions, carbon nanofibers (CNFs) grew on the carbon xerogel matrix forming therefore a carbon xerogel-CNF composite, labelled as XFe6bNF. A 50 - 50 wt.% carbon xerogels – CNF composition was estimated by weighting the materials after the different steps, including only after the H_2 pre-treatment; in this last case, obviously a specific portion of sample was used only for this weight calculation.

The iron contents of the electro-catalysts were determined by burning off a portion of the sample at 800 ºC in air and weighting the residue.

2.2.- CHARACTERIZATION TECHNIQUES

2.2.1.- Adsorption of gases

The porous texture was analyzed by N_2 adsorption at -196 °C. In some cases the CO_2 adsorption at 0°C was used as well. Prior to measuring the adsorption isotherms, the samples were outgassed overnight at 110 ºC under high vacuum (10^{-6} mbar). The BET equation was applied to the N_2 adsorption data from which the apparent surface area, S_{BET}, was obtained. The Dubinin-Radushkevich equation was applied to the N_2 and CO_2 adsorption data in order to obtain the corresponding micropore volume (W_0) and micropore mean width (L_0). Total pore volumes ($V_{0.95}$) were calculated from N_2 adsorption isotherms at -196°C and at 0.95 relative pressures. The BJH method [2] was applied to the desorption branch of the N_2 adsorption isotherms to obtain the pore size distribution (PSD) curves and mesopore volume (V_{BJH}). Mesopore volumes (V_{MESO}) were calculated by difference between $V_{0.95}$ and W_0. S_{DFT} is the

cumulative surface area obtained from the pore size distribution determined applying the quenched solid state functional theory (QSDFT) method for slit-shaped pores [3].

2.2.2.- Mercury porosimetry

Mercury porosimetry was obtained up to a pressure of 2320 kg/cm^2 using Quantachrome Instruments equipment model POREMASTER 33. Macropore volumes (V_{MACRO}) and the pore size distributions from 6.5 nm were obtained with this technique. Prior to the analysis the samples were outgassed.

2.2.3.- Scanning electron microscopy

Scanning electron microscopy (SEM) was performed using a Zeiss SUPRA40VP microscope, equipped with secondary electron detector, back-scatter electron detector, and using an X-Max 50 mm energy dispersive X-ray microanalysis system. All of the samples were crushed before realizing this analysis.

2.2.4.- Transmission electron microscope

High resolution transmission electron microscopy (HRTEM) was carried out using a FEI Titan G2 60-300 microscope with a high-brightness electron gun (X-FEG) operated at 300 kV and equipped with a Cs image corrector (CEOS) and, for analytical electron microscopy (AEM), a SUPER-X silicon-drift window-less EDX detector. The AEM spectra were collected in scanning transmission electron microscopy mode (STEM) using a high angle annular dark field

(HAADF) detector. Digital X-ray maps were also collected on selected areas of the samples.

2.2.5.- Raman spectroscopy

Raman spectra were obtained using a Micro-Raman JASCO NRS-5100 dispersive spectrometer with a 532 nm laser line.

2.2.6.- X-ray diffraction

X-ray diffraction (XRD) patterns were recorded with BRUKER D8 ADVANCE diffractometer using Cu Kα radiation (BRUKER, Rivas-Vaciamadrid, Spain). JCPDS files were searched to assign the different diffraction lines observed. Diffraction patterns were recorded between 5° and 70° (2θ) with a step of 0.02° and a time per step of 96 s. The average crystal size was determined using the Scherrer equation.

2.2.7.- X-ray photoelectron spectroscopy

X-ray photoelectron spectroscopy (XPS) measurements of the fresh samples were performed using a Physical Electronics ESCA 5701 (PHI, Chanhassen, MN, USA) equipped with a Mg Kα X-ray source (hν = 1253.6 eV) operating at 12 kV and 10 mA, and a hemispherical electron analyzer. For these measurements, the binding energy (BE) values were referred to the C 1s peak at 284.7 eV. A base pressure of 10^{-9} mbar was maintained during data acquisition. Survey and multi-region spectra were recorded at C 1s, O 1s, Co 2p, Fe 2p and Ni 2p photoelectron peaks. Each spectral region of interest was scanned several times to obtain good signal-to-noise ratios. The spectra obtained after background signal

correction were fitted to Lorentzian and Gaussian curves in order to obtain the number of components, the position of each peak and the peak areas. For XPS analysis of the samples used in reaction, the procedure was the following: once the reaction was finished, the sample was dried under He flow, impregnated with n-octane, and then transferred to the pre-treatment chamber of the XPS instrument. Prior to the XPS analysis the samples were evacuated at high vacuum and room temperature, and then introduced into the analysis chamber. A base pressure of 10^{-9} mbar was maintained during data acquisition.

2.2.8.- Electro-chemical studies

Linear sweep voltammetry (LSV), cyclic voltammetry (CV), galvanostatic charge–discharge tests, electrochemical impedance spectroscopy (EIS) and floating test have been carried out in different experimental conditions depending on the studied application, and for this reason, their experimental details are described in each Chapter. Experimental reaction conditions for the CO_2 reduction reaction and oxygen reduction reaction also are described in the corresponding Chapter.

BIBLIOGRAPHY

[1] Gallegos-Suarez E.; Perez-Cadenas, A.F.; Maldonado-Hodar, F.J.; Carrasco-Marin, F. On the micro- and mesoporosity of carbon aerogels and xerogels. The role of the drying conditions during the synthesis processes. *Chem. Eng. J.* **2012**, *181-182*, 851-855.

[2] Barrett E.P.; Joyner, L.G.; Halenda, P.P. The Determination of Pore Volume and Area Distributions in Porous Substances. I. Computations from Nitrogen Isotherms. *J. Am. Chem. Soc.* **1951**, *73*, 373-380.

[3] Neimark A.V.; Lin, Y.; Ravikovitch, P.I.; Thommes, M. Quenched solid density functional theory and pore size analysis of micro-mesoporous carbons. *Carbon* **2009**, *47*, 1617-1628.

CHAPTER III: COBALT-DOPED CARBON GELS AS ELECTRO-CATALYSTS FOR THE REDUCTION OF CO_2 TO HYDROCARBONS

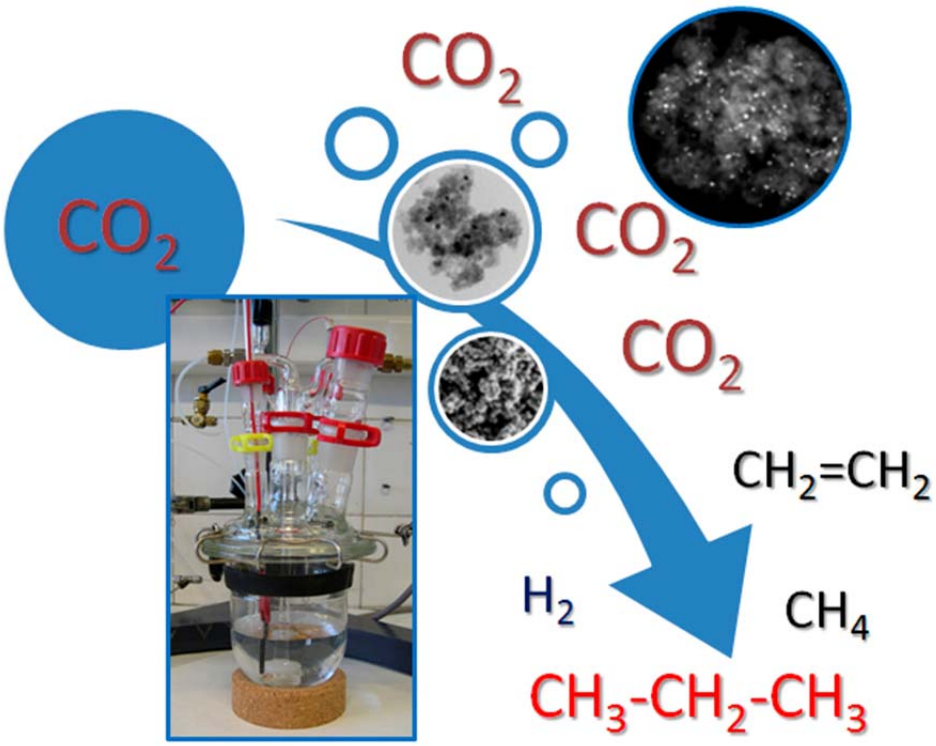

catalysts

MDPI

doi:10.3390/catal7010025

Cobalt-Doped Carbon Gels as Electro-Catalysts for the Reduction of CO_2 to Hydrocarbons

Abdalla Abdelwahab [1,†], Jesica Castelo-Quibén [1], María Pérez-Cadenas [2], Abdelhakim Elmouwahidi [1], Francisco J. Maldonado-Hódar [1], Francisco Carrasco-Marín [1] and Agustín F. Pérez-Cadenas [1,*]

[1] Carbon Materials Research Group, Department of Inorganic Chemistry, Faculty of Sciences, University of Granada. Campus Fuentenueva s/n, Granada 18071, Spain; aabdelwahab@ugr.es (A.A.); jesicacastelo@ugr.es (J.C.-Q.); aelmouwahidi@ugr.es (A.E.); fjmaldon@ugr.es (F.J.M.-H.); fmarin@ugr.es (F.C.-M.)

[2] Department of Inorganic and Technical Chemistry, Science Faculty, UNED, Paseo Senda del Rey 9, Madrid ES28040, Spain; mariaperez@ccia.uned.es

* Correspondence: afperez@ugr.es; Tel.: +34-958-243-316

† Present address: Materials Science and Nanotechnology Department, Faculty of Postgraduate Studies for Advanced Sciences, Beni-Suef University, Beni-Suef 62511, Egypt

Academic Editors: Damien P. Debecker and Keith Hohn
Received: 26 October 2016; Accepted: 5 January 2017; Published: date

Abstract: Two original series of carbon gels doped with different cobalt loadings and well-developed mesoporosity, aerogels and xerogels, have been prepared, exhaustively characterized, and tested as cathodes for the electro-catalytic reduction of CO_2 to hydrocarbons at atmospheric pressure. Commercial cobalt and graphite sheets have also been tested as cathodes for comparison. All of the doped carbon gels catalyzed the formation of hydrocarbons, at least from type C1 to C4. The catalytic activity depends mainly on the metal loading, nevertheless, the adsorption of a part of the products in the porous structure of the carbon gel cannot be ruled out. Apparent faradaic efficiencies calculated with these developed materials were better that those obtained with a commercial cobalt sheet as a cathode, especially considering the much lower amount of cobalt contained in the Co-doped carbon gels. The cobalt-carbon phases formed in these types of doped carbon gels improve the selectivity to C3-C4 hydrocarbons formation, obtaining even more C3 hydrocarbons than CH_4 in some cases.

Keywords: carbon aerogels; carbon xerogels; cobalt; carbon dioxide; electro-catalysis

1. Introduction

The continuous increase of the CO_2 atmospheric concentration is thought to be one of the main causes of global climate change [1]. In particular, CO_2 emission from the use of fossil fuels contributes to the increasing concentration, because it constitutes a continuous net increase in the natural cycle of tropospheric carbon.

Different strategies of CO_2 reduction to valuable compounds are being studied, like catalytic reduction [2], photo-catalytic reduction [3–5], and electro-catalytic reduction [6].

Renewable energy sources such as solar, wind and tidal electricity are also receiving a lot of attention, but they do not produce the constant and tunable currents that fossil fuels provide. Storage of surplus electrical energy produced during peak production periods and its release during peak demand periods is, thus, crucial, especially as peak production and peak demand periods often do not coincide. In this line, the electro-catalytic reduction of CO_2 to hydrocarbons can be an alternative strategy to address the problem of storing temporary and local surpluses of renewable energy [6,7]. In a one-pot process, water is split to provide the required hydrogen atoms/ions which are reacted with CO_2 to form hydrocarbons that can be used directly in the existing infrastructure for transportation fuels. Next to storing the renewable energy, some CO_2 is removed from the atmosphere. O_2 is formed simultaneously, which can be used to burn the hydrocarbons to release the energy whenever required. For this process sheet metal electrodes have mainly been investigated [8–10].

The direct electrochemical reduction of CO_2 in aqueous solution has been studied mainly on metal electrodes in the form of plates, both at atmospheric pressure and at higher pressures [9,11]. So far, copper electrodes have been shown to be quite unique in the activation of CO_2 to hydrocarbons, although the faradaic efficiency is still low as a result of the dissociation of H_2O to H_2. Several studies have been concerned with elucidating the mechanism of electro-reduction of CO_2 to hydrocarbons, which seem to point to a Fischer–Tropsch mechanism of chain propagation [12,13].

Cobalt catalysts supported on carbon for CO_2 electro-reduction have not been studied yet in depth, although recently some studies are appearing in the bibliography focusing mainly in cobalt oxidized phases [14,15] or coordination complexes [16]; however, none of these works reported the formation of C3-C4 hydrocarbons.

On the other hand, some types of carbon materials have been used in electro-catalytic CO_2 reduction as support of platinum catalysts, as carbon nanotubes, carbon cloth, or carbon black [17,18], obtaining a wide distribution of products of up to nine carbon atoms.

Carbon gels, xerogels, and aerogels are nanostructured materials obtained from the carbonization of organic gels, which are prepared by the sol–gel polycondensation of certain organic monomers, typically resorcinol (R) and formaldehyde (F) [19,20]. The

textural characteristics of these materials strongly depend on a careful control of the reactant concentrations and the experimental conditions of the different synthesis steps: gelation, curing, drying and carbonization/activation [21,22]. For this reason, the surface area, pore volume, and pore size distribution are tunable properties related to the synthesis and processing conditions, enabling the preparation of a wide spectrum of materials with unique properties, e.g., for adsorption and catalytic and electrochemical applications [23–28]. Moreover, carbon gels doped with transition metals show a high metal dispersion and a very good distribution of the metals throughout the carbon matrix [29–31]. The majority of metal cations will be embedded into the structure of the carbon gel, which minimizes the leaching of the metals in liquid phase applications. In this respect, these materials may have advantages over those catalysts or electro-catalysts prepared by impregnation of the corresponding metallic phase. Nevertheless, a percentage of the metal phase of the doped carbon gels will not be accessible to the reactants, although preparation techniques are available that minimize this aspect [32].

Recently [33,34], Fe-, Cu-, and Ni-doped carbon xerogels, prepared in film form, have been used as working electrodes in the electro-catalytic reduction of CO_2 to hydrocarbons. The use of these doped xerogels as cathodes, instead of the traditional metallic planar-type, reduced the amount of metal required for a similar hydrocarbon production. Although all doped xerogels formed mainly CH_4, the selectivity varied depending on the doping metal.

As far as we know, these types of cobalt-doped carbon materials have never been used as electro-catalysts in the reduction of CO_2 to hydrocarbons. Therefore, in the present work we show the application of cobalt-doped carbon gels as promising electro-catalysts in the reduction of CO_2 to hydrocarbons. The effect on the activity and selectivity in the reduction of CO_2 to hydrocarbons of the different cobalt contents, porosity, and chemical nature of the cobalt-carbon phases of these electro-catalysts, is studied and discussed.

2. Results

Table 1 summarizes the surface areas and pore volumes of the cobalt-doped carbon gels prepared in this work; the numbers in the sample names indicate the approximate percentage of Co content, while A and X refer to aerogel and xerogel, respectively. All of them are microporous and mesoporous materials, with remarkable mesopore volumes and apparent surfaces areas. The highest surface areas and pore volumes are observed in the case of the samples with less doped Co.

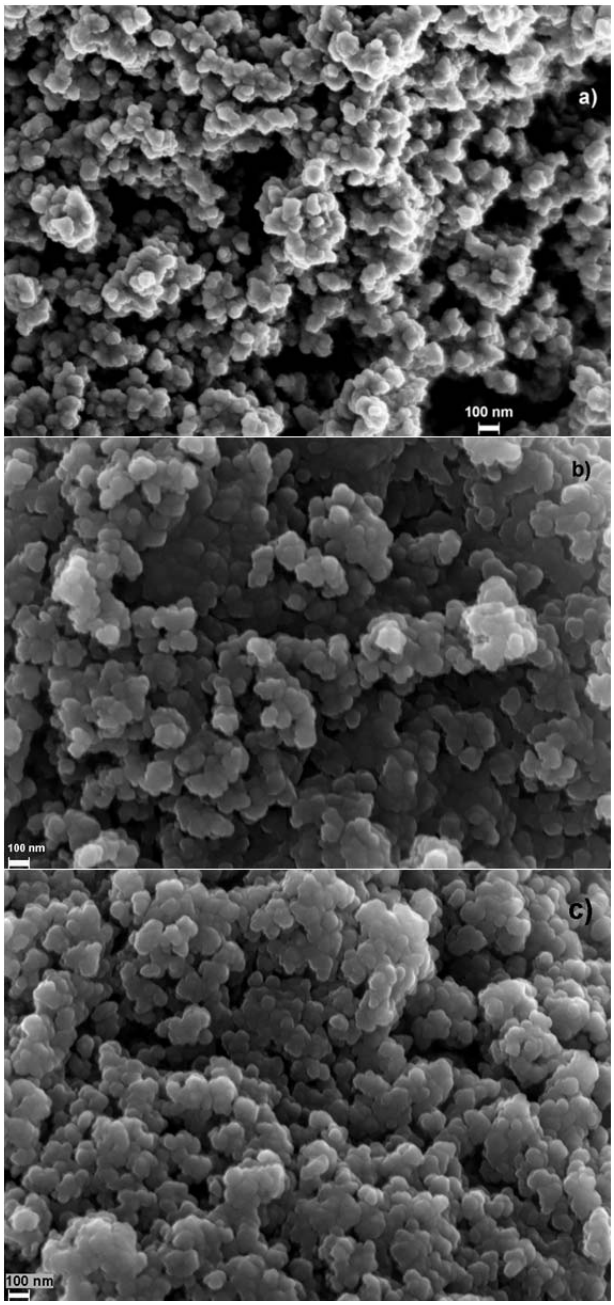

Figure 1. Scanning electron microscopy (SEM) microphotographs obtained at 100.00 KX of magnification: (**a**) XCo6; (**b**) XCo1; and (**c**) ACo6.

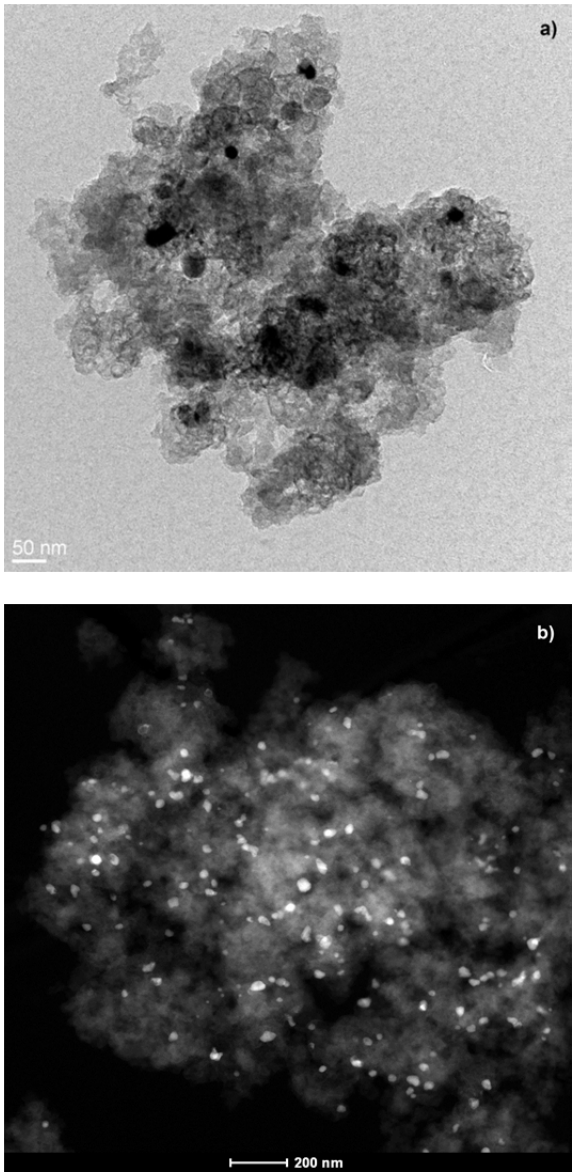

Figure 2. Transmission electron microscopy (TEM) analysis of sample ACo6: (**a**) TEM image; and (**b**) analytical electron microscopy (AEM) spectra collected in scanning transmission electron microscopy (STEM) mode using a high angle annular dark field (HAADF) detector.

Table 1. Name, surface areas, and pore volumes of the doped carbon gels.

Sample	S_{BET} [1] (m^2/g)	S_{DFT} [2] (m^2/g)	$W_0(N_2)$ (cm^3/g)	$L_0(N_2)$ (nm)	$V_{0.95}(N_2)$ (cm^3/g)	$V_{meso}(N_2)$ (cm^3/g)
ACo1	800	871	0.32	0.8	1.09	0.77
ACo4	583	646	0.23	1.1	0.64	0.41
ACo6	589	628	0.23	1.0	0.65	0.42
XCo1	751	816	0.30	1.1	0.89	0.59
XCo4	586	615	0.23	0.9	0.54	0.31
XCo6	586	667	0.23	1.1	0.54	0.30

[1] BET, Brunauer–Emmett–Teller; [2] DFT, Density functional theory.

The carbon gel morphology, which was studied by scanning electron microscopy (SEM) (Figure 1), is typical for R-F carbon gels showing a carbon network formed by nearly spherical particles with different degree of fusion [31], and where a well-developed macroporous structure can also be observed. Apparently there are no significant morphological differences on the non-porous external surface among the samples.

Regarding the Co metal phase characterization, the Co is situated mainly embedded within the carbon matrix, as confirmed by high-resolution transmission electron microscopy (HRTEM) and energy dispersive X-ray analysis (EDAX); these metal particles can be observed in Figure 2a, in which they are very well dispersed throughout the carbon matrix showing a wide range of sizes within a nanometric scale (Figure 2b).

Analysing the X-ray photoelectron spectroscopy (XPS) spectra corresponding to Co 2p, no peaks can be clearly distinguished from the baseline in the spectra corresponding to 1 wt % of Co; therefore, the Co concentration on the external surface of these carbon gels is considered negligible. Only the Co 2p spectra of samples with 6 wt % could be well deconvoluted. A Co $2p_{3/2}$ peak can be observed at 781.1 eV of binding energy (B.E.) in Figure 3, which is assigned to the Co(II) species. The presence of Co(II) species was also corroborated by Raman (Figure 4). Raman spectra of samples with 4% and 6% of cobalt show four peaks at 672, 607, 510, and 466 cm^{-1}, which can be well assigned to the presence of Co_3O_4 nanoparticles [35]. Figure 4 shows two main signals at 1340 and 1580 cm^{-1} approx. corresponding to D and G bands, respectively [36]. It is known that carbon gels are considered as amorphous carbon materials; therefore, the presence of these bands should be analysed into this context: in this type of material, the D band would be associated with alternating ring vibrations in condensed benzene rings [36], while the G band would be associated to the development of the sp^2 carbon structure thought out the material during the carbonization process. Moreover, the presence of Co nanoparticles inside of the organic matrix can also catalyse the development of graphite clusters

around the metal particles, during the carbonization process. This could be detected by X-ray diffraction (XRD) as a broad peak at around 26° in the case of samples with 4 and 6 wt % of cobalt content (Figure 5); this partial graphitization of the Co-doped carbon aerogel structure has been also observed in previous works [30,31]. The XRD peaks detected at 44.22° and 51.50° are assigned to metallic cobalt.

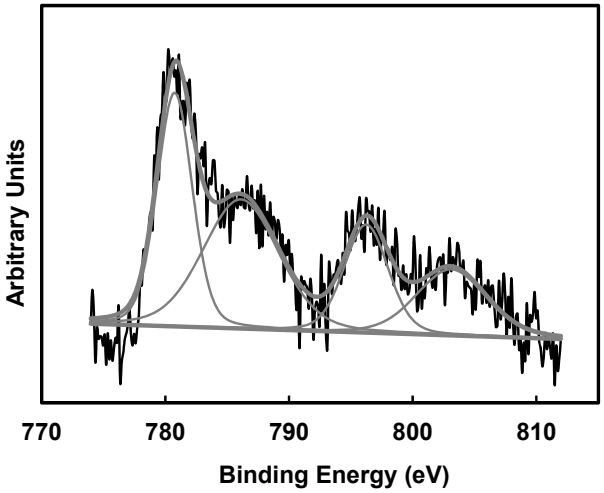

Figure 3. X-ray photoelectron spectroscopy (XPS) spectra of region Co 2p sample ACo6.

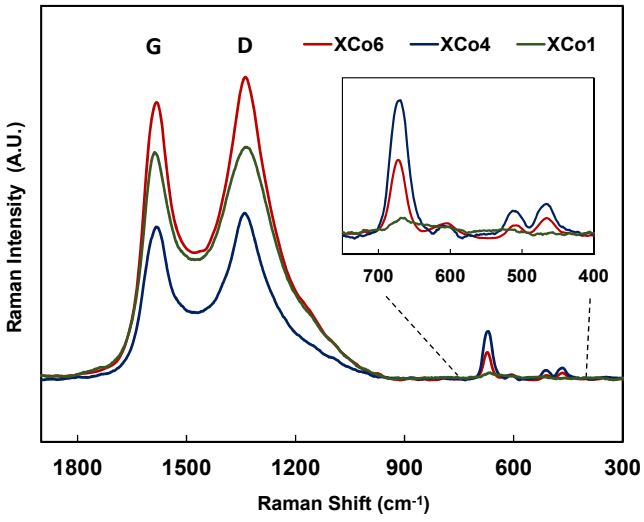

Figure 4. Raman spectra of the doped carbon xerogels.

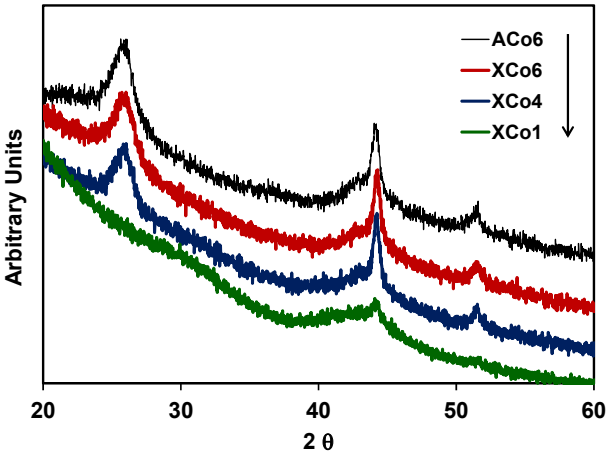

Figure 5. XRD patterns of samples ACo6, XCo6, XCo4, and XCo1.

Cobalt particle sizes estimated by applying the Scherrer equation (d_{XRD}), the chemical composition obtained by XPS, and the total cobalt content of the samples are collected in Table 2. Cobalt particle sizes could not be calculated for samples with the lowest Co content; in the other samples, the main cobalt particle sizes are around 14 nm, with the exception of sample ACo6 in which this value is 21.5 nm. On the other hand, the oxygen surface contents of all the samples range between 3.1 and 3.7 wt %.

Table 2. Chemical characteristics of the carbon gels.

Sample	*Co* TOTAL (wt %)	*Co* XPS [1] (wt %)	*O*XPS (wt %)	d_{XRD} (nm)
ACo1	1.2	n.d. [2]	1.7	n.d
ACo4	4.4	n.d.	3.1	13.9
ACo6	5.9	0.7	3.6	21.5
XCo1	1.1	n.d.	1.5	n.d
XCo4	4.2	n.d.	2.9	14.6
XCo6	5.6	0.6	3.7	14.8

[1] XPS, X-ray photoelectron spectroscopy; [2] n.d.: no determined.

All of the samples were used as a cathode in the electro-catalytic reduction of CO_2. An un-doped carbon xerogel, a cobalt sheet, and the graphite sheet were also tested as cathodes in the electro-catalytic reduction of CO_2; both sheets had dimensions of 50 mm × 8 mm.

The products analysed in the gas phase of the reactor were the following: methane (CH_4), ethane (C_2H_6), ethene (C_2H_4), propane (C_3H_8), propene (C_3H_6), propyne (C_3H_4), and *n*-butane (C_4H_{10}). The molar production will be described in terms of C1, C2, C3, and C4

hydrocarbons, with 1 to 4 being the number of carbon atoms in the molecules in order to simplify the discussion about the reaction selectivity. Nevertheless, methane was the major product in all cases, and minor amounts of other detected products (probably C4 isomers, or C5, hydrocarbons) have not been quantified.

It should be remarked that an "induction period" [33] was not observed and the reaction products were detected since the beginning of the monitoring; this is ascribed to the mesoporosity of the samples which gives good accessibility to the electrolyte inside the porous network, together with the fact that electrodes were submerged in the electrolyte overnight and before the start of the reaction. Nevertheless, the adsorption of a part of the products in the porous structure of the carbon gel cannot be ruled out.

On the other hand, before the discussion, it is necessary to clarify that when an electrolyte free of dissolved CO_2 was used (that is, carrying out the reaction under Ar-saturated solution) no hydrocarbons were detected in any case. Using both under normal experimental reaction conditions, using a graphite sheet or an un-doped carbon xerogel sheet as cathodes, no hydrocarbons were detected.

Data of the total molar productions in the reactor are collected in Figures 6 and 7. These figures show the general tendency that the higher the Co loading, the higher the hydrocarbon formation in both aerogels and xerogels series. This tendency is also clearly observed with the values of the apparent faradaic efficiencies (F.E.) collected in Table 3, being the average of them of the same order that the F.E. calculated for the Co sheet, in spite of the much larger amount of Co used in this last cathode.

Table 3. Apparent faradaic efficiencies (F.E.) for the electro-catalytic CO_2 reduction at −1.65 V vs. Ag/AgCl.

Cathode/Electro-Catalyst	Reaction Time (min)	F.E. (%)
ACo1	60	0.12
ACo4	60	0.17
ACo6	60	0.24
XCo1	60	0.17
XCo4	60	0.29
XCo6	60	0.34
Co sheet-Alfa Aesar® (Karlsruhe, Germany)	60	0.27

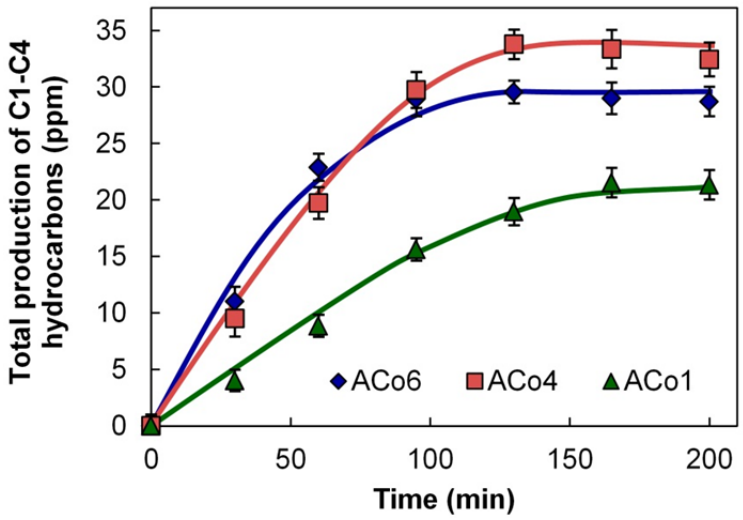

Figure 6. Molar production in the reaction versus time using aerogel based electro-catalysts.

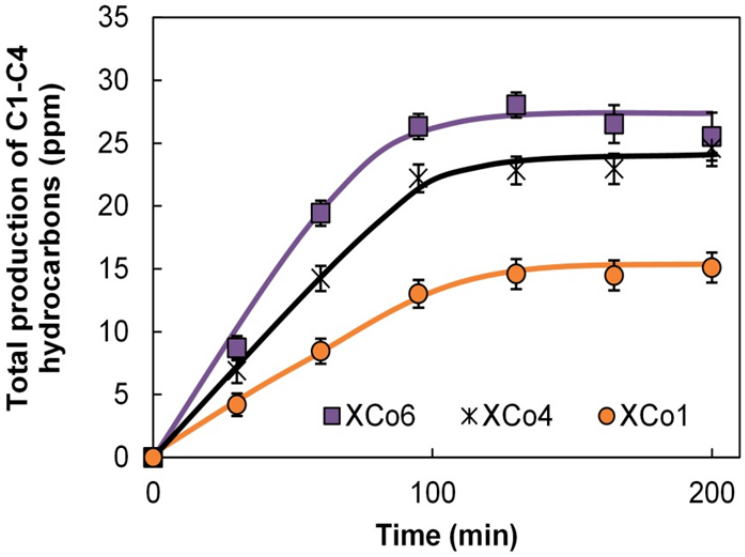

Figure 7. Molar production in the reaction versus time using xerogel based electro-catalysts.

Figure 8 compares the linear sweep voltammetry (LSV) curves of CO_2 reduction obtained with the three aerogels. Current values at –1.44 V clearly increased with the

increase of Co loading, indicating, consecutively, additional CO_2 reduction reaction activity. This tendency is in agreement with the apparent faradaic efficiencies and the total amount of hydrocarbons detected using these electro-catalysts.

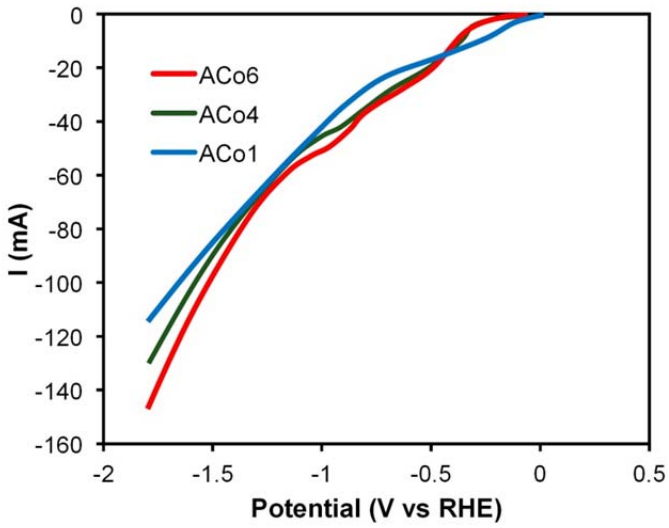

Figure 8. Linear sweep voltammetries obtained from the equilibrium electrode potential to a negative electric potential of −1.79 V vs. RHE. Scan rate: 5 mV/s. Fresh electrodes ACo6, ACo4, and ACo1 in CO_2-saturated 0.1 M $KHCO_3$.

Cobalt leaching in the liquid solutions was studied in all cases by ICP-OES. The detected cobalt concentrations in the liquids were always lower than 100 ppb, which means that Co leaching was not higher than 0.5 wt % of the metal phase in the worst case.

The electrodes were weighed before and after reaction and no weight changes were detected. Finally, the catalysts with the highest cobalt loading were also analysed after reaction by XPS, detecting both Co^{2+} and Co^0 species in a ratio of 4:6, respectively.

3. Discussion

Taking into account all characterization data collected in Section 2, we can conclude that the cobalt-doped gels are materials with a very well-developed porosity, all of them with a remarkable mesoporosity, and with a Co phase well-dispersed and distributed mainly into the carbon matrix. Therefore, Co particles show a broad range of nanometric sizes, being mainly embedded in the carbon matrix with a zero oxidation state, while a very low percentage of the cobalt would be situated in the external non-porous surface

area, being these particles partially oxidized. The carbon matrix macro-structure is very similar among the samples, however, in samples with 4 and 6 wt % of Co, a partial graphitization process has also been detected by XRD.

From the catalytic point of view, a correct comparison of the electro-catalytic behaviour of these materials is, however, not straightforward because the tested cathodes do not have exactly the same textural characteristics, although there is reasonable similarity among them, but also the main Co particle size of ACo1 and XCo1 could not be calculated. Nevertheless, it is demonstrated that the Co-doped carbon gel works as an electro-catalyst in this reaction, the hydrocarbons formation and F.E. increases directly proportional to the total cobalt content, and no previous report has been found in the literature on this type of electro-catalysts.

Analysing more deeply the electro-catalytic results from Figures 6 and 7, we can see that the hydrocarbon formation seems to stop around 100 min of reaction time. In this line, it should be noticed that there are three other different processes that are simultaneously taking place, which can explain this observation: (i) the formation of high amounts H_2 and O_2; (ii) a probable adsorption of hydrocarbons inside of the micropores; and (iii) a partial leaching of the particles situated in the porous and non-porous external surface. The high formation of H_2 and O_2 can provoke a dilution effect of the hydrocarbon formation in the gas phases of the reactor.

As it was mentioned in Section 2, the higher the Co loading, the higher the hydrocarbon production, however this clear general tendency should be commented taking into account not only Co loading, but also the main cobalt particle sizes and the porous texture. In this way, the relative and apparent low catalytic activity of ACo6 in comparison with ACo4 (Figure 6) can be due to the fact that ACo6 has a higher main Co particle size than ACo4 (Table 2). On the other hand, the highest mesoporosity and, mainly, microporosity of samples ACo1 and XCo1 can positively contribute to the above-mentioned tendency because in these two samples the amount of adsorbed hydrocarbons could be higher. Finally, it is very important to remark that processes (i) and (ii) have not been included in the faradaic efficiency calculations. In any case, the more remarkable aspect of this data is the fact that in spite of the much larger amount of Co used with the cobalt sheet (a sheet of 50 mm × 8 mm × 0.25 mm thick versus 80 mg of each carbon gel), all of the apparent F.E. are comparable with the Co sheet, with some of them showing even higher values (Table 3).

Regarding to the selectivity of these materials to the hydrocarbons formation, Figure 9 contains these data at two reaction times, 60 and 200 min. It can be observed in this Figure that the selectivity not only depends on the reaction time, but also of the type of cathode. Co-doped gels are clearly more selective to C3-C4 hydrocarbons, mainly C3, than the Co sheet in all of the cases and independently of the studied reaction time. The selectivity sequence observed at 60 min of reaction time is C1 > C2 > C3 > C4 (Figure 9a,c);

being the carbon gels already more selective to C3 than the Co sheet at this reaction time. At a higher reaction time (200 min) using carbon gels, especially with ACo4 and XCo4, the above mentioned sequence changes, being the C3 hydrocarbon production close to or even higher than the C1 one (Figure 9b,d). This change on the selectivity does not seem to be due to an effect of the carbon matrix mesoporosity because the corresponding A-X couples show similar selectivity; however, it might be due to an effect of the metal-carbon interaction.

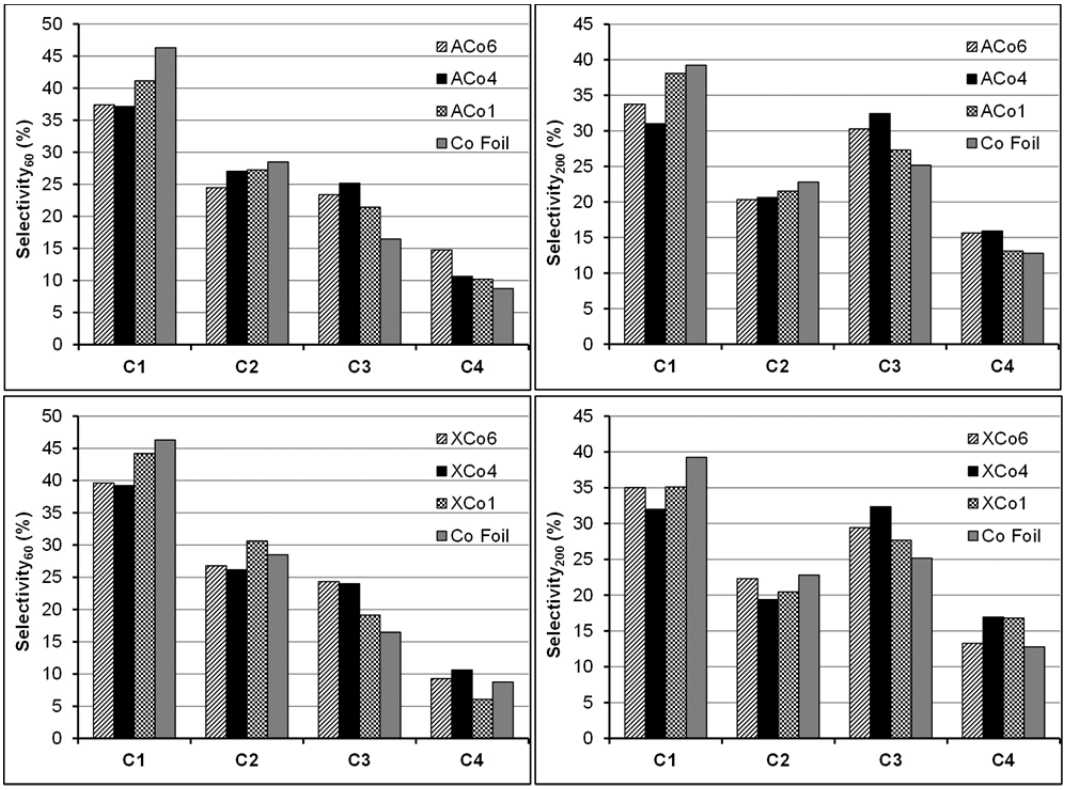

Figure 9. Product distribution (%) in terms of carbon selectivity in gas phase products after 60 (**a**,**c**) and 200 (**b**,**d**) min of reaction time for the aerogel (**a**,**b**)- and xerogel (**c**,**d**)-based electro-catalysts, respectively.

Therefore, the presented results show that this type of cobalt-carbon composites are very interesting as electro-catalysts in the CO_2 reduction reaction, not only because they show better faradaic efficiencies than traditional Co sheet but because this combination of phases improves the selectivity to C3-C4 hydrocarbons formation. In this line and for a

future work, the effect of the metal particle size is an important aspect that should be studied in order to better understand the electro-catalytic selectivity of cobalt in this reaction, for this proposal will be necessary the preparation of cobalt-carbon composites with different mean cobalt particle sizes.

4. Materials and Methods

Cobalt-doped carbon gels were prepared by dissolving resorcinol (R) and formaldehyde (F) in water (W) and using the corresponding metal acetate as a catalyst precursor (C). The used (R/F) and molar ratio (R/W) were 1:2 and 1:17, respectively. Different amounts of C were used in order to obtain three different Co loadings (1, 4, and 6 wt %, approx.) among the final carbon aerogels and xerogels. The mixture was stirred to obtain homogeneous solutions that were cast into glass molds and cured for one day at 40 °C, and for five days at 80 °C, obtaining the corresponding organic gels. Then, the organic gels were immersed in acetone to exchange the solvent media. Two different drying processes, supercritical CO_2 or thermal oven, were carried out in order to obtain the aerogel (A) or xerogel (X) series, respectively. Finally, the organic gels were carbonized in a N_2 flow at 900 °C during 5 h, and using a heating rate of 1 °C/min. The names of the obtained carbon gels were the following: ACo1, ACo4, ACo6, XCo1, XCo4, and XCo6, indicating the numbers the approximate percentage of Co content. The cobalt contents of the samples were determined by burning off a portion of carbon gel at 800 °C in air and weighing the residue.

The characterization of the samples was carried out using gas adsorption, scanning electron microscopy (SEM), high-resolution transmission electron microscopy (HRTEM), Raman spectroscopy, X-ray diffraction (XRD), X-ray photoelectron spectroscopy (XPS), and linear sweep voltammetry (LSV).

The porous texture was analyzed by N_2 adsorption at −196 °C. Prior to measuring the N_2 adsorption isotherms, the samples were outgassed overnight at 110 °C under high vacuum (10^{-6} mbar). The BET equation was applied to the N_2 adsorption data from which the apparent surface area, S_{BET}, was obtained. The Dubinin-Radushkevich (DR) equation was applied to the N_2 adsorption data in order to obtain the corresponding micropore volume (W_0) and micropore mean width (L_0). Total pore volumes ($V_{0.95}$) are calculated from N_2 adsorption isotherms at −196°C and at 0.995 relative pressure, and the corresponding mesopore volumes (V_{MESO}) were calculated by difference between $V_{0.95}$ and W_0. Finally, S_{DFT} is the cumulative surface area obtained from the pore size distribution determined applying the quenched solid state functional theory (QSDFT) method for slit-shaped pores.

SEM was performed using a Zeiss SUPRA40VP scanning electron microscope (Carl Zeiss AG, Oberkochen, Germany), equipped with secondary electron detector, back-

scatter electron detector, and using an X-Max 50 mm energy dispersive X-ray microanalysis system. All of the samples were crushed before realizing this analysis.

HRTEM was carried out using a FEI Titan G2 60-300 microscope (FEI, Eindhoven, The Netherlands) with a high-brightness electron gun (X-FEG) operated at 300 kV and equipped with a Cs image corrector (CEOS) and, for analytical electron microscopy (AEM), a SUPER-X silicon-drift window-less EDX detector. The AEM spectra were collected in STEM (scanning transmission electron microscopy) mode using a HAADF (high angle annular dark field) detector. Digital X-ray maps were also collected on selected areas of the samples.

Raman spectra were obtained using a Micro-Raman JASCO NRS-5100 dispersive spectrometer with a 532 nm laser line (JASCO Inc., Easton, MD, USA).

XRD patterns were recorded with BRUKER D8 ADVANCE diffractometer using Cu Kα radiation (BRUKER, Rivas-Vaciamadrid, Spain). JCPDS files were searched to assign the different diffraction lines observed. Diffraction patterns were recorded between 5° and 70° (2θ) with a step of 0.02° and a time per step of 96 s. The average crystal size was determined using the Scherrer equation.

XPS measurements of the fresh samples were performed using a Physical Electronics ESCA 5701 (PHI, Chanhassen, MN, USA) equipped with a Mg Kα X-ray source (hν = 1253.6 eV) operating at 12 kV and 10 mA, and a hemispherical electron analyzer. For these measurements, the binding energy (BE) values were referred to the C 1s peak at 284.7 eV. A base pressure of 10^{-9} mbar was maintained during data acquisition. Survey and multi-region spectra were recorded at C 1s, O 1s, and Co 2p photoelectron peaks. Each spectral region of interest was scanned several times to obtain good signal-to-noise ratios. The spectra obtained after background signal correction were fitted to Lorentzian and Gaussian curves in order to obtain the number of components, the position of each peak and the peak areas. For XPS analysis of the samples used in reaction, the procedure was the following: once the reaction was finished, the sample was dried under He flow, impregnated with n-octane, and then transferred to the pretreatment chamber of the XPS instrument. Prior to the XPS analysis the samples were evacuated at high vacuum and room temperature, and then introduced into the analysis chamber. A base pressure of 10^{-9} mbar was maintained during data acquisition.

Electro-catalytic conversion of CO_2 was carried out in a three-electrode cell of 300 cm^3 of capacity at ambient temperature and pressure. A Biologic VMP multichannel potentiostat was used to induce an electro-catalytic reduction by applying adequate potential differences over the electrodes. A platinum electrode was employed as a counter electrode, and Ag/AgCl as the reference electrode. A CO_2-saturated 0.1 M potassium bicarbonate aqueous solution (150 cm^3) was used as the electrolyte. The setup was used in potentiostatic mode at −1.65 V, because at this voltage maximum hydrocarbon formation has been typically reported in CO_2 electro-catalytic reductions,

using Ag/AgCl as the reference electrode [13] (−1.44 V vs. reversible hydrogen electrode, RHE). Prior to the electro-catalytic CO_2 reduction, the solution was saturated with CO_2 by bubbling through for 3 h. After saturation, the pH of the solution was 6.7. The CO_2 feed and exit lines were closed off, and the reactor was operated in batch mode. The amount of carbon gel used as electro-catalyst in the working electrode was 80 mg which was homogeneously pasted on the both face of a graphite sheet with dimensions of 50 mm × 8 mm. In the preparation of the working electrode the carbon gel was mixed with the corresponding amount of PTFE in a weight ratio of (80:7) using a PTFE (60%) water solution. Working electrodes were kept in 0.1 M potassium bicarbonate aqueous solution overnight before being used in the electro-reactor.

All cobalt-doped carbon gels were characterized by LSV. The cathodic sweep analysis was conducted from the equilibrium electrode potential to negative electric potential (−1.79 V vs. RHE), with a scan rate of 5 mV/s, using the same experimental conditions and reactor set-up that those for the electro-catalytic CO_2 conversion.

Gas phase hydrocarbons produced by the electrochemical reduction of CO_2 at the fixed potential were analyzed using a gas chromatograph (GC) where gases were directly injected into the column for GC analysis using a gas recirculating pump for low flows. The GC was equipped with a FID and TCD detectors (carrier gas: He, column: Chrompack Poraplot Q, 50 m × 0.53 mm). Production of CO was below the detection limit of the TCD applied in the GC analysis after separation.

The distribution of gaseous products is expressed in terms of the carbon selectivity S_{Ci}, the amount of carbon (from CO_2) in a specific product, relative to the total amount of carbon in the detected hydrocarbons:

$$S_{Ci}(\%) = \frac{i \cdot n_{Ci}}{\sum_i i \cdot n_{Ci}} \times 100\% \quad (1)$$

where nCi represents the mol of product C_i, and i the number of carbon atoms in that product.

The water phase was also analyzed by headspace gas chromatography-mass spectrometry in order to determine the formation and concentration of organic products, using other GC equipped with a HP-INNOWax 30 m × 0.25 mm × 0.25 μm column (Agilent Technologies, Santa Clara, CA, USA), which was coupled to a MS-Triple quadrupole. The presence of alcohols or carboxylic acids of one to four carbon atoms were not detected.

For comparative purposes a commercial Alfa Aesar® (Karlsruhe, Germany) cobalt sheet (99.95% metal basis, 0.25 mm thick), a sheet of graphite from Alfa Aesar® (99.8%, 0.25 mm thick) and an un-doped carbon aerogel were also tested as cathodes.

The amount of cobalt leached into the solution during reaction was determined by inductively coupled plasma optical emission spectrometry (ICP-OES) using an ICP-OES PerkinElmer OPTIMA 8300 spectrometer (PerkinElmer, Madrid, Spain).

5. Conclusions

Two series of carbon gels doped with different cobalt loadings and well-developed mesoporosity, aerogels and xerogels, have been prepared to be used as cathodes for the electro-catalytic reduction of CO_2 to hydrocarbons, at atmospheric pressure. All of the doped carbon gels catalyzed the formation of C1 to C4 hydrocarbons: the higher the Co loading, the higher the hydrocarbon formation with both aerogel and xerogel series; this tendency was also obtained with the apparent faradaic efficiencies which were comparatively much better than those obtained with a pure cobalt sheet. The cobalt-carbon phases formed in this type of doped carbon gels improve the selectivity to C3-C4 hydrocarbons formation, obtaining even more C3 hydrocarbons than CH_4 in some cases.

Acknowledgments: This research is supported by the European Regional Development Fund (FEDER) and the Spanish projects CTQ2013-44789-R of Ministry of Industry, Economy and Competitiveness (MINECO), and P12-RNM-2892 of Junta de Andalucía. Abdalla Abdelwahab and Abdelhakim Elmouwahidi are grateful to the European Union for their Erasmus Mundus fellowships, Programs ELEMENT and Al Idrissi, respectively. Jesica Castelo-Quibén is grateful to the Junta de Andalucía for her research contract (P12-RNM-2892).

Author Contributions: Agustín F. Pérez-Cadenas, Francisco Carrasco-Marín and María Pérez-Cadenas conceived and designed the experiments; Abdalla Abdelwahab, Abdelhakim Elmouwahidi, Jesica Castelo-Quibén and Francisco Carrasco-Marín performed the experiments; Abdalla Abdelwahab, Jesica Castelo-Quibén, Agustín F. Pérez-Cadenas, Francisco Carrasco-Marín and Francisco J. Maldonado-Hódar analyzed the data; María Pérez-Cadenas contributed with XPS analysis; Agustín F. Pérez-Cadenas, Francisco Carrasco-Marín and Francisco J. Maldonado-Hódar wrote the paper.

Conflicts of Interest: The authors declare no conflict of interest.

References

1. Word Meteorological Organization 2016. Available online: http://www.wmo.int/ (accessed on 25 October 2016).
2. Kumar, N.; Camaioni, D.M.; Dupuis, M.; Raugei, S.; Appel, A.M. Mechanistic insights into hydride transfer for catalytic hydrogenation of CO_2 with cobalt complexes. *Dalton Trans.* **2014**, *43*, 11803–11806.
3. Liu, J.Y.; Garg, B.; Ling, Y.C. $Cu_xAg_yIn_zZn_kSm$ solid solutions customized with RuO_2 or $Rh_{1.32}Cr_{0.66}O_3$ co-catalyst display visible light-driven catalytic activity for CO_2 reduction to CH_3OH. *Green Chem.* **2011**, *13*, 2029–2031.

4. Wang, J.J.; Jing, Y.H.; Ouyang, T.; Zhang, Q.; Chang, C.T. Photocatalytic reduction of CO_2 to energy products using Cu-TiO_2/ZSM-5 and Co-TiO_2/ZSM-5 under low energy irradiation. *Catal. Commun.* **2015**, *59*, 69–72.
5. Truong, Q.D.; Le, T.H.; Liu, J.Y.; Chung, C.C.; Ling, Y.C. Synthesis of TiO_2 nanoparticles using novel titanium oxalate complex towards visible light-driven photocatalytic reduction of CO_2 to CH_3OH. *Appl. Catal. A* **2012**, *437–438*, 28–35.
6. Centi, G.; Perathoner, S. Heterogeneous catalytic reactions with CO_2: Status and perspectives; In *Carbon Dioxide Utilization for Global Sustainability*; Park, S.E., Chang, J.S., Lee, K.W., Eds.; Elsevier: Amsterdam, The Netherlands, 2004.
7. Bell, A.T.; Gates, B.C.; Ray, D.; Thompson, M.R. *Basic Research Needs: Catalysis for Energy*; U.S. Department of Energy Pub: Washington, DC, USA, 2007.
8. Jitaru, M.; Lowy, D.A.; Toma, M.; Toma, B.C.; Oniciu, L. Electrochemical reduction of carbon dioxide on flat metallic cathodes. *J. Appl. Electrochem.* **1997**, *27*, 875–889.
9. Gattrell, M.; Gupta, N.; Co, A. A review of the aqueous electrochemical reduction of CO_2 to hydrocarbons at copper. *J. Electroanal. Chem.* **2006**, *594*, 1–19.
10. Chaplin, R.P.S.; Wragg, A.A. Effects of process conditions and electrode material on reaction pathways for carbon dioxide electroreduction with particular reference to formate formation. *J. Appl. Electrochem.* **2003**, *33*, 1107–1123.
11. Ougitani, Y.; Aizawa, T.; Sonoyama, N.; Sakata, T. Temperature dependence of the probability of chain growth for hydrocarbon formation by electrochemical reduction of CO_2. *Bull. Chem. Soc. Jpn.* **2001**, *74*, 2119–2122.
12. Schwartz, M.; Vercauteren, M.E.; Sammells, A.F. Fischer-Tropsch electrochemical CO_2 reduction to fuels and chemicals. *J. Electrochem. Soc.* **1994**, *141*, 3119–3127.
13. Shibata, H.; Moulijn, J.A.; Mul, G. Enabling electrocatalytic Fischer-Tropsch synthesis from carbon dioxide over copper-based electrodes. *Catal. Lett.* **2008**, *123*, 186–192.
14. Gao, S.; Lin, Y.; Jiao, X.; Sun, Y.; Luo, Q.; Zhang, W.; Li, D.; Yang, J.; Xie, Y. Partially oxidized atomic cobalt layers for carbon dioxide electroreduction to liquid fuel. *Nature* **2016**, *529*, 68–71.
15. Gao, S.; Jiao, X.; Sun, Z.; Zhang, W.; Sun, Y.; Wang, C.; Hu, Q.; Zu, X.; Yang, F.; Yang, S.; et al. Ultrathin Co_3O_4 layers realizing optimized CO_2 electroreduction to formate. *Angew. Chem. Int. Ed.* **2016**, *55*, 698–702.
16. Quezada, D.; Honores, J.; Garcia, M.; Armijo, F.; Isaacs, M. Electrocatalytic reduction of carbon dioxide on a cobalt tetrakis(4-aminophenyl)porphyrin modified electrode in $BMImBF_4$. *New J. Chem.* 2014, 38, 3606–3612.
17. Centi, G.; Perathoner, S.; Wine, G.; Gangeri, M. Electrocatalytic conversion of CO_2 to long carbon-chain hydrocarbons. *Green Chem.* **2007**, *9*, 671–678.
18. Centi, G.; Perathoner, S. Problems and perspectives in nanostructured carbon-based electrodes for clean and sustainable energy. *Catal. Today* **2010**, *150*, 151–162.
19. Pekala, R.W.; Alviso, C.T.; Kong, F.M.; Hulsey, S.S. Aerogels derived from multifunctional organic monomers. *J. Non-Cryst. Solids* **1992**, *145*, 90–98.

20. Pekala, R.W. Low Density, Resorcinol-Formaldehyde Aerogels. U.S. Patent 4,873,218, 10 October 1989.
21. ElKhatat, A.M.; Al-Muhtaseb, S.A. Advances in tailoring resorcinol-formaldehyde organic and carbon gels. *Adv. Mater.* **2011**, *23*, 2887–2903.
22. Gallegos-Suarez, E.; Perez-Cadenas, A.F.; Maldonado-Hodar, F.J.; Carrasco-Marin, F. On the micro- and mesoporosity of carbon aerogels and xerogels. The role of the drying conditions during the synthesis processes. *Chem. Eng. J.* **2012**, *181–182*, 851–855.
23. Maldonado-Hodar, F.J.; Moreno-Castilla, C.; Carrasco-Marin, F.; Perez-Cadenas, A.F. Reversible toluene adsorption on monolithic carbon aerogels. *J. Hazard. Mater.* **2007**, *148*, 548–552.
24. Moreno-Castilla, C.; Maldonado-Hódar, F.J. Carbon aerogels for catalysis applications: An overview. *Carbon* **2005**, *43*, 455–465.
25. Perez-Cadenas, M.; Moreno-Castilla, C.; Carrasco-Marin, F.; Perez-Cadenas, A.F. Surface chemistry, porous texture, and morphology of N-doped carbon xerogels. *Langmuir* **2009**, *25*, 466–470.
26. Duarte, F.; Maldonado-Hodar, F.J.; Perez-Cadenas, A.F.; Madeira, L.M. Fenton-like degradation of azo-dye Orange II catalyzed by transition metals on carbon aerogels. *Appl. Catal. B* **2009**, *85*, 139–147.
27. Morales-Torres, S.; Maldonado-Hodar, F.J.; Perez-Cadenas, A.F.; Carrasco-Marin, F. Design of low-temperature Pt-carbon combustion catalysts for VOC's treatments. *J. Hazard. Mater.* **2010**, *183*,
814–822.
28. Pandolfo, A.G.; Hollenkamp, A.F. Carbon properties and their role in supercapacitors. *J. Power Sources* **2006**, *157*, 11–27.
29. Moreno-Castilla, C.; Maldonado-Hodar, F.J.; Perez-Cadenas, A.F. Physicochemical surface properties of Fe, Co, Ni, and Cu-doped monolithic organic aerogels. *Langmuir* **2003**, *19*, 5650–5655.
30. Maldonado-Hodar, F.J.; Moreno-Castilla, C.; Rivera-Utrilla, J.; Hanzawa, Y.; Yamada, Y. Catalytic graphitization of carbon aerogels by transition metals. *Langmuir* **2000**, *16*, 4367–4373.
31. Maldonado-Hodar, F.J.; Moreno-Castilla, C.; Perez-Cadenas, A.F. Surface morphology, metal dispersion, and pore texture of transition metal-doped monolithic carbon aerogels and steam-activated derivatives. *Micropor. Mesopor. Mat.* **2004**, *69*, 119–125.
32. Maldonado-Hodar, F.J.; Jirglova, H.; Perez-Cadenas, A.F.; Morales-Torres, S. Chemical control of the characteristics of Mo-doped carbon xerogels by surfactant-mediated synthesis. *Carbon* **2013**, *51*, 213–223.
33. Perez-Cadenas, A.F.; Ros, C.H.; Morales-Torres, S.; Perez-Cadenas, M.; Kooyman, P.J.; Moreno-Castilla, C.; Kapteijn, F. Metal-doped carbon xerogels for the electro-catalytic conversion of CO_2 to hydrocarbons. *Carbon* **2013**, *56*, 324–331.
34. Perez-Cadenas, A.F., Moreno-Castilla, C., Carrasco-Marín, F., Maldonado-Hódar, F., Morales-Torres, S., Kapteijn, F.; Ros, C.H. Doped Carbon Material for the Electrocatalytic Conversion

of CO_2 into Hydrocarbons, Uses of the Material and Conversion Method Using Said Material. WO/2013/004882, 1 October 2013.
35. Rashad, M.; Rüsing, M.; Berth, G.; Lischka, K.; Pawlis, A. CuO and Co_3O_4 nanoparticles: Synthesis, characterizations, and Raman spectroscopy. *J. Nanomater.* **2013**, *2013*, 82.
36. Schwan, J.; Ulrich, S.; Batori, V.; Ehrhardt, H.; Silva, S.R.P. Raman spectroscopy on amorphous carbon films. *J. Appl. Phys.* **1996**, *80*, 440–447.

CHAPTER IV: CARBON GELS DOPED WITH IRON FOR THE ELECTRO-REDUCTION OF CO_2 TO HYDROCARBONS: THE ROLE OF THE IRON PARTICLE SIZE

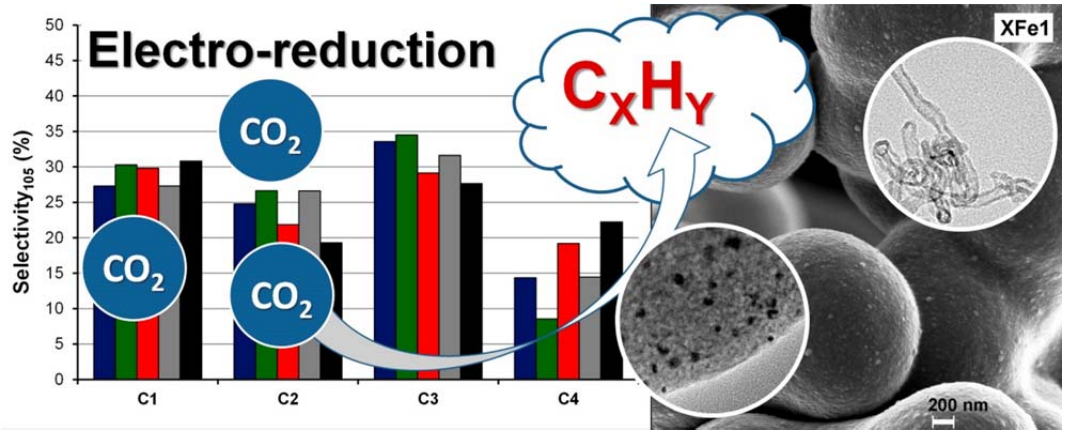

4.1.- ABSTRACT

Different types of carbon gels doped with iron, in particular an aerogel, three xerogels with different iron contents, and a carbon xerogel – carbon nanofiber composite have been prepared, exhaustively characterized, and tested as cathodes for the electro-catalytic reduction of CO_2 to hydrocarbons at atmospheric pressure. Commercial iron and graphite sheets have also been tested as cathodes for comparison.

All electro-catalysts promoted the formation of C1 to C4 hydrocarbons showing a high selectivity to C3 hydrocarbons. The carbon xerogel – carbon nanofiber composite was the most selective to C4 hydrocarbons, even over long reaction times. The iron particle size is a very important parameter involved in the hydrocarbon formation. A linear correlation between mean iron particle sizes and the faradaic efficiency of the materials has been found: the smaller the iron particle size, the higher the faradaic efficiency. Iron nano-particles smaller than 4 nm seem to increase significantly the formation of hydrocarbons.

4.2.- EXPERIMENTAL

4.2.1.- Preparation and characterization of the materials

Iron-doped carbon gels were prepared by dissolving resorcinol (R) and formaldehyde (F) in water (W) and using the corresponding metal acetate as catalyst precursor (C). The used (R/F) and molar ratio (R/W) were 1:2 and 1:17 respectively. Different amounts of C were used in order to obtain two different Fe loadings (1 and 6 wt.%, approx.) among de final carbon aerogels and xerogels. The mixture was stirred to obtain homogeneous solutions that were cast into glass moulds and cured 1 day at 40 ºC, and 5 days at 80 ºC, obtaining the corresponding wet organic gels. Then, the organic gels were introduced in acetone to exchange the solvent media [1]. Two different drying processes, supercritical CO_2 or thermal oven, were carried out in order to obtain the dry organic sample: aerogel (A) or xerogel (X), respectively. Finally, all the organic gels were carbonized in a N_2 flow at 900 ºC during 5 h, and using a heating rate of 1 ºC/min. The prepared carbon gels will be referred as follow: AFe1, XFe1 and XFe6, being 1 and 6 the weight percentage of metal loading in the aerogel and xerogel samples. On the other hand, a second type carbon xerogel, hereafter as XFe6b, was obtained avoiding the exchange with acetone before the thermal drying. An additional material was prepared by heating sample XFe6b at 700 ºC in H_2 flow during 1 h, and after that, the H_2 flow was changed *in situ* by a mixture of $He:C_2H_4:H_2$ with a volumetric ratio of 90:10:20, respectively, keeping the same temperature during 2 h. In these conditions, carbon nanofibers (CNFs) grew on the carbon xerogel matrix forming therefore a carbon xerogel-CNF composite, labelled as XFe6bNF. A 50 - 50 wt.% carbon xerogels – CNF composition was estimated by weighting

the materials after the different steps, including only after the H_2 pre-treatment; in this last case, obviously a specific portion of sample was used only for this weight calculation.

The iron contents of the electro-catalysts were determined by burning off a portion of the sample at 800 ºC in air and weighting the residue.

The characterization of the samples was carried out using physical adsorption of nitrogen, mercury porosimetry, scanning electron microscopy (SEM), high resolution transmission electron microscopy (HRTEM), Raman, X-ray diffraction (XRD), X-ray photoelectron spectroscopy (XPS), and linear sweep voltammetry (LSV).

4.2.2.- Electro-catalytic reduction of CO_2

Electro-catalytic conversion of CO_2 was carried out in a three-electrode cell of 300 cm^3 of capacity at ambient temperature and pressure. A Biologic VMP multichannel potentiostat was used to induce electro-catalytic reduction by applying adequate potential differences over the electrodes. A platinum electrode was employed as a counter electrode, and Ag/AgCl as reference electrode. A CO_2-saturated 0.1 M potassium bicarbonate aqueous solution (150 cm^3) was used as electrolyte. The setup was used in potentiostatic mode at -1.65 V, reproducing the voltage conditions of previous works, using Ag/AgCl as reference electrode [2]. Prior to the electro-catalytic CO_2 reduction, the solution was saturated with CO_2 by bubbling through for 3 h. After saturation, the pH of the solution was 6.7. The CO_2 feed and exit lines were closed off, and the reactor was operated in batch mode. The amount of carbon gel used as electro-catalyst in the working electrode (cathode) was 80 mg which was homogeneously pasted on the both face of a

graphite sheet with dimensions of 50 mm x 8 mm. In the preparation of the working electrode the carbon gel was mixed with the corresponding amount of polytetrafluoroethylene (PTFE) in a weight ratio of (80:7) using a PTFE (60%) water solution. Working electrodes were kept in 0.1 M potassium bicarbonate aqueous solution overnight before being used in the electro-reactor. All electro-catalysts were also tested carrying out the reaction under Ar-saturated solution, and therefore using electrolytes free of CO_2.

4.2.3.- Analysis of the reaction products

Gas phase hydrocarbons produced by the electrochemical reduction of CO_2 at the fixed potential were analysed using a gas chromatograph (GC), where gases were directly injected into the GC column using a gas recirculating pump for low flows. The GC was equipped with a FID and TCD detectors (carrier gas: He, column: Chrompack Poraplot Q, 50 m × 0.53 mm). Production of CO was below the detection limit of the TCD applied in the GC analysis after separation.

The distribution of gaseous products is expressed in terms of the carbon selectivity, the amount of carbon (from CO_2) in a specific product relative to the total amount of carbon in the detected hydrocarbons.

$$S_{C_i}\ (\%) = \frac{i \cdot n_{C_i}}{\sum_i i \cdot n_{C_i}} \times 100\%$$

Here n_{Ci} represents the mol of product Ci, and i the number of carbon atoms in that product.

Water phase was also analysed by Headspace Gas Chromatography-Mass Spectrometry in order to determine the formation and concentration of organic products, using other GC equipped with a HP-INNOWax 30 m x 0.25 mm x 0.25 μm column, which was coupled to a MS-Triple quadrupole. The presence of alcohols or carboxylic acids of one to four carbon atoms were not detected.

4.2.4.- Linear sweep voltammetry

All electro-catalysts were characterized by LSV. The cathodic sweep analysis was conducted from the equilibrium electrode potential to negative electric potential of −2.0 V vs. Ag/AgCl, with a scan rate of 5 mV/s, using the same experimental conditions and reactor set-up that those for the electro-catalytic CO_2 conversion.

4.2.5.- Other tested materials

For comparative purposes a commercial Alfa Aesar® iron sheet (99.995% metal basis, 0.25 mm thick, Puratronic®), a sheet of graphite from Alfa Aesar® (99.8%, 0.25 mm thick) and an un-doped carbon aerogel were also tested as cathodes.

4.2.6.- Lixiviation measurements

The amount of Fe leached into the solution during reaction was determined by inductively coupled plasma optical emission spectrometry (ICP-OES) using an ICP-OES PerkinElmer OPTIMA 8300 spectrometer.

4.3.- RESULTS

Table 4.1 summarizes the surface areas and pore volumes of the doped carbon materials. All carbon gels prepared in this work are microporous, mesoporous and macroporous materials. Xerogels with the highest iron content (i.e., XFe6 and XFe6b) show the highest mesopore volumes (V_{BJH}), all of them with similar mean mesopore width and low micropore volumes. XFe6b has lower macro- and mesopore volumes, and apparent surface area than XFe6 because it was obtained without the acetone exchange step before the thermal drying [1].

Table 4.1. Name, surface area and pore volumes of the doped carbon materials.

Sample	S_{BET} m^2/g	W_0 cm^3/g	L_0 nm	$V_{0.95}$ cm^3/g	L_{BJH} nm	V_{BJH} cm^3/g	V_{MACRO} cm^3/g
AFe1	427	0.16	0.8	0.32	3.4	0.27	1.13
XFe1	445	0.17	0.7	0.30	3.4	0.23	1.27
XFe6	473	0.18	0.8	0.40	3.8	0.62	1.71
XFe6b	275	0.10	1.0	0.26	3.8	0.46	0.47
XFe6bNF	62	0.02	1.2	0.15	7.0	0.37	1.73

On the other hand, the carbon xerogel - carbon nanofiber composite, XFe6bNF, is a macro-mesoporous material with a remarkable mesopore volume but with mean mesopore sizes wider than the other samples. In the preparation of XFe6bNF, the initial microporosity of the carbon xerogel was nearly destroyed (i.e., W_0 = 0.10 *vs.* 0.02 cm^3/g for XFe6b and XFe6bNF, respectively) probably due to a partial gasification of the carbon xerogel matrix catalysed by the Fe

nanoparticles during the H_2 pre-treatment, followed by a blocking of the porosity assisted by the carbon nanofiber (CNF) growth.

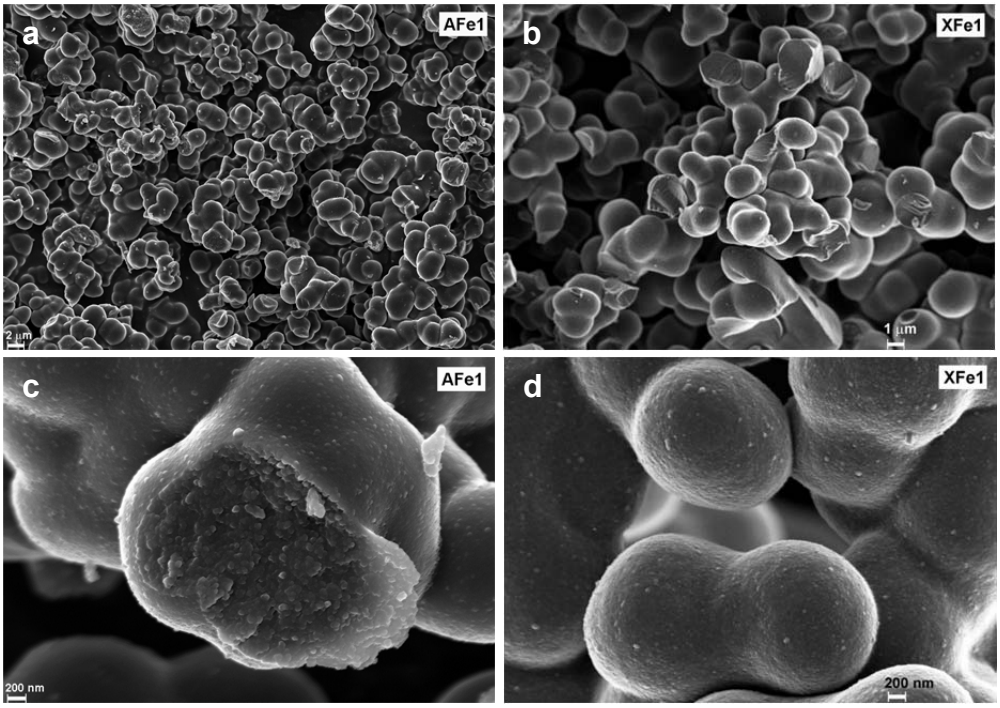

Figures 4.1a-d. SEM microphotographs showing the morphology of samples AFe1 and XFe1.

SEM images of the carbon gels are collected in Figure 4.1. The morphology is typical for R-F carbon gels showing a carbon network mainly formed by nearly spherical nanoparticles with different degree of fusion [3], and where a well-developed macroporous structure can be also observed in all cases. However, we can distinguish significant differences among them: AFe1 and XFe1 are formed in turn by carbon microspheres partially fused (Figures 4.1a-d), which are

constituted by the same type of carbon network that throughout all the structure in XFe6b and XFe6 (Figures 4.1e and g, respectively). The morphology of the carbon xerogel - CNF composite is clearly formed by CNFs with very different lengths and also widths, which have grown from the carbon xerogel matrix (Figures 4.1f and h); an average width of 70 nm for the CNFs has been estimated. Thus, the HRTEM analysis revealed that these CNFs are really hollow nanofibers (Figures 4.2e and f), in which sometimes the iron particle can be identified inside of the nanofiber channel.

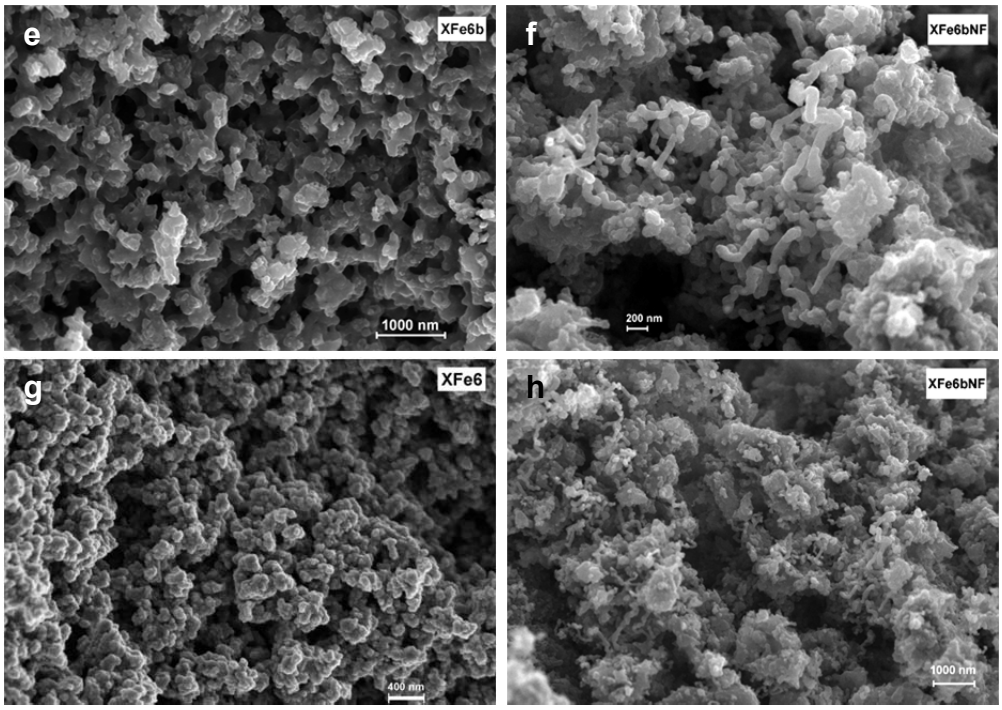

Figures 4.1e-h. SEM microphotographs showing the morphology of samples XFe6b, XFe6bNF and XFe6.

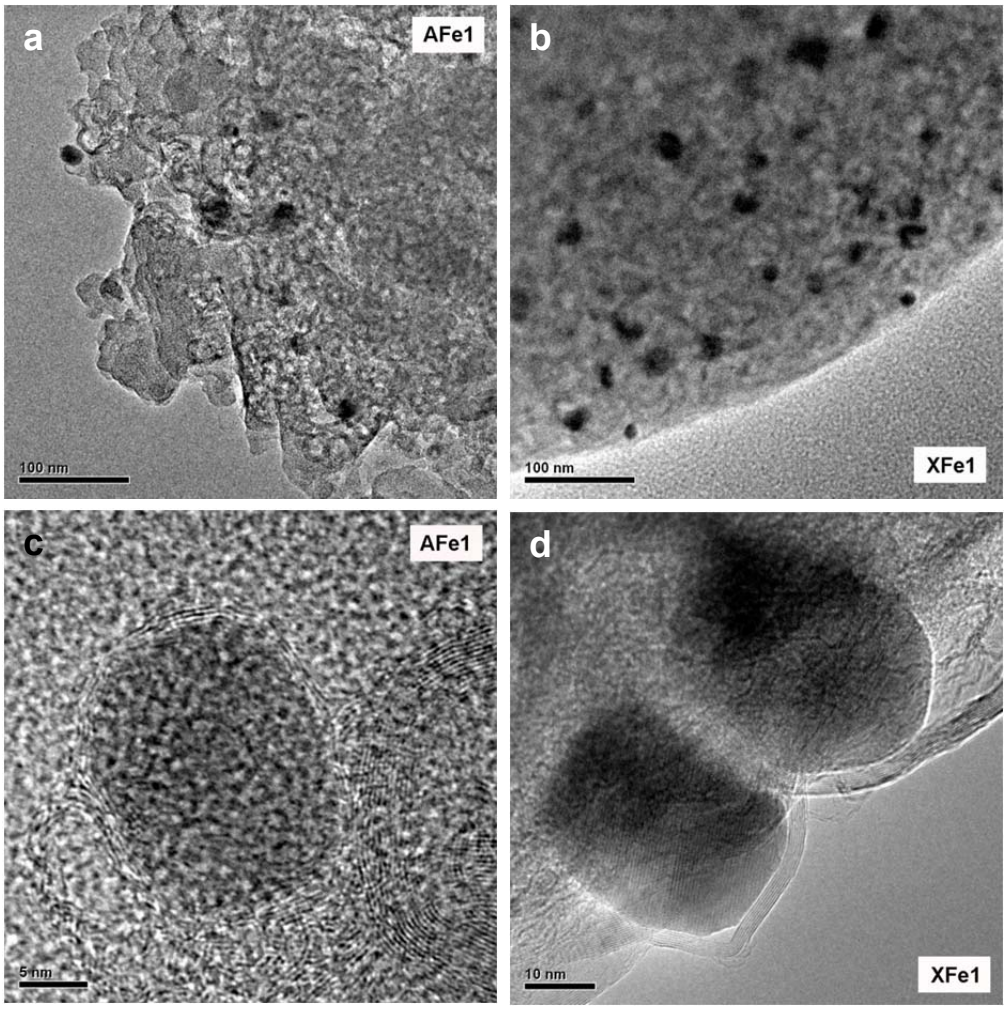

Figures 4.2a-d. HRTEM images of samples AFe1 (a, c), XFe1 (b, d).

Regarding the Fe metal phase characterization in the carbon gels, Fe is mainly embedded within the carbon matrix, as confirmed by XPS, HRTEM and EDAX analysis; these metal particles can be identified in Figure 2, in which they are well-dispersed throughout the carbon matrix showing a wide range of sizes

within a nanometric scale (Figures 4.2a-b and Figure 4.3). In this way, the presence of iron inside of the organic matrix catalysed the development of graphite clusters surrounding the nanoparticles in all carbon gels during the carbonization process; two examples of these graphitic lines are clearly observed in Figures 4.2c-d, samples AFe1 and XFe1, respectively. This partial graphitization of the carbon gel structure by metal particles was already reported in previous works [3,4], and corroborated by XRD analysis, where a well-defined peak (002) at around 26º is clearly observed in the spectra collected in Figure 4.4. A second broad peak, typically of partially graphitized carbon materials, can be also observed around 44º corresponding with the 101 diffraction peak of graphite. The mean stack height of the graphite crystallites, L_c, was obtained by applying Scherrer equation to the 002 diffraction peak. The values obtained are compiled in Table 4.2.

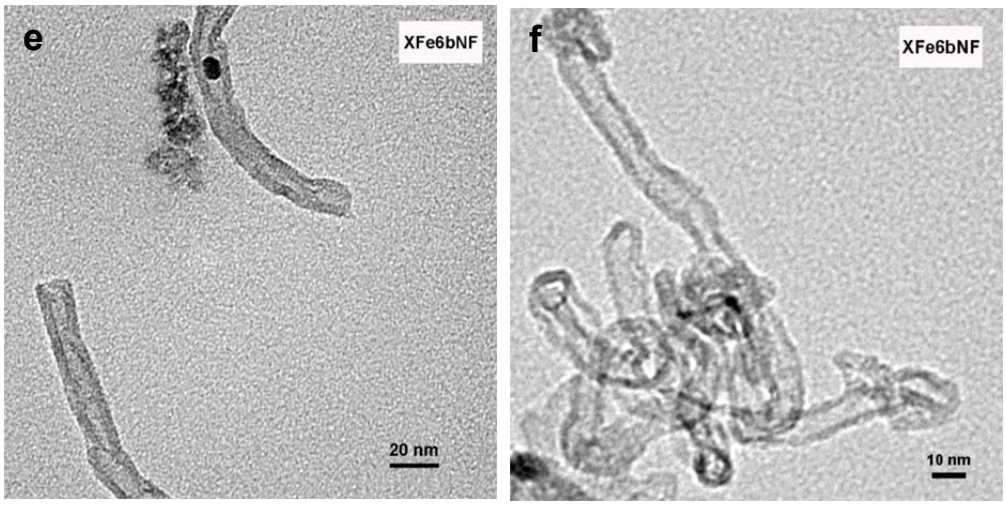

Figures 4.2e-f. HRTEM images of sample XFe6bNF (e, f).

Table 4.2. Chemical characteristics of the different carbon gels.

Sample	Fe_{TOTAL} wt.%	Fe_{XPS} wt.%	O_{XPS} wt.%	d_{DRX} nm	L_C nm	I_D/I_G
AFe1	1.1	n.d.	n.d.	16.7	5.5	n.d.
XFe1	1.0	n.d.	n.d.	< 4	5.1	1.18
XFe6	5.9	0.5	2.8	28.3	4.7	1.12
XFe6b	6.2	1.1	3.1	20.9	5.8	1.01
XFe6bNF	7.6	< 0.1	1.4	18.9	6.3	1.03

n.d: no determined

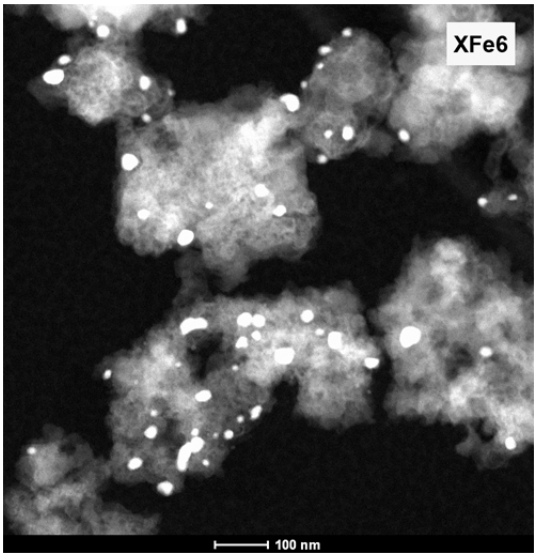

Figure 4.3. Scanning transmission electron microscopy (STEM) image using a high angle annular dark field (HAADF) detector of the XFe6 sample.

Figure 4.5 shows two main signals in the Raman spectra placed at ~1340 and ~1580 cm^{-1} corresponding to D and G bands, respectively [5]. It is well-known

that carbon gels are considered as amorphous carbon materials and therefore, the presence of these bands should be analysed into this context: in this type of materials, the D band would be associated with alternating ring vibrations in condensed benzene rings [5] or loss of hexagonal symmetry in the carbon structure [4], while the G band would be associated to the development of the sp^2 carbon structure throughout the material during the carbonization process, this fact being always observed in all carbon and graphite materials. It should be noted than the intensity of the G band (I_G) in XFe6b and XFe6bNF is higher than that for the D band (I_D), while the opposite trend is observed in XFe1 and XFe6, i.e., a higher I_D/I_G. This fact indicates an improvement of the stacking of the graphitic layers in both XFe6b and XFe6bNF materials, which is in agreement with the L_c values obtained by XRD (Table 4.2). On the hand, the smallest Fe loading of XFe1 and the so large d_{DRX} value of XFe6 might justify the previous explanation.

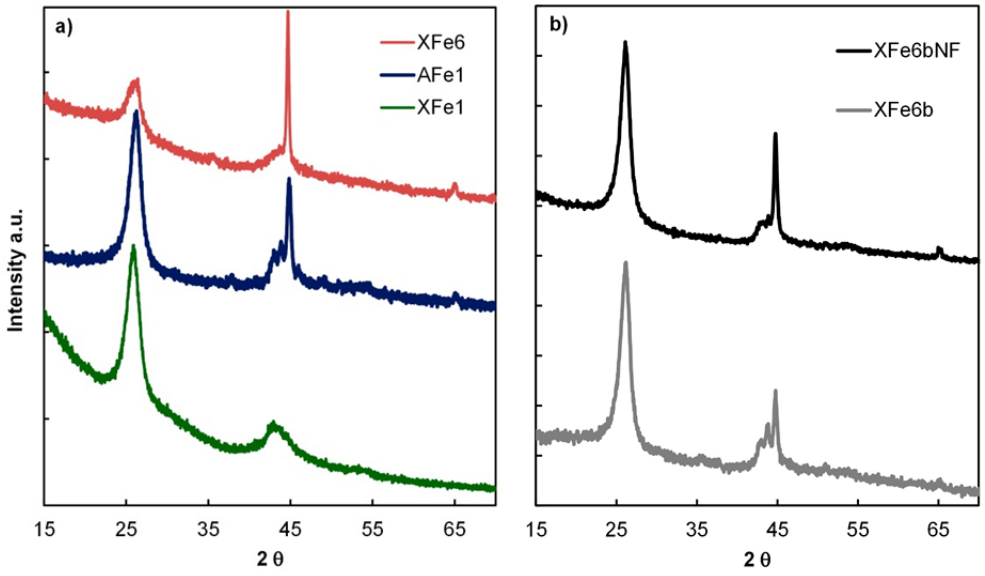

Figure 4.4. XRD patterns of the samples.

Regarding the Fe crystalline phase, two peaks placed at 44.6º and 65.2º corresponding to Fe(0) were observed in XRD patterns of all samples with exception of XFe1. XFe1 does not show any metal diffraction peak because the Fe particles should have probably mean sizes smaller than 4 nm or very slim laminar shapes. On the other hand, some samples seem to show a small peak located at 43.5º indicating the presence of iron oxide particles, which were not totally reduced by the organic matrix during the heat treatment. Fe particle sizes estimated by applying the Scherrer equation, chemical composition obtained by XPS and total iron content of the samples are collected in Table 4.2.

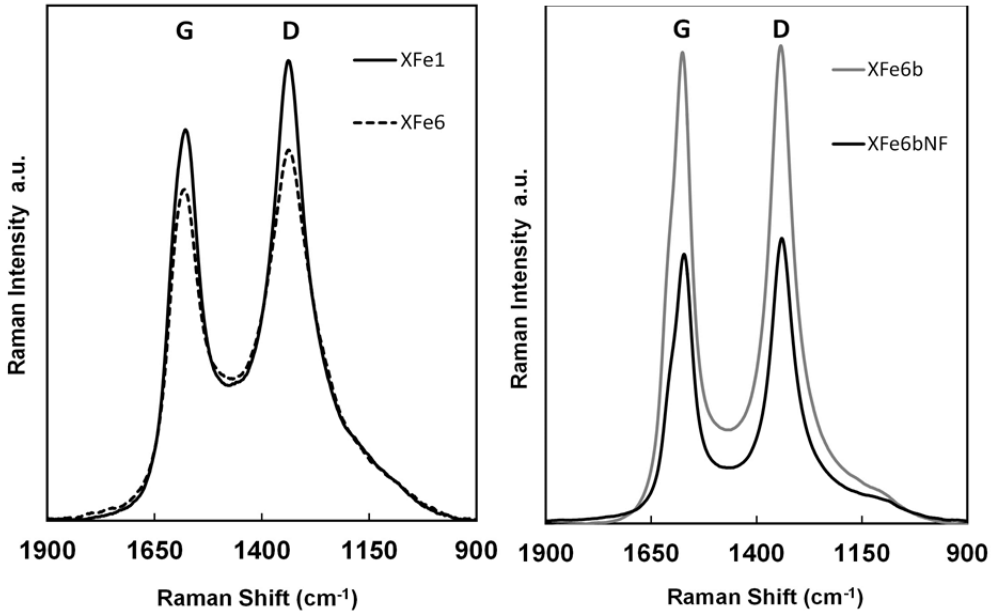

Figure 4.5. Raman spectra of the carbon xerogels and the carbon xerogel-CNF composite.

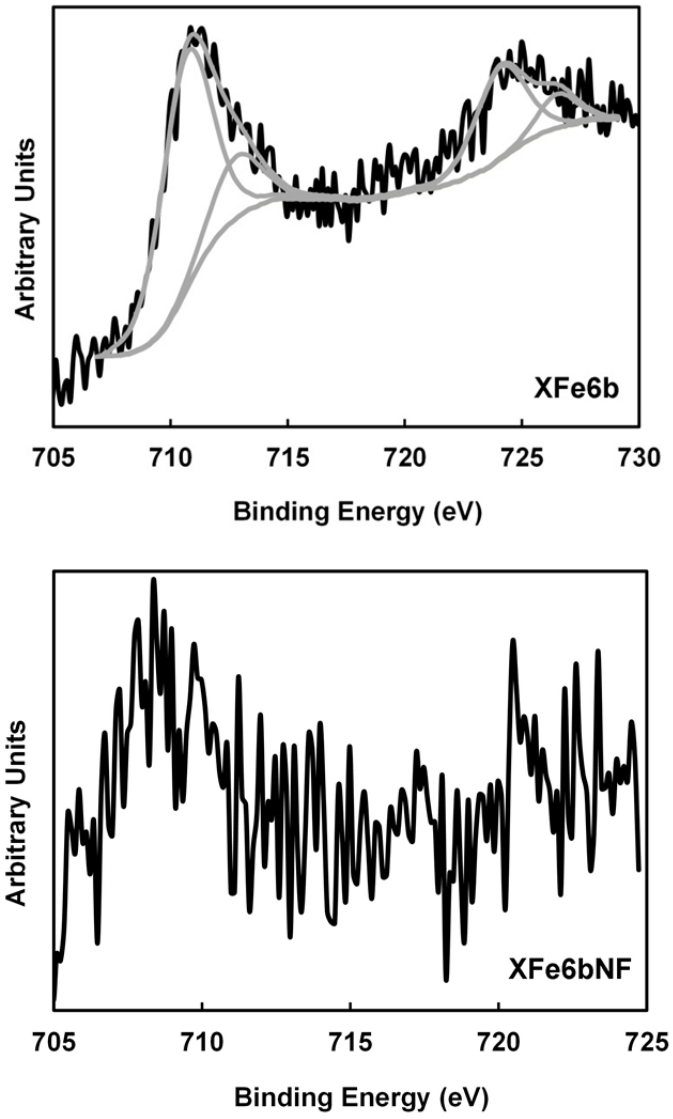

Figure 4.6. XPS analysis and deconvolution of the Fe_{2p} region of XFe6b and XFe6bNF.

Analysing the XPS spectra corresponding to the Fe_{2p} region, no peaks can be clearly distinguished from the base line in the spectra corresponding to 1 wt.% of Fe (i.e., AFe1 and XFe1) and therefore, the Fe concentration on the external surface of these carbon gels is considered negligible. Only Fe_{2p} spectra of samples with 6 wt.% could be deconvoluted showing two different type of iron species at 710.7 and 712.8 eV, which are assigned to Fe_2O_3 (79.2%) and Fe_3O_4 (20.8%), respectively (Figure 4.6). Small particles of iron on the external surface are easier to be oxidized than large particles embedded in the inner surface.

On the other hand, the iron surface content determined for XFe6bNF was markedly lower than that for its precursor carbon gel (i.e., < 0.1 and 1.1 wt.% for XFe6bNF and XFe6b, respectively).

All the samples were used as a cathode in the electro-catalytic reduction of CO_2. An un-doped carbon xerogel, an iron sheet, and the graphite sheet were also tested as cathodes in the electro-catalytic reduction of CO_2, both sheets with dimensions of 50 mm x 8 mm.

The products analysed in the gas phase of the reactor were the following: methane (CH_4), ethane (C_2H_6), ethene (C_2H_4), propane (C_3H_8), propene (C_3H_6), propyne (C_3H_4) and n-butane (C_4H_{10}). The molar production will be described in terms of C_1, C_2, C_3 and C_4 hydrocarbons, being 1 to 4 the number of carbon atoms in the molecules in order to simplify the discussion about the reaction selectivity. Nevertheless, methane was the major product in all cases, and minor amounts of other detected products (probably C4 isomers, or C5, hydrocarbons) have not been quantified.

It should be remarked that an ‘induction period’ [6] was not observed and the reaction products were detected since the beginning of the monitoring; this is

ascribed to the mesoporosity of the samples which favours a good accessibility to the electrolyte inside the porous network, together with the fact that electrodes were submerged in the electrolyte overnight and before of starting the reaction. Nevertheless, the adsorption of a part of the products in the porous structure of the carbon gel cannot be ruled out.

On the other hand, before the discussion, it is necessary to clarify that when an electrolyte free of dissolved CO_2 was used (that is, carrying out the reaction under Ar-saturated solution) hydrocarbons, CO or CO_2 were not detected in any case. Similarly, in presence of CO_2 (normal experimental reaction conditions) and using cathodes of both pure phases (graphite sheet, un-doped carbon xerogel sheet or iron sheet), no hydrocarbons were detected.

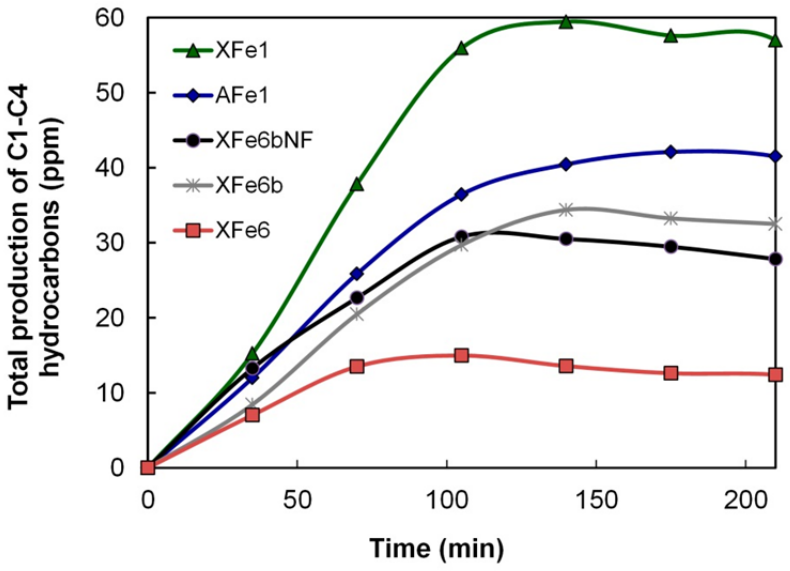

Figure 4.7. Molar production versus time obtained with the electro-catalysts.

Data of the total molar productions of hydrocarbons in the reactor are collected in Figure 4.7. After one hour of reaction the following tendency can clearly be observed: XFe1 > AFe1 > XFe6bNF > XFe6b > XFe6, which is in agreement with the apparent faradaic efficiencies calculated at 70 min of reaction time (Table 4.3).

Table 4.3. Apparent faradaic efficiencies (F.E.) for the electro-catalytic CO_2 reduction determined at 70 min of reaction time at −1.65 V *vs.* Ag/AgCl.

Cathode / Electro-catalyst	F.E. (%)
AFe1	0.42
XFe1	0.61
XFe6	0.10
XFe6b	0.26
XFe6bNF	0.30

It has to be clarified that only the detected hydrocarbons (nor H_2 neither O_2 formation) have been included in the faradaic efficiencies calculations.

The first observation is that electro-catalysts based on doped carbon gels with the lowest Fe loading are the most active, and in particular XFe1. On the other hand, the carbon xerogel-CNF composite works better than both, XFe6 and XFe6b, i.e., carbon xerogels with similar Fe loading. It should be mentioned that cathodes were used in a second run of reaction renovating the electrolyte and saturating with CO_2; all of them showed again similar profiles than those collected in Figure 4.7. After drying, no significant weight differences were appreciated

between the cathodes after first and second runs. Iron leaching in the liquid solutions was studied in all cases by ICP-OES. The detected iron concentrations in the liquids were always lower than 100 ppb, which means that Fe leaching was not higher than 0.5 wt. % of the metal phase in the worst case. Figure 4.8 compares the LSV curves of CO_2 reduction obtained with all electro-catalysts. The increase of the current values at -1.65 V of the electro-catalysts shows a tendency opposite to their apparent activities and faradaic efficiencies

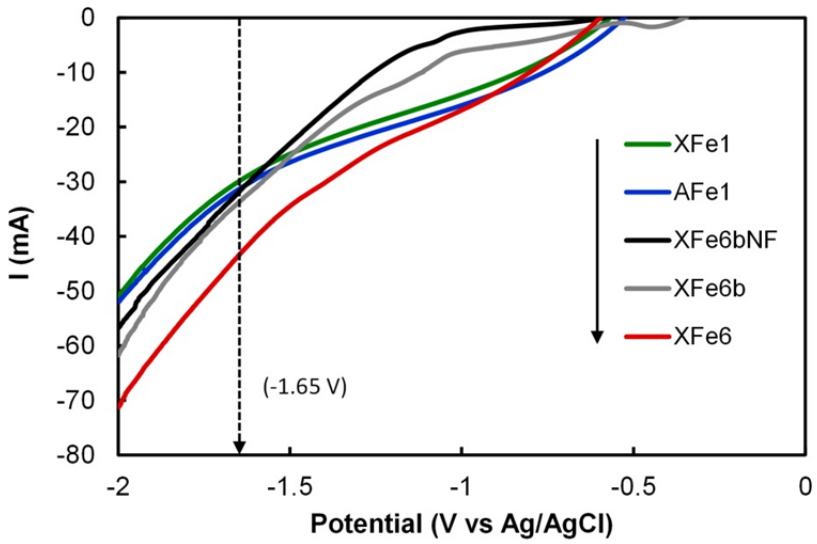

Figure 4.8. Linear sweep voltammetries obtained from the equilibrium electrode potential to a negative electric potential of −2.00 V vs. Ag/AgCl. Scan rate: 5 mV/s. Fresh electrodes in CO_2 saturated 0.1M $KHCO_3$.

.

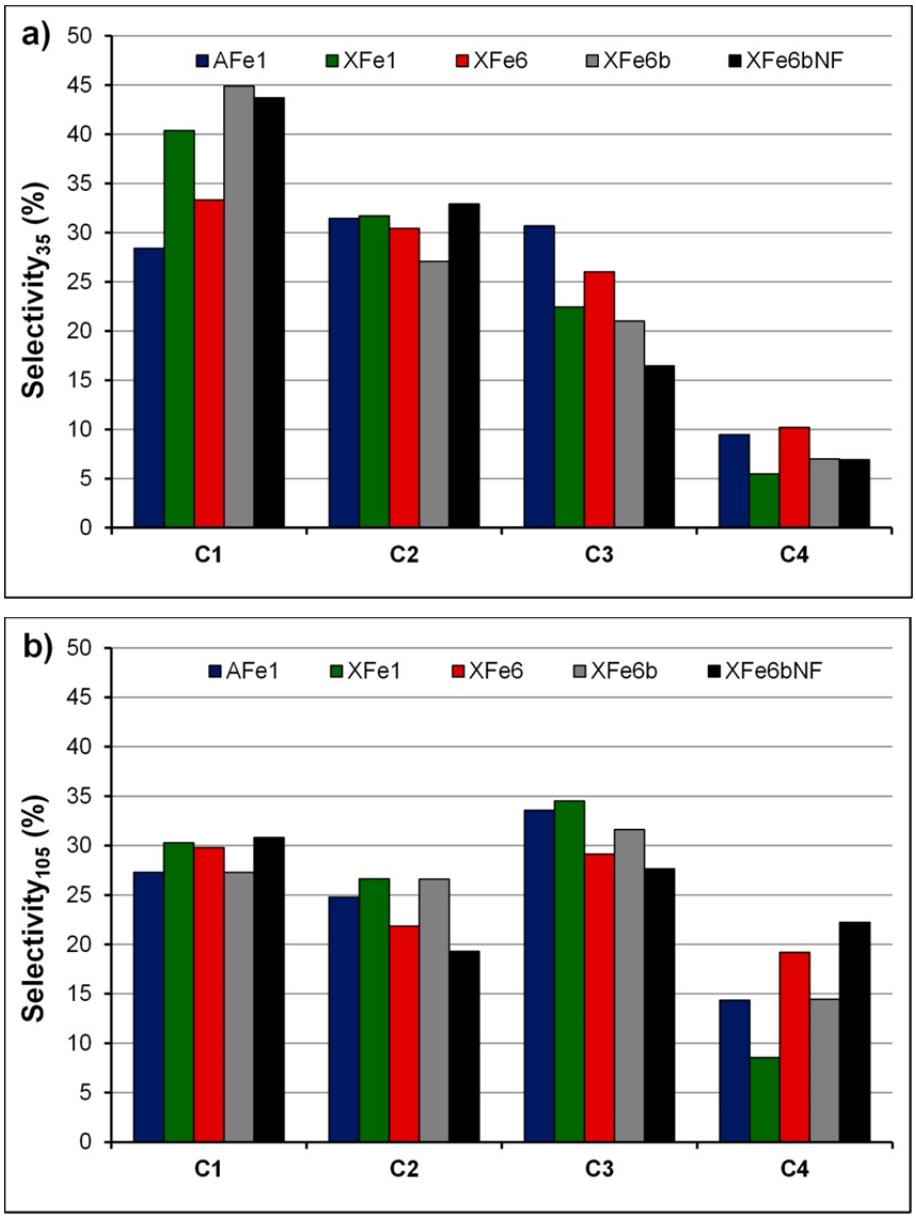

Figure 4.9.- Product distribution (%) in terms of carbon selectivity in gas phase products after 35 and 105 min of reaction time.

Regarding to the selectivity of these materials to the hydrocarbon formation, Figure 4.9 contains these data at two reaction times, 35 and 105 min. It can be observed that the selectivity not only depends on the reaction time, but also of the type of cathode used. Once the maximum production of hydrocarbons is apparently close to be achieved in the reactor (around 100 min of reaction time), all electro-catalysts show high selectivity to C3 hydrocarbons, even more, XFe1 and AFe1 clearly show higher selectivity to C3 hydrocarbons than to CH_4 (Figure 4.9b). The XFe6bNF composite is the most selective to C4 products.

4.4.- DISCUSSION

Taking in account all characterization data introduced in the previous section, Fe-doped carbon gels are materials with a well-developed porosity. The highest Fe loading seems to increase the mesoporosity (V_{BJH}), while the small Fe loadings of 1 wt.% produce a particular morphology in shape of partially overlapped microspheres with large macroporous openings among them. The development of CNFs in the xerogel matrix leads to a strong reduction of the initial microporosity of the XFe6b support.

Iron crystalline phases are well-dispersed and distributed mainly into the carbon matrix. Fe particles are anchored or mainly embedded in the carbon matrix with a broad range of nano-metric sizes and mostly with a zero oxidation state, although small amounts of iron oxides on the external surface also have been detected. Iron particles have catalysed the development of graphite clusters during the carbonization process and thereby, a very low iron percentage only has been

detected in the external non-porous surface area of samples with the highest Fe loading, with the exception of the carbon xerogel – CNF composite (XFe6bNF), in which the majority of the iron particles are embedded in the composite matrix, part of them inside of the hollow CNFs.

From the catalytic point of view, the adequate comparison of the behaviour of these materials is not straightforward because the tested materials do not present similar textural characteristics or iron loadings. However, it is demonstrated that all Fe-doped carbons gel work as electro-catalysts in this reaction, and they are able to produce the CO_2 transformation to at least C4 hydrocarbons, showing a high selectivity to C3 products over long reaction times. Among all tested materials, XFe6bNF composite is the most selective to C4 products.

Analysing more deeply the electro-catalytic results from Figure 4.7, we can see that the rate of hydrocarbon formation apparently tends to decrease after ~100 min of reaction depending on the sample. This type of catalytic behaviour has been previously observed [7] and explained by a high formation of H_2 and O_2, which can provoke a dilution effect of the hydrocarbon formation in the gas phase of the reactor [8], although a partial adsorption of hydrocarbons inside the porosity cannot be discarded. On the other hand, the absence of stirring and the continuous consumption of the reaction product may result in a locally CO_2 deplete, and after certain time the active sites could suffer a mass transfer limitation of the still available CO_2 in the solution. Other authors have reported deactivation processes as consequence of poisoning of the active sites [9], but it does not seems to justify our results since very similar profiles were obtained in a second run using the same electro-catalysts.

On the other hand, the activity trend XFe1 > AFe1 > XFe6bNF > XFe6b > XFe6 cannot be only justified neither by the metal loading nor by the textural characteristics of the samples. XFe1 and AFe1 present very comparable textural properties, iron loading (1 wt.%) and morphology but they produce different significant amounts of hydrocarbons. XFe6 with a high iron content shows the highest V_{BJH} value and BET surface area; however its electro-catalytic behaviour is apparently the worst. The results obtained in a previous work [7] concerning cobalt-doped carbon gels pointed out to a possible influence of the metal particle size on the activity of the electro-catalysts, being the cathode with a lower Co loading and smaller mean particle size, more active than other with higher Co loading and larger mean particle size of cobalt. Therefore, taking into account that the catalysts of this work present large differences of mean iron particle size, the d_{DRX} values (Table 4.2) have been plotted against the faradaic efficiency (F.E.) in Figure 4.10, and a clear relationship can be observed: the smaller the d_{DRX}, the higher the F.E. The well-fitted linear dependence between d_{DRX} and F.E. values cannot obviously exclude other important factors that have not been normalized for an adequate comparison, such as the iron loading or the porosity. Nevertheless, in our opinion the results of this work show clear evidence that the iron particle size is a crucial parameter involved in the hydrocarbon formation. In addition, the commercial iron sheet did not work under the same experimental conditions, while iron nano-particles smaller than 4 nm seem to increase significantly the formation of hydrocarbons. Recently, electro-catalysts based on Au [10] and Ag [11] reached similar conclusions in the case of CO_2 reduction to CO, but for the best of our knowledge, no previous work has been found in the

literature describing this particle size effect with iron-based electro-catalysts applied to the CO_2 reduction to hydrocarbons.

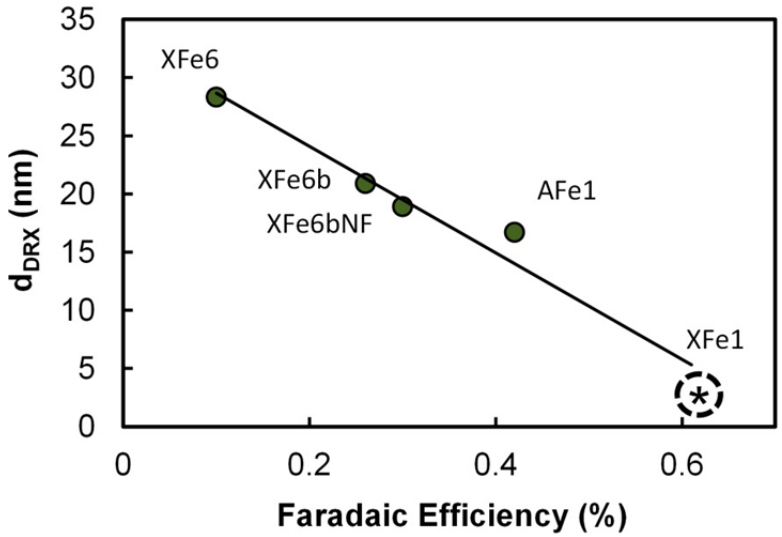

Figure 4.10.- Mean iron particle size obtained by XRD *versus* faradaic efficiency obtained at 70 min of reaction time. (*) Mean iron particle size < 4nm.

Finally, the high selectivity to C3 obtained with the iron-doped carbon gels and the good selectivity to C4 obtained with the carbon xerogel – carbon nanofiber composite should be also remarked. These results have also evidenced that the selectivity in the products of CO_2 reduction on iron-doped carbon gels electrodes should depend on both the characteristic of carbon matrix itself and the nature of the metal nanoparticles; this influence on the selectivity and product distribution of the carbon support has been also recently proposed when Co-doped carbon gels [7], and Fe supported on carbon nanotubes [12] were used as electrodes in the CO_2 reduction.

CONCLUSIONS

Different types of carbon gels doped with iron, in particular an aerogel, three xerogels with different iron contents, and a carbon xerogel – carbon nanofiber composite have been prepared to be used as cathodes for the electro-catalytic reduction of CO_2 to hydrocarbons, at atmospheric pressure. All electro-catalysts promoted the formation of C1 to C4 hydrocarbons showing a high selectivity to C3 hydrocarbons. The carbon xerogel – carbon nanofiber composite was the most selective to C4 hydrocarbons, even over long time reaction. The iron particle size is a very important parameter involved in the hydrocarbon formation. A well-fitted linear correlation between mean iron particle sizes obtained by XRD and the faradaic efficiency has been found among all electro-catalysts of this work: the smaller the d_{DRX}, the higher the F.E.

BIBLIOGRAPHY

[1] Gallegos-Suarez E.; Perez-Cadenas, A.F.; Maldonado-Hodar, F.J.; Carrasco-Marin, F. On the micro- and mesoporosity of carbon aerogels and xerogels. The role of the drying conditions during the synthesis processes. *Chem. Eng. J.* **2012**, *181-182*, 851-855.

[2] Shibata H.; Moulijn, J.A.; Mul, G. Enabling electrocatalytic Fischer-Tropsch synthesis from carbon dioxide over copper-based electrodes. *Catal. Lett.* **2008**, *123*, 186-192.

[3] Maldonado-Hodar F.J.; Moreno-Castilla, C.; Perez-Cadenas, A.F. Surface morphology, metal dispersion, and pore texture of transition metal-doped monolithic carbon aerogels and steam-activated derivatives. *Micropor. Mesopor. Mat.* **2004**, *69*, 119-125.

[4] Maldonado-Hodar F.J.; Moreno-Castilla, C.; Rivera-Utrilla, J.; Hanzawa, Y.; Yamada, Y. Catalytic graphitization of carbon aerogels by transition metals. *Langmuir* **2000**, *16*, 4367-4373.

[5] Schwan J.; Ulrich, S.; Batori, V.; Ehrhardt, H.; Silva, S.R.P. Raman spectroscopy on amorphous carbon films. *J. Appl. Phys.* **1996**, *80*, 440-447.

[6] Perez-Cadenas A.F.; Ros, C.H.; Morales-Torres, S.; Perez-Cadenas, M.; Kooyman, P.J.; Moreno-Castilla, C.; Kapteijn, F. Metal-doped carbon xerogels for the electro-catalytic conversion of CO_2 to hydrocarbons. *Carbon* **2013**, *56*, 324-331.

[7] Abdelwahab A.; Castelo-Quibén, J.; Pérez-Cadenas, M.; Elmouwahidi, A.; Maldonado-Hódar, F.J.; Carrasco-Marín, F.; Pérez-Cadenas, A.F. Cobalt-doped carbon gels as electro-catalysts for the reduction of CO_2 to hydrocarbons. *Catalysts* **2017**, *7*, 25

[8] Goncalves M.R.; Gomes, A.; Condeco, J.; Fernandes, R.; Pardal, T.; Sequeira, C.A.C.; Branco, J.B. Selective electrochemical conversion of CO_2 to C_2 hydrocarbons. *Energy Convers. Manage.* **2010**, *51*, 30-32.

[9] Hori Y.; Konishi, H.; Futamura, T.; Murata, A.; Koga, O.; Sakurai, H.; Oguma, K. "Deactivation of copper electrode" in electrochemical reduction of CO_2. *Electrochim. Acta* **2005**, *50*, 5354-5369.

[10] Nursanto E.B.; Jeon, H.S.; Kim, C.; Jee, M.S.; Koh, J.H.; Hwang, Y.J.; Min, B.K. Gold catalyst reactivity for CO_2 electro-reduction: From nano particle to layer. *Catal. Today* **2016**, *260*, 107-111.

[11] Back S.; Yeom, M.S.; Jung, Y. Active Sites of Au and Ag Nanoparticle Catalysts for CO_2 Electroreduction to CO. *ACS Catal.* **2015**, *5*, 5089-5096.

[12] Genovese C.; Ampelli, C.; Perathoner, S.; Centi, G. Electrocatalytic conversion of CO_2 on carbon nanotube-based electrodes for producing solar fuels. *J. Catal.* **2013**, *308*, 237-249.

CHAPTER V: CARBON AEROGELS DOPED WITH TRANSITION METALS FOR OXYGEN REDUCTION REACTION CATALYSTS

5.1.- ABSTRACT

A series of carbon aerogels doped with iron, cobalt and nickel were prepared. Samples with different Ni content were obtained in order to test the influence of the metal proportion. Samples were characterized to analyse their textural properties, surface chemistry and crystal structures. These metal doped gels are materials with a very well developed porosity, all of them with a remarkable mesoporosity. Ni doped carbon xerogels were the ones with the largest surface area and the smallest graphitization. They also presented larger mesopore volumes than Co and Fe doped xerogels. These materials were tested as electro-catalysts for oxygen reduction reaction. Results showed a strong influence of carbonaceous structure on electro-catalytic behaviour of aerogels. In fact, aerogel doped with Ni was the most active one, followed by Fe and Co doped ones which presented similar results. As the Ni content was larger, E^0_{onset} was reduced and kinetic current densities were increased.

5.2.- EXPERIMENTAL

5.2.1.- Preparation and characterization of the materials

Carbon aerogels doped with Ni, Co and Fe were prepared by dissolving resorcinol (R) and formaldehyde (F) in water (W) and using the corresponding metal acetate as catalyst precursor (C). The used (R/F) and molar ratio (R/W) were 1:2 and 1:17 respectively. Different amounts of C were used in order to obtain three different Ni loadings (1, 4 and 6 wt.%, approx.) among de final carbon aerogels. Fe and Co doped aerogels were prepared only with a 6 wt.%, approx. of metal loading. The mixture was stirred to obtain homogeneous solutions that were cast into glass moulds and cured 1 day at 40 ºC, and 5 days at 80 ºC, obtaining the corresponding organic aerogels. Then, the organic aerogels were introduced in acetone to exchange the solvent media. After that the organic aerogels were dried using supercritical CO_2. Finally, the organic aerogels were carbonized in a N_2 flow at a 900 ºC during 5 h, and using a heating rate of 1 ºC/min. The names of the obtained carbon aerogels (A) were the following: ANi1, ANi4, ANi6, AFe6 and ACo6, indicating the numbers the approximate percentage of metal content. The cobalt contents of the samples were determined by burning off a portion of carbon gel at 800 ºC in air and weighting the residue.

The characterization of the samples was carried out using gas adsorption, scanning electron microscopy (SEM), high resolution transmission electron microscopy (HRTEM), Raman spectroscopy, X-ray diffraction (XRD), X-ray photoelectron spectroscopy (XPS). Samples performance for Oxygen Reduction Reaction was tested by means of cyclic voltammetry (CV) and linear sweep voltammetry (LSV).

5.2.2.- Electro-chemical studies Oxygen reduction reaction

Cyclic Voltammetry (CV) and Linear Sweep Voltammetry (LSV) experiments were conducted on a three electrode cell controlled by a Biologic VMP multichannel potentiostat. A Rotating Disk Electrode (RDE) Metrohm AUTOLAB RDE-2 with a 3 mm Glassy Carbon tip, was used as working electrode. 5 mg of electro-catalyst were suspended on 1 mL of a solution which contained Nafion (5%) and water in a 1:9 (v:v) ratio. Subsequently, 10 μL of this suspension were loaded on RDE tip and dried under an infrared lamp [1]. The glassy carbon electrode had been previously polished with 1, 0.3 and 0.05 μm alumina powder and sonicated in deionized water and ethanol. Ag/AgCl was chosen as reference electrode and Pt-wire as counter electrode. The three electrodes were immersed in a 0.1M KOH (electrolyte) solution in water.

Oxygen reduction reaction may occur by two different pathways: One implies the formation of peroxide species (Equation 1) which could damage the electro-catalytic layer and a 2 e^-_s transference and it is undesired; the other leads only to the formation of hydroxide and it occurs by a 4 e^-_s (Equation 2) which is the wished one.

$$O_2 + H_2O + 2\,e_s^- \rightarrow HO_2^- + OH^- \qquad \text{Equation 1}$$

$$O_2 + 2\,H_2O + 4\,e_s^- \rightarrow 4\,OH^- \qquad \text{Equation 2}$$

CV experiments were carried out while N_2 or O_2 bubbled through the electrolyte solution during measurements. The chosen potential window ranged from -0.8 to 0.4 V (at 5 $mV \cdot s^{-1}$ and 50 $mV \cdot s^{-1}$). LSV curves were obtained in O_2-

saturated 0.1 M KOH solutions at different rotation speed and sweeping voltage, from 0.4 to -0.8 V (5 $mV \cdot s^{-1}$). Data were fitted to the Koutecky-Levich model (Equations 3 and 4) in order to evaluate the electro-catalytic performance of samples and the transferred electron number for each of them [1].

$$\frac{1}{j} = \frac{1}{j_k} + \frac{1}{B\omega^{0.5}} \qquad \text{Equation 3}$$

$$B = 0.2nF(D_{O_2})^{2/3}v^{-1/6}C_{O_2} \qquad \text{Equation 4}$$

where j, current density; j_k, kinetic current density; ω, rotation speed; F, Faraday constant; D_{O2}, oxygen diffusion coefficient ($1.9 \cdot 10^{-5} cm^2 \cdot s^{-1}$); ν, viscosity ($0.01 cm^2 \cdot s^{-1}$); C_{O2}, oxygen concentration ($1.2 \cdot 10^{-6}$ $mol \cdot cm^{-3}$).

5.3.- RESULTS

Table 5.1 summarizes the used names, the surface areas and pore volumes of the metal-doped carbon aerogels prepared in this work. All of them are microporous and mesoporous materials, with remarkable mesopore volumes and apparent surfaces areas.

Aerogels doped with Ni have the highest surface areas and pore volumes, specially the highest micropore volumes; among the Ni samples ANi6 is the more microporous material. In the opposite site, AFe6 has the lower surface area and pore volumes.

The carbon gel morphology, which was studied by SEM (Figure 5.1), is typical for R-F carbon gels showing a carbon network formed by nearly spherical

particles with different degree of fusion [2], and where also a well-developed macroporous structure can be observed. Apparently there are no significant morphological differences on the non-porous external surface among all metal doped aerogels.

Table 5.1. Name, surface areas and pore volumes of the doped carbon gels**.**

Sample	S_{BET} m^2/g	W_0 (N_2) cm^3/g	L_0 (N_2) nm	W_0 (CO_2) cm^3/g	L_0 (CO_2) cm^3/g	$V_{0.95}$ (N_2) cm^3/g	V_{BJH} (N_2) cm^3/g
ANi1	663	0.258	1.07	0.276	0.63	0.82	1.70
ANi4	685	0.268	0.96	0.280	0.63	0.71	1.60
ANi6	698	0.273	0.90	0.294	0.64	0.69	1.58
ACo6	589	0.230	1.00	0.181	0.57	0.65	1.56
AFe6	461	0.177	1.00	0.182	0.62	0.41	0.61

Regarding the metal phase characterization, metals are situated mainly embedded within the carbon matrix, as confirmed by HRTEM and EDAX analysis; the metal particles can be clearly observed in Figure 5.2 and 5.3, in which they are very well dispersed throughout the carbon matrix showing a wide range of sizes within a nanometric scale. Moreover, the presence these metallic nanoparticles inside of the organic matrix have catalysed the development of graphite clusters around the metal particles, during the carbonization process, in all the samples; two examples of these graphitic lines can be observed in Figure 5.2, samples ANi6 and AFe6. This partial graphitization of the carbon aerogel structure has been also observed in previous works [3,4] with Co, Fe and Ni as doping metals. This can be also detected by XRD as a broad peak at around 26

θ specially in the case of aerogels ACo6 and AFe6 (Figure 5.4), although this signal hardly can be observed in the case of the Ni doped samples, which would indicate that the graphitic clusters in the Ni samples should have mean sizes smaller than 4 nm or a very slim laminar shape.

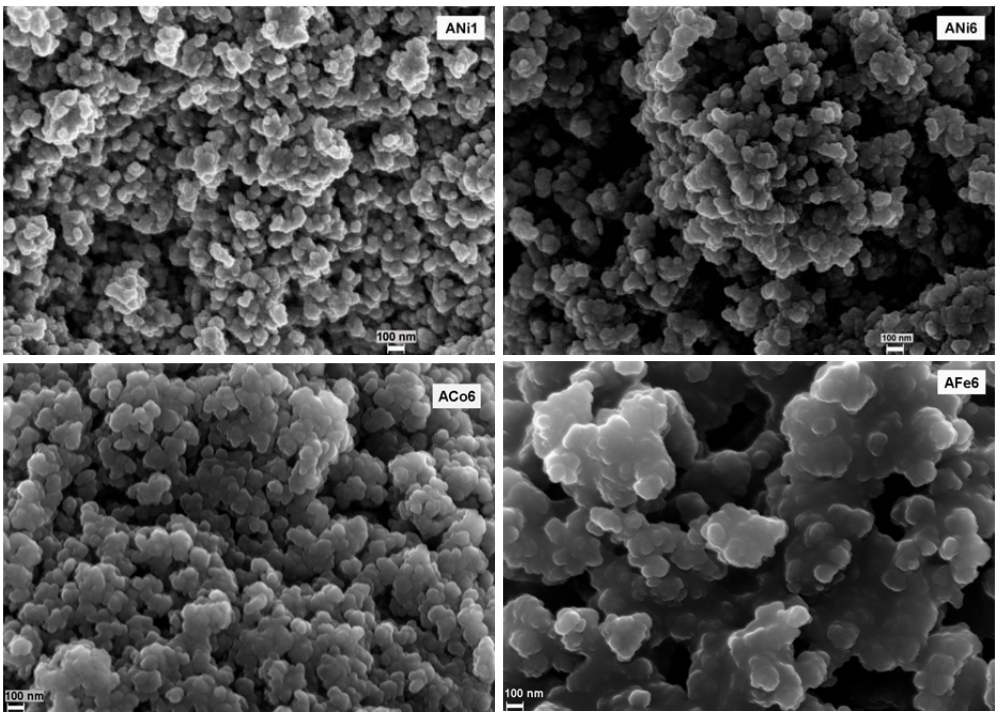

Figure 5.1. SEM microphotographs obtained at 100.00 KX of magnification of samples ANi1, ANi6, ACo6 and AFe6.

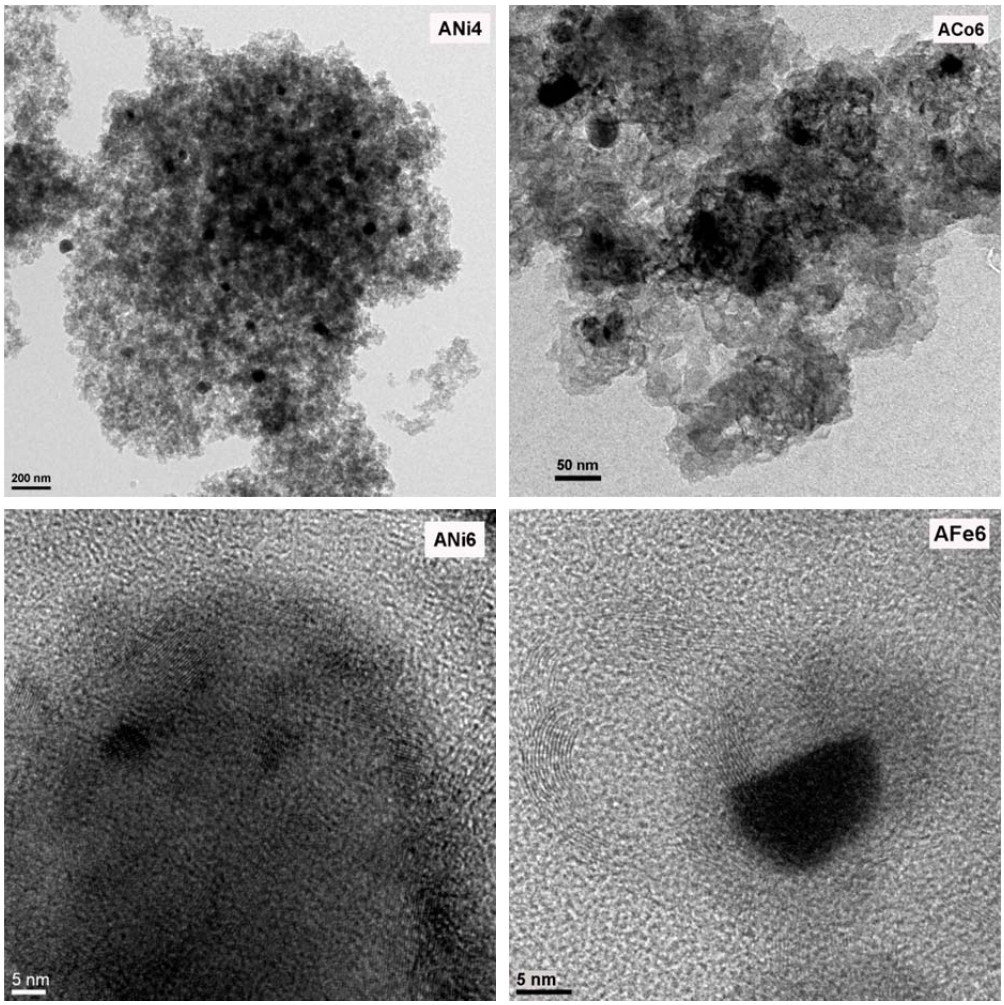

Figure 5.2. HRTEM images of the samples ANi4, ACo6, ANi6 and AFe6.

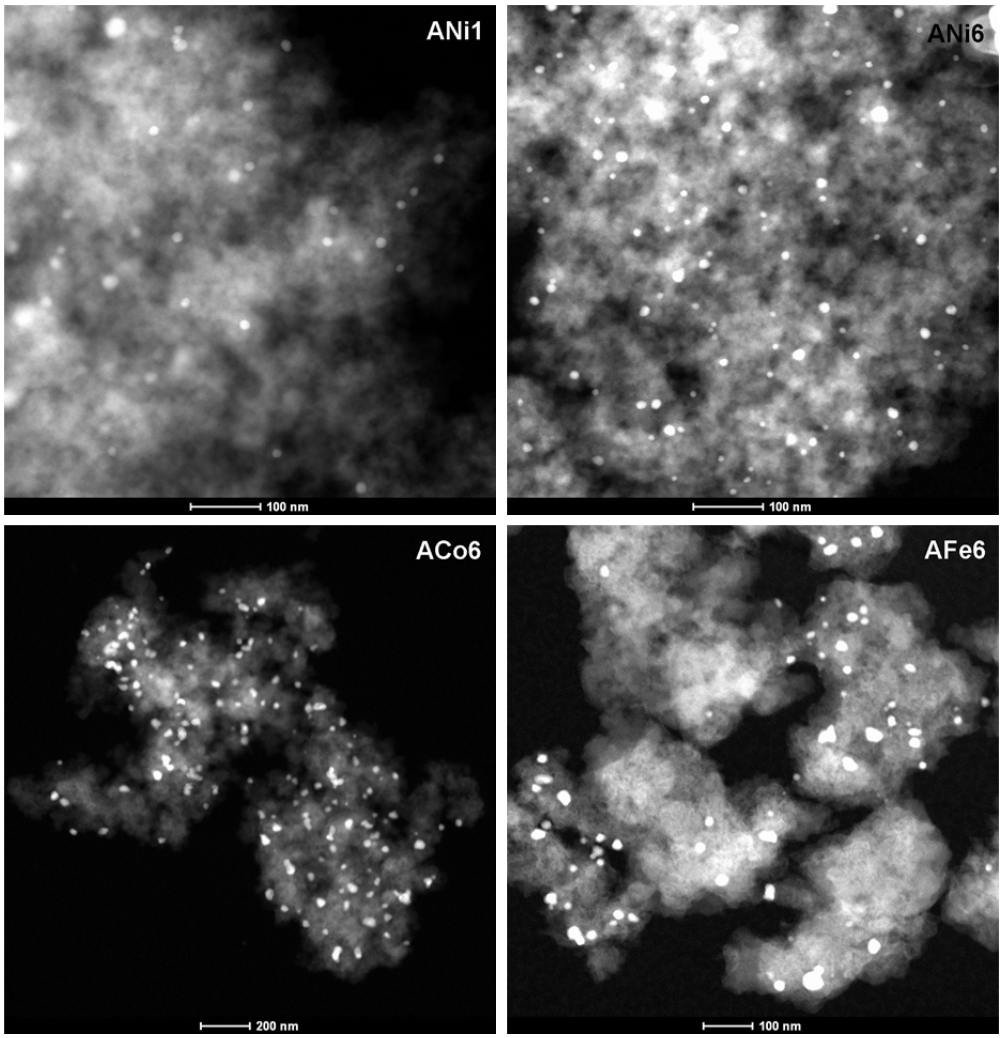

Figure 5.3. AEM spectra collected in STEM mode using a HAADF detector of the samples ANi4, ACo6, ANi6 and AFe6

On the other hand, the XRD peaks in Figure 5.4 clearly show the presence of Ni and Co completely reduced. Only in the case of sample AFe6 a mixture of Fe(0) (peaks at 44.6, and 65.2º) and Fe(III) (at 43.5º) are detected.

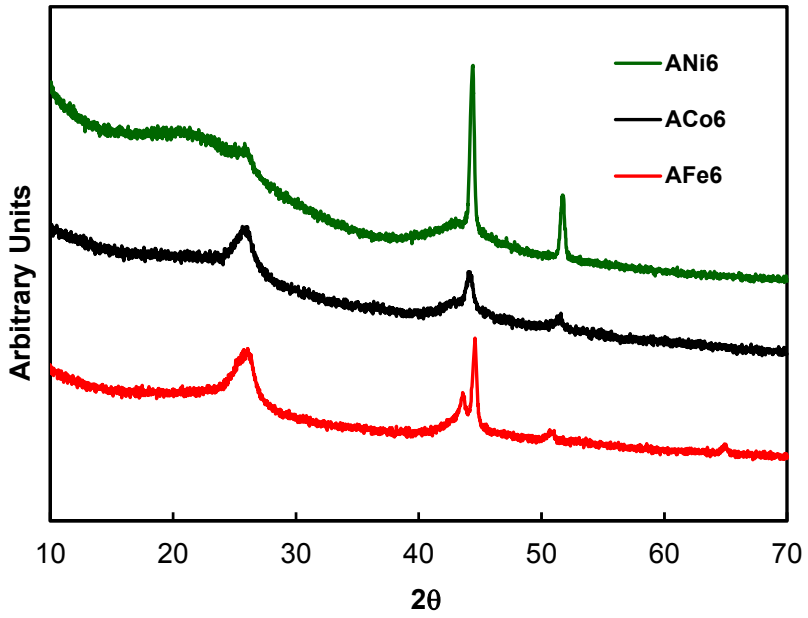

Figure 5.4. XRD patterns of samples ANi6, ACo6 and AFe6

Analysing the XPS spectra no peaks corresponding with metal phases can be clearly distinguished from the base line in the case of ANi1 and ANi4, therefore the Ni concentration on the external surface of these carbon gels is considered negligible. Only Ni, Co and Fe2p spectra of samples with 6 wt.% could be deconvoluted. Figure 5.5 shows in the Ni2p spectra only one $Ni2p_{3/2}$ signal at 853.3 eV which is assigned to Ni (II); its corresponding satellite peak can be clearly observed at 859.8 eV. In this line, only one $Co2p_{3/2}$ signal can be also

observed at 781.1 eV of B.E together its corresponding satellite at 786.1 eV, which is also assigned to Co (II) species. Finally, the Fe2p spectra shows two different type of iron species at 710.7 and 712.7 eV which are assigned to Fe_2O_3 (76.5%) and Fe_3O_4 (23.5%), respectively.

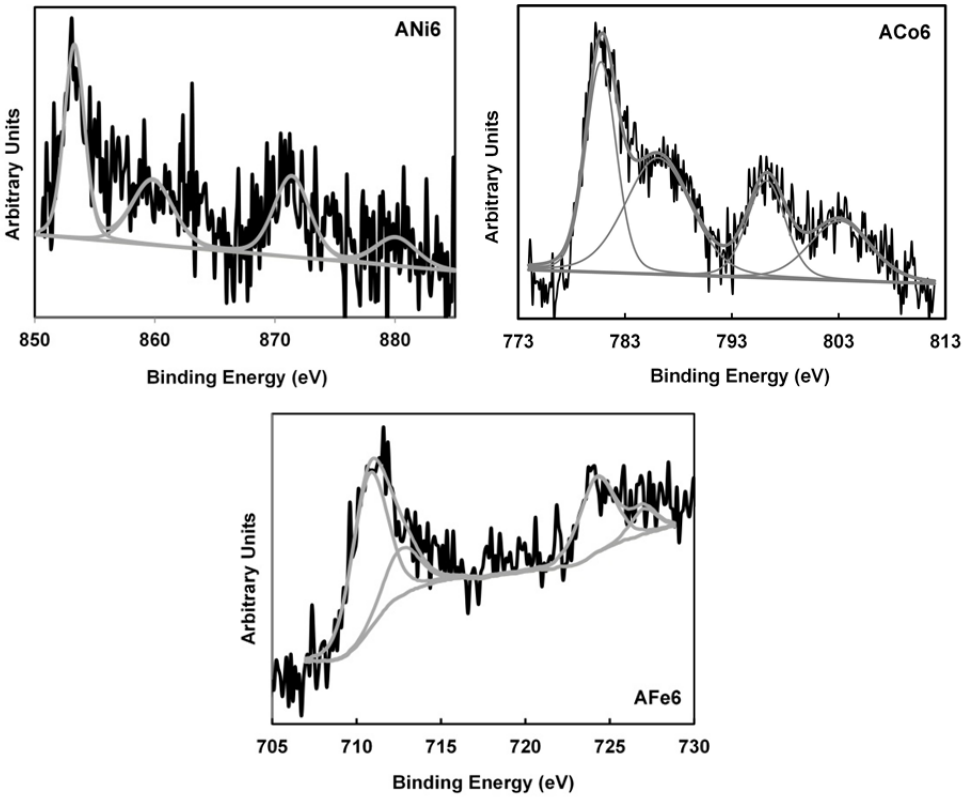

Figure 5.5. XPS spectra of the doped carbon aerogels.

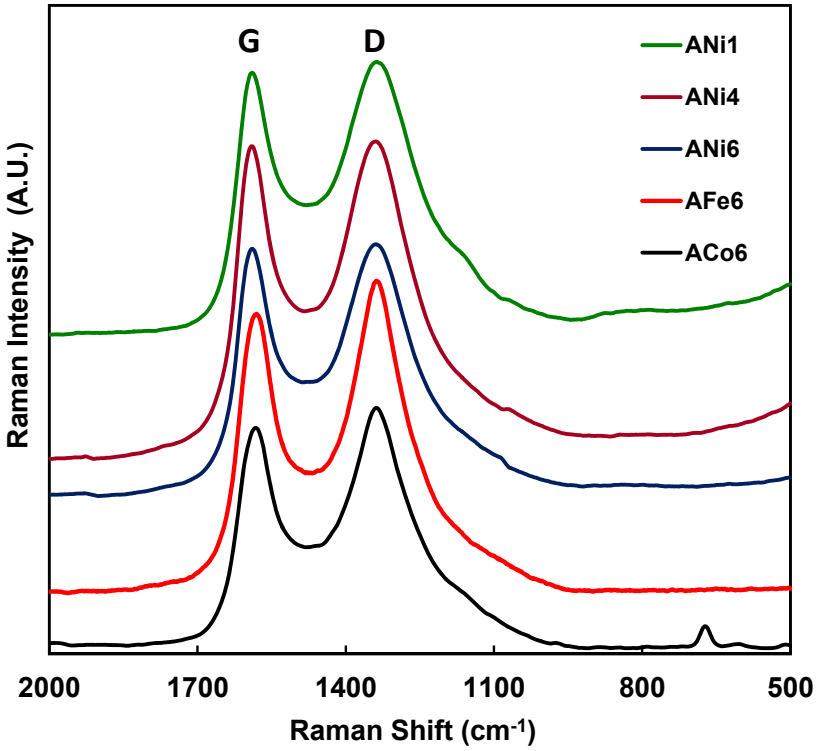

Figure 5.6. Raman spectra of the doped carbon aerogels.

Figure 5.6 shows two main signals in the Raman spectra at 1340 and 1580 cm^{-1} approx. corresponding to D and G bands respectively [5]. It is known that carbon gels are considered as amorphous carbon materials, therefore the presence of these bands should be analysed into this context: in this type of materials, D band would be associated with alternating ring vibrations in condensed benzene rings [5], while G band would be associated to the development of the sp^2 carbon structure thought out the material during the carbonization process. It should be noted than the intensity of the G band (I_G) with respect with its D band (I_D) is

higher in the Ni doped aerogels than in the case of Fe or Co samples, and among the Ni samples this ratio I_G/I_D is clearly higher in ANi6 and ANi4 than in ANi1.

Metal particle sizes estimated by applying the Scherrer equation, chemical composition obtained by XPS and total metal content of the samples are collected in Table 5.2. Among the Ni samples, the main cobalt particle size clearly decreases with the metal loading; however the samples ANi6, ACo6 and AFe6 show very similar value around 21 nm.

Table 5.2. Chemical characteristics of the carbon aerogels**.**

Sample	**$Metal_{TOTAL}$** **wt.%**	**$Metal_{XPS}$** **wt.%**	**O_{XPS}** **wt.%**	**d_{DRX}** **nm**
ANi1	1.2	n.d	1.6	15.9
ANi4	3.9	n.d	1.6	17.4
ANi6	5.8	0.3	2.5	21.1
ACo6	5.9	0.7	3.6	21.5
AFe6	6.1	0.4	2.9	21.6

n.d: no determined

Regarding Rotating Disk Electrode (RDE) experiments, cyclic voltammetry was used in order to observe the difference between samples behaviour on N_2-saturated electrolyte (KOH 0.1M) and O_2-saturated one. Figure 5.7 shows CV curves for ANi6 sample at 5 $mV \cdot s^{-1}$ and at 50 $mV \cdot s^{-1}$, where a peak corresponding to oxygen reduction can be observed when the curve is obtained on O_2-saturated electrolyte.

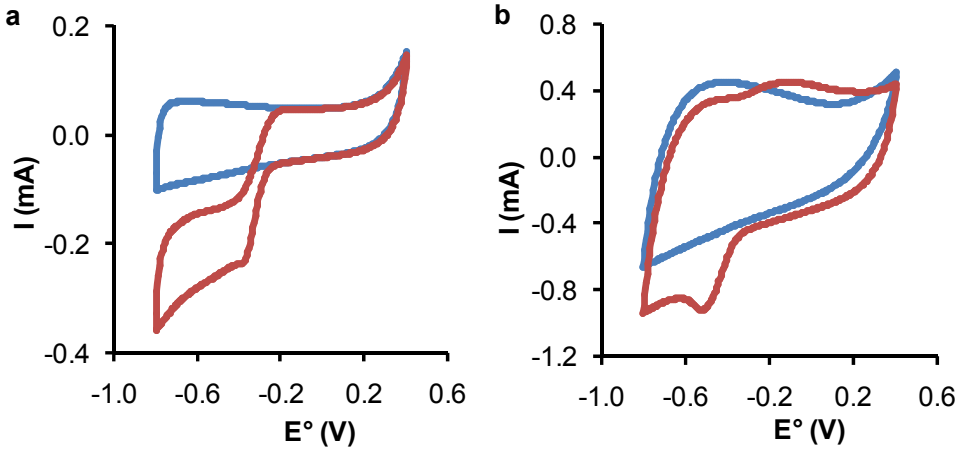

Figure 5.7. CV for ANi6 on N_2-saturated KOH 0.1 M (blue) and O_2-saturated KOH 0.1 M (red). a) 5 $mV \cdot s^{-1}$; b) 50 $mV \cdot s^{-1}$.

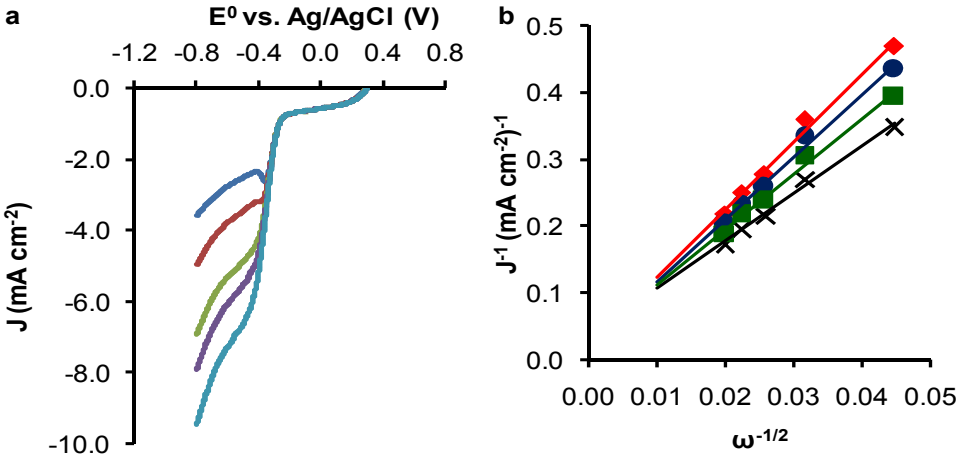

Figure 5.8. a) LSV for ANi6 at different RDE rotating speed. b) Koutecky-Levich fits at different potentials: from -0.5 (◆) to -0.8 V (×).

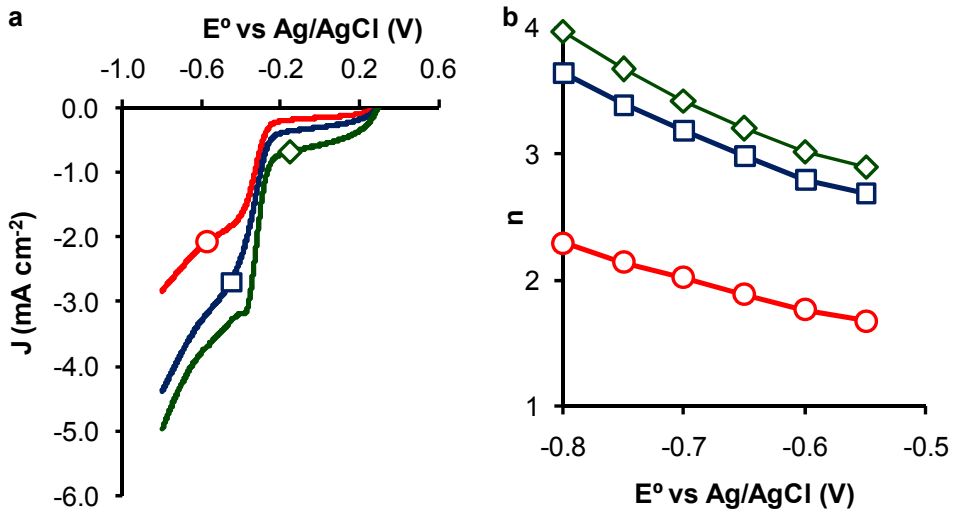

Figure 5.9. a) LSV curves at 1000 rpm, and b) variation of n with E^0 vs Ag/AgCl for samples ANi1 (○), ANi4 (□), ANi6 (◇).

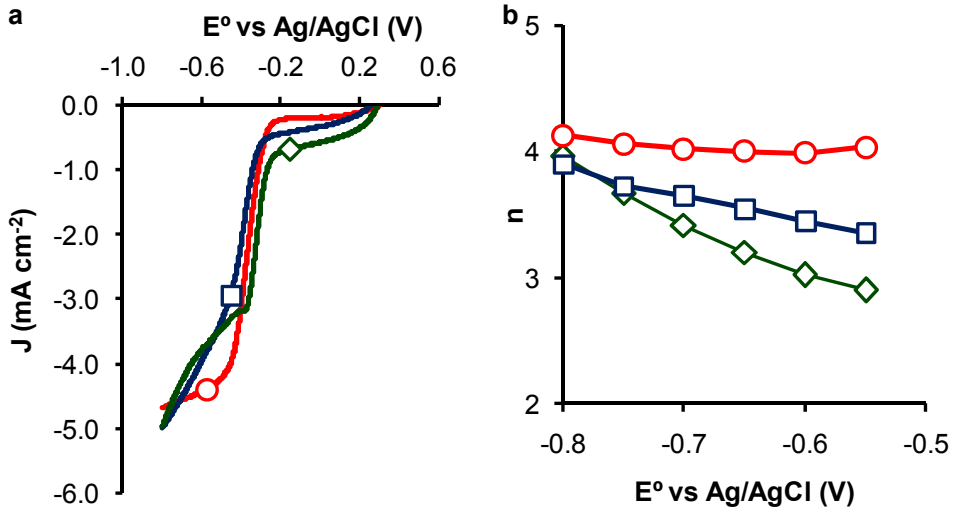

Figure 5.10. a) LSV curves at 1000 rpm, and b) variation of n with E^0 vs Ag/AgCl for samples AFe6 (□), ACo6 (○), ANi6 (◇).

After CV, Linear Sweep Voltammetry (LSV) was used to test the electro-catalytic performance of samples for oxygen reduction. The experiments were conducted at different rotating speed in order to apply Koutecky-Levich Equation. This analysis is shown in Figure 5.8 for ANi6 sample.

From this analysis the number of electrons transferred at a given potential can be obtained (Table 5.3). Aerogels with different content in Ni where tested in order to analyse the influence of the metal content in electro-catalytic behaviour of samples on LSV (Figure 5.9.a) and number of electron transferred (Figure 5.9.b). Finally, aerogels with different metals (ANi6, ACo6 and AFe6) were compared as well (Figure 5.10).

Table 5.3. Parameters obtained from the analysis of LSV curves (values of n refer to K-L fitting for data at -0.8V)**.**

Sample	$\mathbf{E^0_{onset}}$ **V**	$\mathbf{j_k}$ **mA·cm^{-2}**	**n**
ANi1	-0.25	11.1	2.3
ANi4	-0.24	19.8	3.6
ANi6	-0.23	27.7	4.0
ACo6	-0.25	21.7	4.1
AFe6	-0.26	22.3	3.9

5.4.- DISCUSSION

Taking in account all characterization data collected in Section 5.3, we can conclude that these metal doped gels are materials with a very well developed porosity, all of them with a remarkable mesoporosity. Aerogels doped with Ni have the highest surface areas and pore volumes, specially the highest micropore volumes. The metal phase is well dispersed and distributed mainly into the carbon matrix in all cases, and the metal particles show a broad range of nano-metric sizes, being them mainly embedded in the carbon matrix with a zero oxidation state, only with the exception of sample AFe6 which has a mixture of Fe (0) and Fe(III); while a very low percentage of the metal would be situated in the external non porous surface area, being these particles partially oxidized. The carbon matrix macro-structure is very similar among the samples; thus, a partial graphitization process around the metal particles has also been detected in the case of the three different metals. In this line carbon aerogels doped with Ni seem to have the smallest and the best developed graphitic cluster.

Regarding electro-catalytic experiments, it can be observed that increasing Ni loading improved the electro-catalytic performance of the aerogel (Figure 5.9). In fact, when the Ni percentage was really small (ANi1), the oxygen reduction occurred by the unwished $2e^-_s$ mechanism. As the Ni content increased the number of electron transferred did too and oxygen reduction occurred with an electronic transfer of 4 e^-_s on both ANi4 and ANi6. Also the reaction started at lower potentials as denoted by the change on E^0_{onset} (Table 5.3).

With respect to the type of metal, small differences are observed (Figure 5.10), being ANi6 the sample where the oxygen reduction occurs at lower E^0_{onset} and with larger current densities. According to bibliography [6-8] the order on

electro-catalytic activity should be Fe > Co > Ni, and this would be related to the ability of the metal to produce the dissociation of the oxygen molecule. Nevertheless, in the case of our sample, it needs to be considered the larger micropore volume and the smaller size of graphitic clusters in the case of ANi6 sample. In fact, electro-catalytic behaviour of carbon materials on Oxygen Reduction Reaction is closely related to the type of carbon structure present on the material and to its porosity. The presence of edge defect on graphitic clusters favours the electro-catalytic performance [8-10]. As it was commented in previous paragraphs graphitic clusters for ANi6 are much smaller than in the case of AFe6 and ACo6 so its better performance could be related to it.

CONCLUSIONS

All the prepared samples showed a very promising behaviour in oxygen reduction reaction. The well-developed porosity joint to the proper dispersion in carbon surface lead to materials with very high electro-catalytic activity on ORR.
As expected, as the metal content was increased, the electro-catalytic behaviour improved. Nevertheless, ANi6 presented better results than AFe6 and ACo6, since E^0_{onset} was lower and j_k rose up to larger values for this material. This result contrasts with others found in bibliography which claim that cobalt and iron should be more active than nickel for ORR. However, other authors relate the electro-catalytic behaviour of carbon materials doped with transition metals to changes in carbon crystalline structure and porosity. This could be the case in our samples, since ANi6 is the one with the largest micropore and mesopore volumes and also the one with the smallest graphitic clusters. The presence of graphitic

domains with a large concentration of edge defect in ANi6 sample favours the electro-catalytic reduction of oxygen.

BIBLIOGRAPHY

[1] Elmouwahidi A.; Vivo-Vilches, J.F.; Pérez-Cadenas, A.F.; Maldonado-Hódar, F.J.; Carrasco-Marín, F. Free metal oxygen-reduction electro-catalysts obtained from biomass residue of the olive oil industry. *Chemical Engineering Journal* **2016**, *306*, 1109-1115.

[2] Maldonado-Hodar F.J.; Moreno-Castilla, C.; Perez-Cadenas, A.F. Surface morphology, metal dispersion, and pore texture of transition metal-doped monolithic carbon aerogels and steam-activated derivatives. *Micropor. Mesopor. Mat.* **2004**, *69*, 119-125.

[3] Maldonado-Hodar F.J.; Moreno-Castilla, C.; Perez-Cadenas, A.F. Surface morphology, metal dispersion, and pore texture of transition metal-doped monolithic carbon aerogels and steam-activated derivatives. *Micropor. Mesopor. Mat.* **2004**, *69*, 119-125.

[4] Maldonado-Hodar F.J.; Moreno-Castilla, C.; Rivera-Utrilla, J.; Hanzawa, Y.; Yamada, Y. Catalytic graphitization of carbon aerogels by transition metals. *Langmuir* **2000**, *16*, 4367-4373.

[5] Schwan J.; Ulrich, S.; Batori, V.; Ehrhardt, H.; Silva, S.R.P. Raman spectroscopy on amorphous carbon films. *J. Appl. Phys.* **1996**, *80*, 440-447.

[6] Sarapuu A.; Kreek, K.; Kisand, K.; Kook, M.; Uibu, M.; Koel, M.; Tammeveski, K. Electrocatalysis of oxygen reduction by iron-containing nitrogen-doped carbon aerogels in alkaline solution. *Electrochimica Acta* **2017**, *230*, 81-88.

[7] Sarapuu A.; Samolberg, L.; Kreek, K.; Koel, M.; Matisen, L.; Tammeveski, K. Cobalt- and iron-containing nitrogen-doped carbon aerogels as non-precious metal catalysts for electrochemical reduction of oxygen. *Journal of Electroanalytical Chemistry* **2015**, *746*, 9-17.

[8] Chen Z.; Higgins, D.; Yu, A.; Zhang, L.; Zhang, J. A review on non-precious metal electrocatalysts for PEM fuel cells. *Energy Environ. Sci.* **2011**, *4*, 3167-3192.

[9] Chao S.; Zhang, Y.; Wang, K.; Bai, Z.; Yang, L. Flower–like Ni and N codoped hierarchical porous carbon microspheres with enhanced performance for fuel cell storage. *Applied Energy* **2016**, *175*, 421-428.

[10] Shin D.; An, X.; Choun, M.; Lee, J. Effect of transition metal induced pore structure on oxygen reduction reaction of electrospun fibrous carbon. *Catalysis Today* **2016**, *260*, 82-88.

CHAPTER VI: INSIGHT OF THE EFFECT OF GRAPHITIC CLUSTERS IN THE PERFORMANCE OF CARBON AEROGELS DOPED WITH NICKEL AS ELECTRODES FOR SUPERCAPACITORS

6.1.- ABSTRACT

A series Ni-doped carbon aerogels were prepared dissolving resorcinol (R) and formaldehyde (F), molar ratio R/F = 1/2 in water R/W = 1/17 and using nickel acetate as catalyst (C). Different amounts of C were used in order to obtain three different Ni loadings (1, 4 and 6 wt.%, approx.) among de final carbon aerogels. A carbon aerogel without Ni was prepared but in this case, Na_2CO_3 was used as polymerization catalyst, R/C = 300.

Carbon aerogels was extensively characterized by N_2 and CO_2 adsorption at -196 and 0 °C, respectively, Raman spectroscopy, scanning and high-resolution transmission microscopy, SEM and HRTEM and by X-ray photoelectron spectroscopy to determine their surface area, porosity, and the formation of graphitic cluster on nickel particles. Electrocapacitive properties were studied by cyclic voltammetry, chronopotentiometry, and electrochemical impedance spectroscopy in a three and two-electrode cell in acidic media and non-aqueous aprotic electrolyte. Results obtained showed that using Ni as polymerization catalysts slightly decrease the micropore volume of the carbon aerogels but a great increase in their mesopore volume were obtained by N_2 adsorption. Electrochemical characterization of the electrodes and cells show that samples present high gravimetric capacitances, ranging from 182 and 219 F g^{-1} in 1 M H_2SO_4 and 49 and 63 F g^{-1} in 1 M TEATFB. The prepared capacitors showed that the equivalent series resistance decrease as Ni content increase and the capacitance increase in the same sense.

6.2.- EXPERIMENTAL

6.2.1.- Preparation and characterization of the materials

Ni-doped carbon aerogels were prepared dissolving resorcinol (R) and formaldehyde (F), molar ratio R/F = 1/2 in water R/W = 1/17 and using nickel acetate as catalyst (C). Different amounts of C were used in order to obtain three different Ni loadings (1, 4 and 6 wt.%, approx.) among de final carbon aerogels. A carbon aerogel without Ni was prepared but in this case, Na_2CO_3 was used as polymerization catalyst, R/C = 300. The mixtures were stirred to obtain a homogeneous solution that was cast into glass molds (45 cm length × 0.5 cm i.d.). Glass molds were sealed, and the mixtures were cured for 5 days at different temperatures from 40 up to 80 °C. After the curing cycle, hydrogel rods were cut into 5-mm pellets and introduced in acetone to exchange the solvent media. After that the organic aerogels were dried using supercritical CO_2. Dried organic gels were pyrolyzed under N_2 flow (300 cm^3 min^{-1}) at a heating rate of 1 °C min^{-1} up to 900 °C with a soaking time of 5 h. The textural and chemical characterization of the samples was carried out using gas adsorption, scanning electron microscopy (SEM), high resolution transmission electron microscopy (HRTEM), Raman spectroscopy and X-ray photoelectron spectroscopy (XPS).

6.2.2.- Electro-chemical study

Cyclic voltammetries (CV), galvanostatic charge–discharge tests, and electrochemical impedance spectroscopy (EIS) were performed in one or two electrodes systems using an EC-lab VMP system (Biologic) at 25 ºC. Different

electrolytes were studied, 1 M H_2SO_4 and tetraethylammonium tetrafluoroborate (TEATBF) 1 M in acetonitrinile as non-aqueous aprotic electrolyte.

The standard procedure for electrode preparation was as follow, a paste was prepared by vigorous mixing powdered carbon aerogel (90 wt.%) and PTFE (10 wt.%) in water. The mixture was pasted on graphite, 1 × 5 cm rectangular shape or discs, 0.5 cm in diameter. The electrodes were dried overnight at 100 ºC and pressed at 5 bar with a uniaxial press. The mass loading of the dried electrodes was 18–20 mg cm^{-2}. The graphitic electrodes were impregnated with the respective electrolyte during 48 h before electrochemical characterization. Each sample was analysed at least three times in order to get an error lower than 1 %.

Single electrodes were characterized by CV in a standard test cell using a three-electrode configuration (Ag/AgCl as reference and Pt wire as counter electrode) at scan rates ranging from 1 to 10 mV s^{-1}. The specific capacitance of the carbon aerogels, C_s, was calculated from the integral of the CV curves using the Equation 1 [1,2].

$$C_s = \frac{\sum |I| \times \Delta t}{2m \times \Delta V} \qquad \text{(Eq. 1)}$$

where $\Sigma|I|\Delta t$ is the area of the current (A) against time (s) curve, m the mass of active material in the electrode (g), and ΔV the potential window (V).

Symmetric supercapacitors were built by assembling glass fibrous material between two disc carbon electrodes of the same weight in a PFA Swagelok® cell. Electrochemical behaviour of the supercapacitors was investigated by galvanostatic charge–discharge by using currents ranging from 0.25 to 5 A g^{-1}.

The gravimetric capacitance from these measurements, C_{scap} (F/g), was calculated by Equation 2 [3-4]:

$$C_{scap} = \frac{I_d \times \Delta t}{m \times \Delta V} \qquad \text{(Eq. 2)}$$

where I_d was the current density (A/g), Δt the discharge time (h), ΔV the voltage interval without the IR drop and m was the total mass of active sample (g).

Impedance spectroscopy experiments were studied from a frequency of 1 mHz to 100 kHz with a sinusoidal signal amplitude of 10 mV and the capacitance value, C_{max}, was obtained by Equation 3.

$$C_{max} = \frac{-Z''}{2\pi f |Z|^2} \qquad \text{(Eq. 3)}$$

where f was the frequency and $|Z|^2 = |Z'|^2 + |Z''|^2$, where Z' and Z'' are the real and imaginary parts of the complex impedance, respectively [5].

Typically, the specific capacitance for one single electrode C_s (F g^{-1}) is calculated according to $C_s = 4 \times C$ where C is the specific cell capacitance for the two-electrode supercapacitor calculated from the charge–discharge curves, C_{scap}, or impedance spectroscopy, C_{max}.

6.3.- RESULTS AND DISCUSSION

6.3.1.- Surface and chemical properties

The shapes of N_2 adsorption isotherms, Figure 6.1a, differ among the samples. Sample A has a type I isotherm [6] with no hysteresis cycle, which is typical of microporous solids, although there is a slight increase in N_2 as the relative pressure increase after micropore filling. This is indicative of the presence of mesopores of 16.8 nm in size, Figure 6.1b. Ni-doped carbon aerogels show type IV isotherms, typical of micro mesoporous materials with mesopores ranging from 16 to 17 nm. It is important to note that mesopore size distribution is similar for all samples.

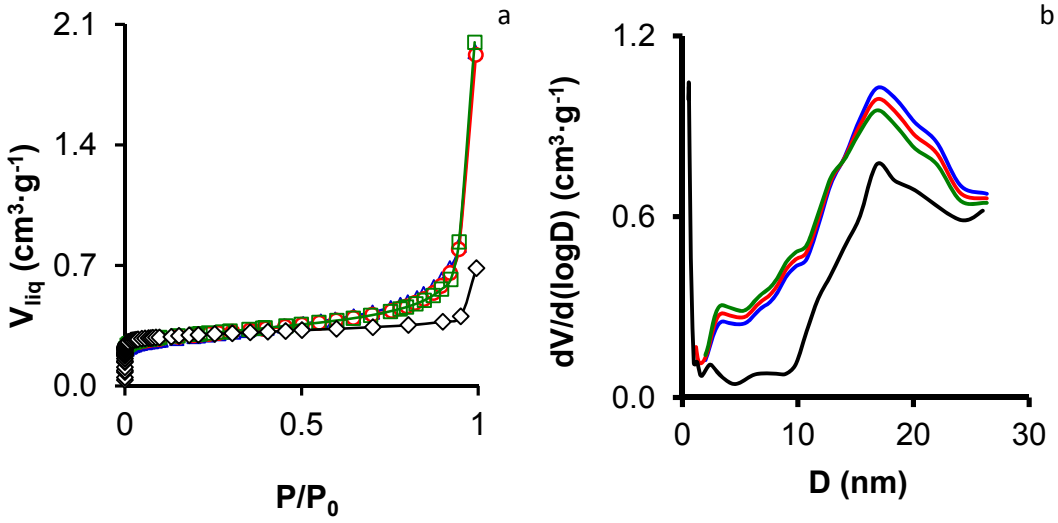

Figure 6.1. a) N_2 adsorption isotherms at -196 °C. b) Pore size distribution obtained by applying QSDFT theory to N_2 adsorption isotherms. Samples: ◇, A; △, ANi1; ○, ANi4; □, ANi6.

Table 6.1 summarizes the results obtained from isotherm data, surface areas and pore volumes of the non-doped and Ni-doped carbon aerogels prepared. All of them are microporous and mesoporous materials, with significant apparent surfaces areas and mesopore volumes in the case of the Ni-doped carbon aerogels.

The micropore volume obtained from CO_2 adsorption at 0 °C yields the volume of narrow micropores (below approximately 0.7 nm in width), whereas N_2 adsorption at −196 °C yields the total micropore volume if there are no very narrow micropores or have constricted entrances [7]. The micropore volume obtained from CO_2 adsorption at 0 °C yields the volume of narrow micropores (below approximately 0.7 nm in width), whereas N_2 adsorption at −196 °C yields the total micropore volume if there are no very narrow micropores or have constricted entrances [7].

Table 6.1. Name, surface areas and pore volumes of the carbon aerogels**.**

Sample	S_{BET} m^2/g	W_0 (N_2) cm^3/g	L_0 (N_2) nm	W_0 (CO_2) cm^3/g	L_0 (CO_2) cm^3/g	$V_{0.95}$ (N_2) cm^3/g	V_{meso} (N_2) cm^3/g
A	724	0.278	0.61	0.246	0.65	0.41	0.132
ANi1	663	0.258	1.07	0.276	0.63	0.82	0.548
ANi4	685	0.268	0.96	0.280	0.63	0.71	0.442
ANi6	698	0.273	0.90	0.294	0.64	0.69	0.417

In all the samples $W_0(N_2) \approx W_0(CO_2)$ and L_0 (CO_2) around 0.65 nm denoting the absence of N_2 diffusional restrictions to the microporosity indicating a well-developed meso and micropore network.

Both micropores and mesopores are very important for their use as electrodes in energy storage applications because they have different roles with respect to

fast charge transfer and the double layer formation of electrolyte ions in the porosity of the electrode [8].

The carbon gel morphology was studied by SEM, results are presented in Figure 6.2, micrographs are typical for R-F carbon gels showing them to be composed of rounded primary particles which are interconnected to each other [9], this leaves well-opened accessible mesopores. The mesopore network constitutes the inter-primary-particle structure and it is directly related with the primary particle size as well as its different degree of aggregation. Sample A presents the smallest primary particle size and because of this it presents the lowest mesopore volume and $L_0(N_2)$ values.

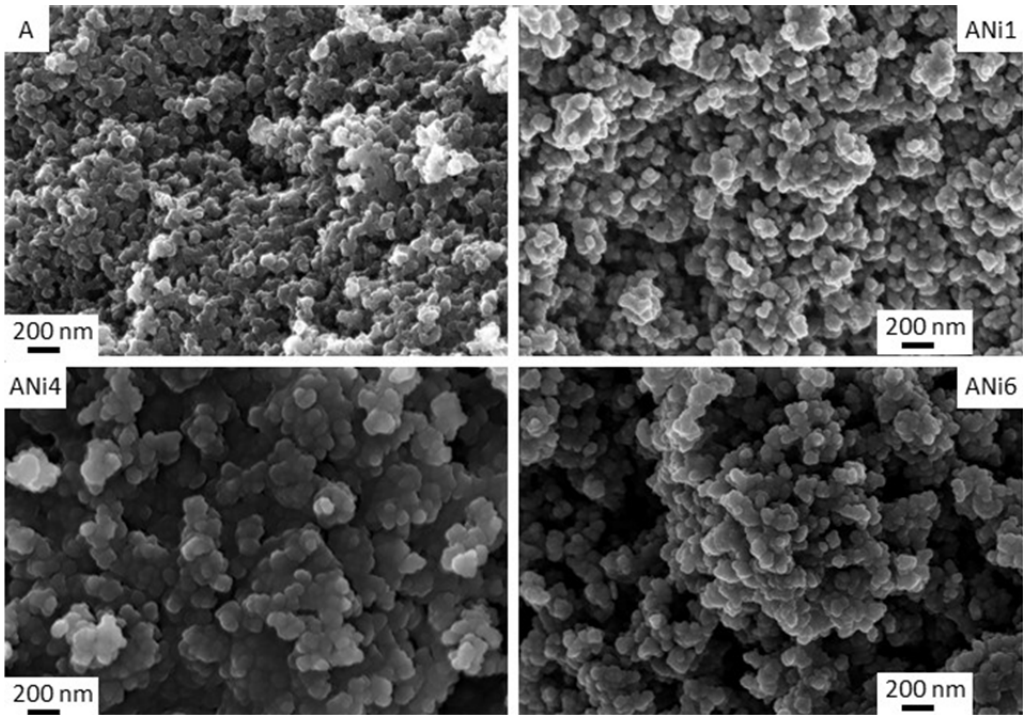

Figure 6.2. SEM microphotographs of samples A, ANi1, ANi4 and ANi6.

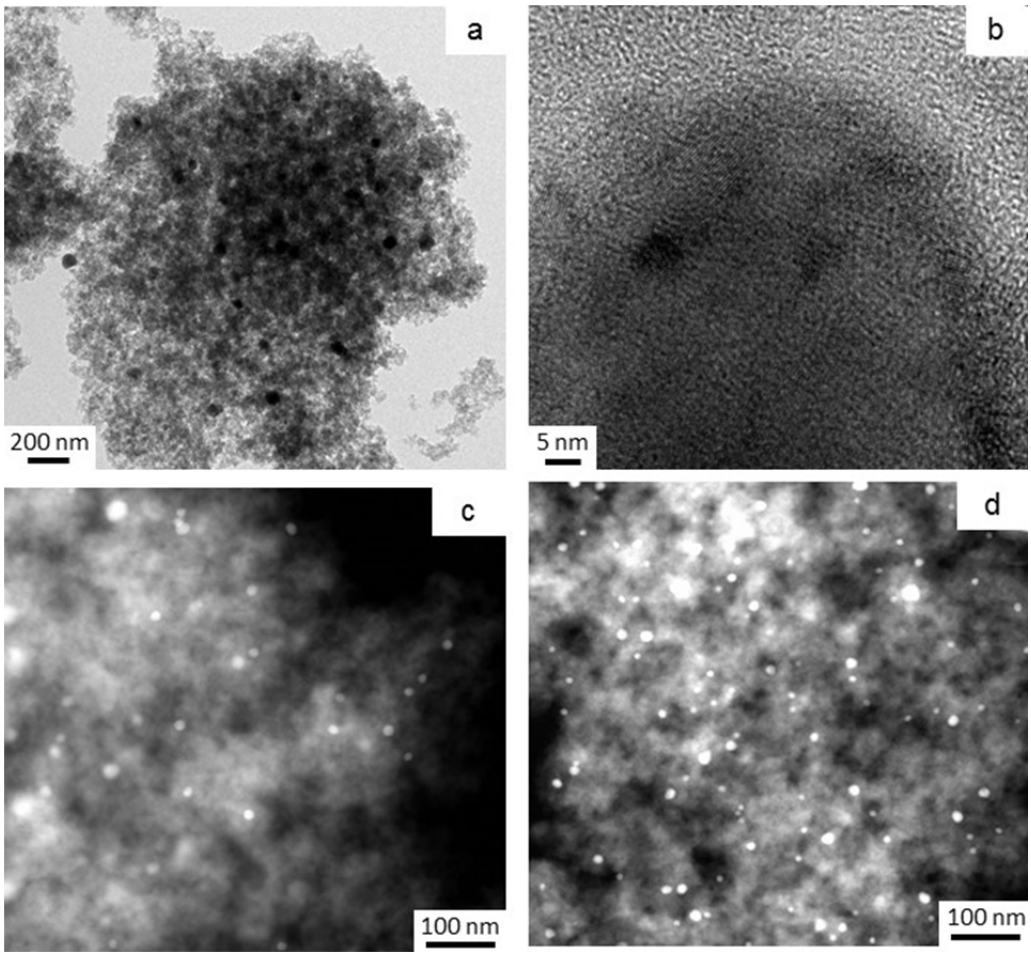

Figure 6.3. HRTEM images of the samples a, ANi4 and b, ANi6. AEM spectra collected in STEM mode using a HAADF detector of the samples ANi1 and ANi6.

TEM images, Figure 6.3, show that Ni particles are very well dispersed throughout the carbon matrix, Figures 6.3 a, c and d, and they are embedded within the carbon matrix, Figure 6.3 b. The metallic nanoparticles inside of the

organic matrix catalysed the development of graphite clusters around the metal particles, during the carbonization process. The partial graphitization of the carbon aerogel has been also observed in previous works [10] with Cr, Fe, Co and Ni as doping metals.

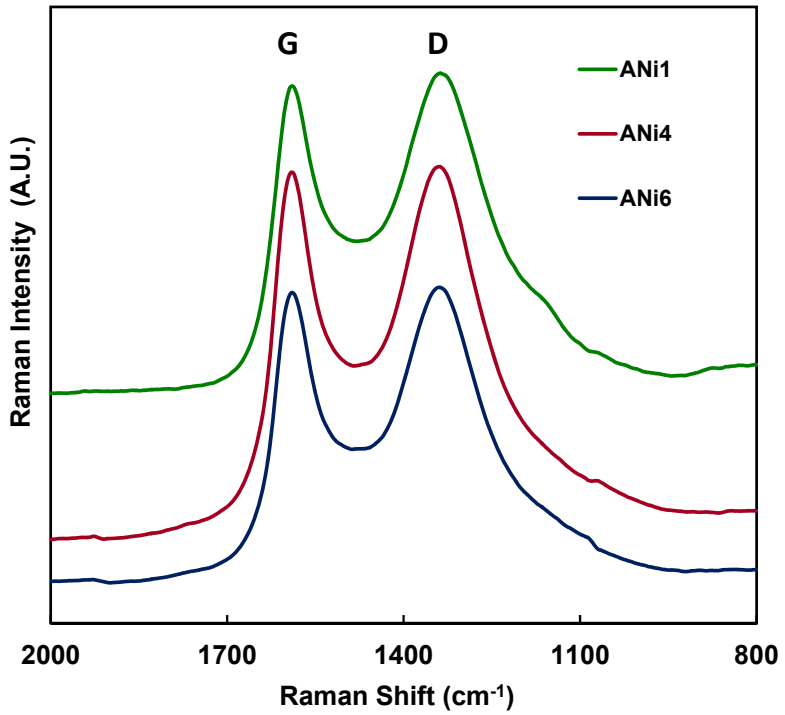

Figure 6.4. Raman spectra of the doped carbon aerogels.

Figure 6.4 shows two main signals in the Raman spectra at 1340 and 1580 cm^{-1} approx. corresponding to D and G bands respectively [11]. It is known that carbon gels are considered as amorphous carbon materials, therefore the presence of these bands should be analysed into this context. In this type of materials, the

D-mode is caused by disordered structure of graphenic layers. The presence of disorder in sp^2-hybridized carbon systems results in resonance Raman spectra, and thus makes Raman spectroscopy one of the most sensitive techniques to characterize disorder in sp^2 carbon materials. The G-mode is at about 1583 cm^{-1}, and is due to E_{2g}. G-band arises from the stretching of the C-C bond in graphitic materials, and is common to all sp^2 carbon systems. It should be noted than the intensity of the G band (I_G) with respect with its D band (I_D) is higher in ANi6 and ANi4 than in ANi1 indicating an increase in the graphitic crystal size and consequently an increase in the electrical conductivity.

C1s XP spectra are presented in Figure 6.5 and the results obtained from their deconvolution compiled in Table 6.2. C1s XP spectra present the same profile for all Ni-doped carbon aerogel, with the same number of components. Briefly, the component positions are maintained although, the FWHM for 284.6 eV peak values decreased and the area of the peak at ≈ 285.7 eV decreases as the Ni content increased due to formation of graphite cluster. At the same time, the area of the C=C peak centred at 284.6 eV, attributed to largely delocalized sp^2 bonding, increase. Yang et al. [12] show that after Ar^+ irradiation of a Highly Oriented Pyrolytic Carbon the component positions, eV, are maintained although the FWHM values increased on irradiation due to disruption of the alternant hydrocarbon structure. Estrade-Szwarckopf [13] shows that an increase during the thermal treatment of an anthracene derived carbon produced a decrease in the crystal defects and a decrease in the FWHM C=C peak.

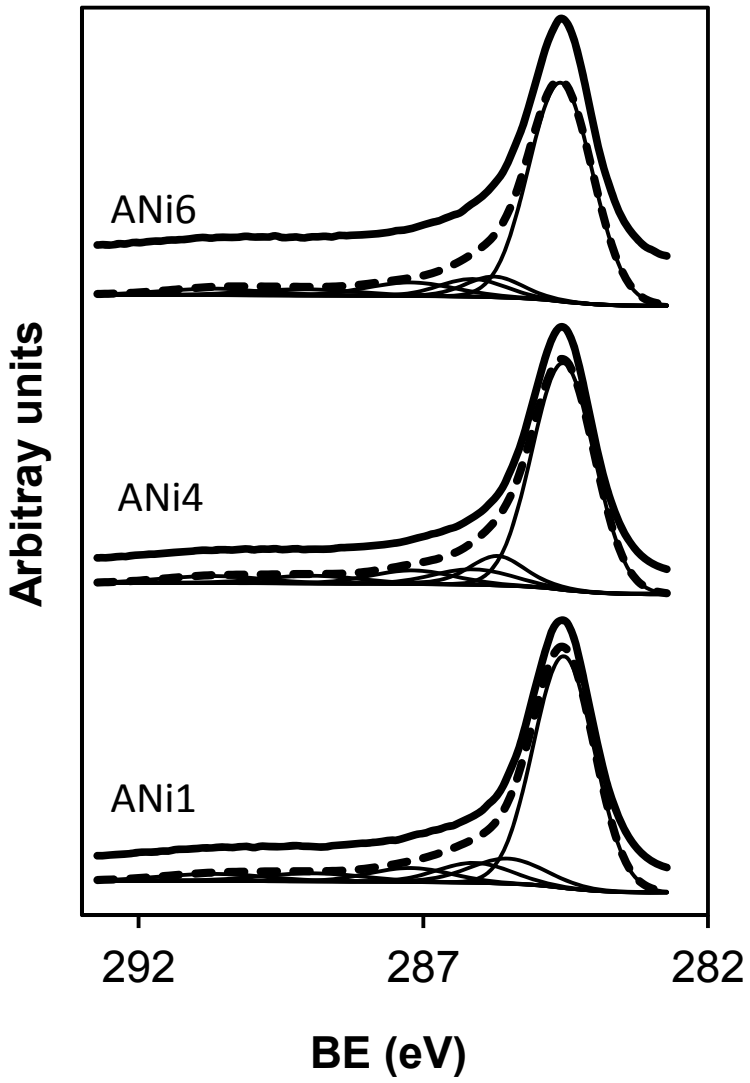

Figure 6.5. Deconvolution of high resolution C1s XP spectra.

Table 6.2. Results obtained from the deconvolution of C1s XP spectra

Muestra	Peak Position eV	FWHM (eV) eV	Peak area %
ANi1	284.6	1.31	70
	285.8		10
	286.1		7
	287.2		6
	289.1		4
	290.7		4
ANi4	284.5	1.28	71
	285.7		9
	286.1		6
	287.2		6
	288.9		4
	290.7		4
ANi6	284.5	1.26	74
	285.5		6
	286.1		6
	287.2		7
	288.9		3
	290.7		4

6.3.2.- Electro-chemical study

6.3.2.1.- Cyclic voltammetry

Cyclic voltammetry were performed in different electrolytes, 1 M H_2SO_4 and 1 M TEATFB in ACN and a several scan rate from 1 to 10 mV s^{-1}. Figure 6.6 shows the results obtained at 5 mV s^{-1} as an example.

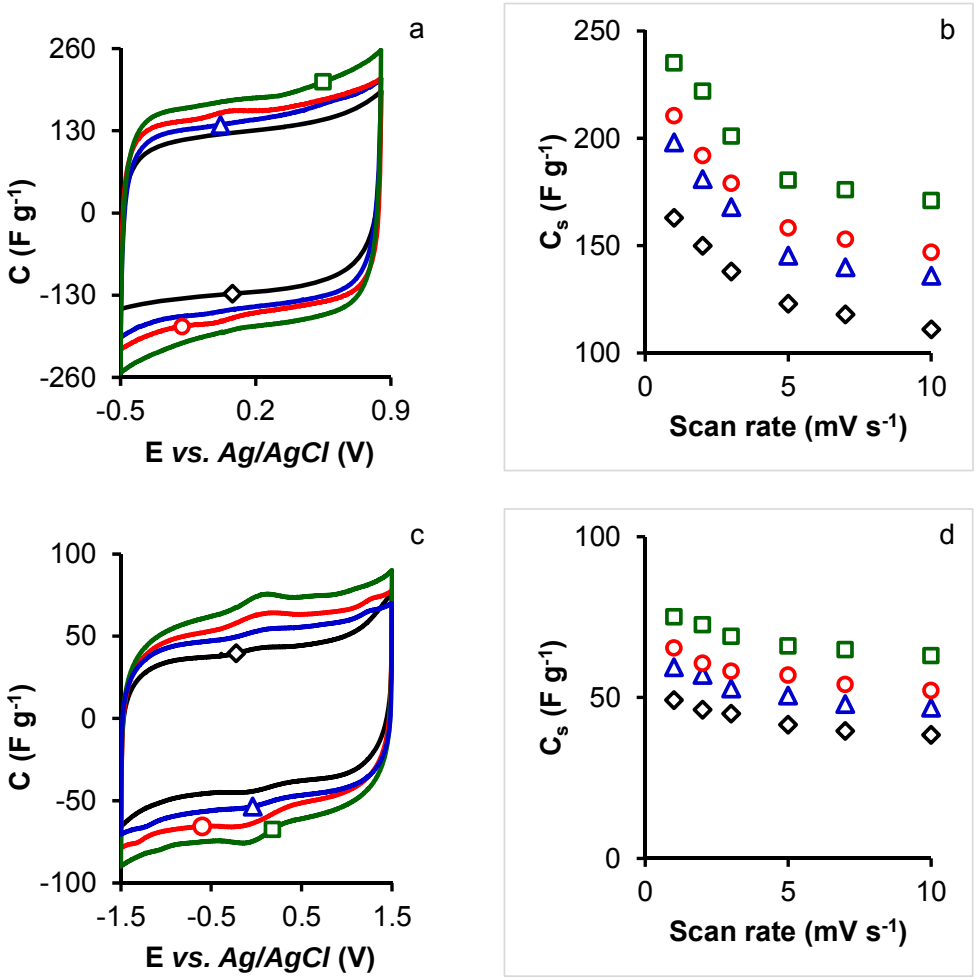

Figure 6.6. Cyclic voltammograms for electrodes at 5 mV s^{-1} (a, c) and variation of the specific capacitance for the electrodes (b, d) in different electrolytes: 1 M H_2SO_4 (a, b), and 1 M TBATFB in acetonitrile (c, d). Carbon aerogels: ◇, A; △, ANi1; ○, ANi4; □, ANi6.

All carbon aerogel showed a quasi-rectangular voltammograms typical for electrochemical double-layer (EDL) capacitors with a low diffusional restriction

to H_2SO_4. Nevertheless, in some cases a resistive component can be observed, especially for samples A and ANi1. This resistive component practically disappear for samples ANi4 and ANi6, that is for samples with higher proportion of graphitic cluster as previously described. This is in good correlation with the absence of significant amount of functional groups, oxygen content, O_{XPS}, ≈ 2 %. Conversely, all samples exhibits a distorted CV shape in acetonitrile possibly due to the porosity saturation caused by the large size of the organic ions that cannot easily penetrate into the pores more than to electrical conductivity problems. This effect has previously been reported for activated carbons in which the surface of the electrode is completely occupied with a lower energy of the electrolyte decomposition [14].

The scan rate effect in capacitance is shown in Figures 6.6 b, d and f. for all carbon aerogel in different media. As expected, C_s is affected by the scan rate in all activated carbons and electrolytes. The capacitance retention is higher for ANi4 and ANi6 doped-carbon aerogel. As an example, for A and ANi1 samples the capacitance retention is around 68 % whereas for ANi6 is ≈ 73 %. This increase in capacity retention should be due to the increase in mesoporosity of the samples as increasing the Ni content [8] and a better electrical conductivity due the formation of the graphitic cluster [12, 13] around the Ni particles.

6.3.2.2.- Galvanostatic charge–discharge experiments

Symmetric supercapacitors were charged and discharged at different current densities to investigate its electrochemical behaviour. Chronopotentiograms (CPs) obtained are depicted in Figure 6.7 (a, b) at a current load of 1 A g^{-1} in different electrolytes and results obtained are compile in Table 6.3.

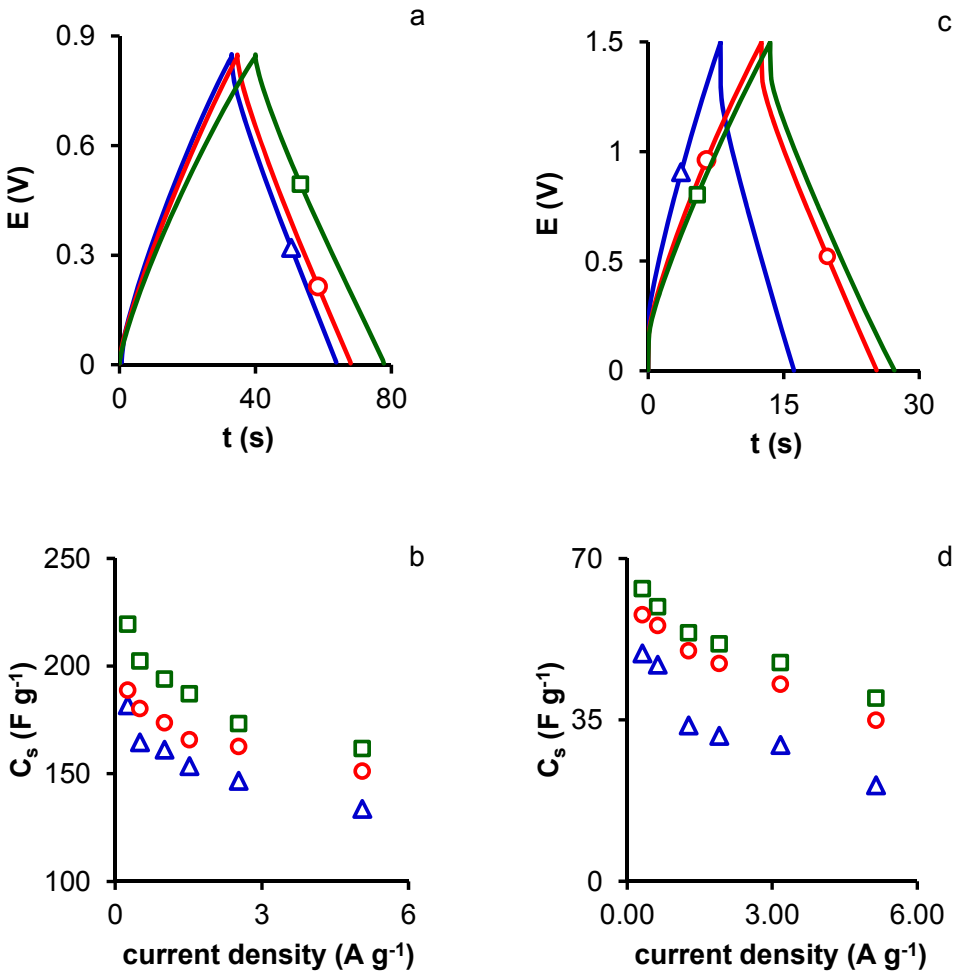

Figure 6.7. Chronopotentiograms obtained at a current density of 1 A g^{-1} for different cells studied (a, b, c) and variation of the specific capacitance for the electrodes (d, e, f) in different electrolytes: 1 M H_2SO_4 (a), (d), 1 M KOH (b), (e), and 1 M TBATFB in acetonitrile (c), (f). Carbon aerogels: △, ANi1; ○, ANi4; □, ANi6.

CPs show quasi-triangular shapes, in 1 M H_2SO_4 which indicate that the samples behave as ideal electrochemical double-layer electrodes (EDL) with low resistance and a good diffusion of the electrolyte inside the pores. The equivalent series resistance, ESR_{GD}, was determined from the I drop at 1 A g^{-1}, Figure 6.8, clearly there is a linear relationship between the FWHM for the C=C peak and the ESR determined for both electrolytes. However, voltage profile of doped-carbon aerogels acetonitrile present an important I drop and consequently higher ESR_{GD} are obtained. This is in agreement with the corresponding distorted CV curves and might be explained by the pore saturation due to the large size of the cations compared with the small pores [14]. Fig. 7 (c, d) depicts Cs obtained from galvanostatic cycling at the different current densities in the two media. Similarly, to cyclic voltammetry studies, higher C_s are obtained in acidic medium for all carbons. This could be due to the different effective sizes of the ions involved, especially the positively charged ions. Thus, the effective size is around 0.7 and 0.46 nm [16, 17] for TEA^+ and $BF4^-$, respectively, whereas it ranges between 0.36 and 0.42 for hydronium [18] and is around 0.53 nm for hydrated bisulfate ion [19]. For all samples, the capacitance decreases with the increasing of the current density due to the difficulty of the formation of the electrochemical double layer in the micropores at high current intensities [8].

Different capacitance retentions, RC_s, were obtained comparing data at 0.250 and 5.15 A g^{-1}. Similar results are showed previously; authors explain this fact that depending on the pore size and the amount of oxygen in the surface which can retard/delay the diffusion of the electrolyte in the micropores [15]. In our case samples present very similar textural properties, Figure 6.1, thus the differences found should be due to the different resistance of Ni-doped carbon gel, Figure 6.8

Table 6.3. C_s at 0.250 and 5 A g^{-1}, from galvanostatic charge-discharge. C_{max}, ESR and τ from EIS**.**

Sample	1 M H_2SO_4					
	$C_s^{0.25}$ F g^{-1}	C_s^{5} F g^{-1}	RC_s %	C_{max} F g^{-1}	ESR Ω	τ s
ANi1	182	134	74	169	0.38	0.8
ANi4	189	151	80	184	0.39	1.1
ANi6	219	162	74	211	0.33	1.1
	1 M TEATFB					
	$C_s^{0.25}$ F g^{-1}	C_s^{5} F g^{-1}	RC_s %	C_{max} F g^{-1}	ESR Ω	τ s
ANi1	49	21	42	40	4.6	2.7
ANi4	58	35	60	52	4.6	3.6
ANi6	63	40	63	59	4.3	4.8

RC_s percentage of retention capacity at 5 A g^{-1} compare to 0.250 A g^{-1}

Finally, Figure 6.8 depicts the Nyquist plots from Ni-doped carbon aerogels in H_2SO_4 and in TEATBF/ACN non-aqueous electrolyte. These impedance plots show typical features of porous electrodes, i.e., resistance at high frequency and capacitance at low frequency. At the highest frequencies, the imaginary part of the impedance tends to zero and the resistance measured is composed of several terms: the intrinsic resistance of the electrodes, the contact resistance at the interface active material/current collector and the ionic resistance of the electrolyte. It is considered, generally, that the width of the semicircle showed at high frequencies reflects the resistance of the active material, because the same electrolyte and technique are used to prepare the electrodes in the experiments. This can justify why at very high frequencies the resistance of the cells, mainly

determined by the electrolyte, is practically the same, in spite of the intrinsic resistance of the carbons is different.

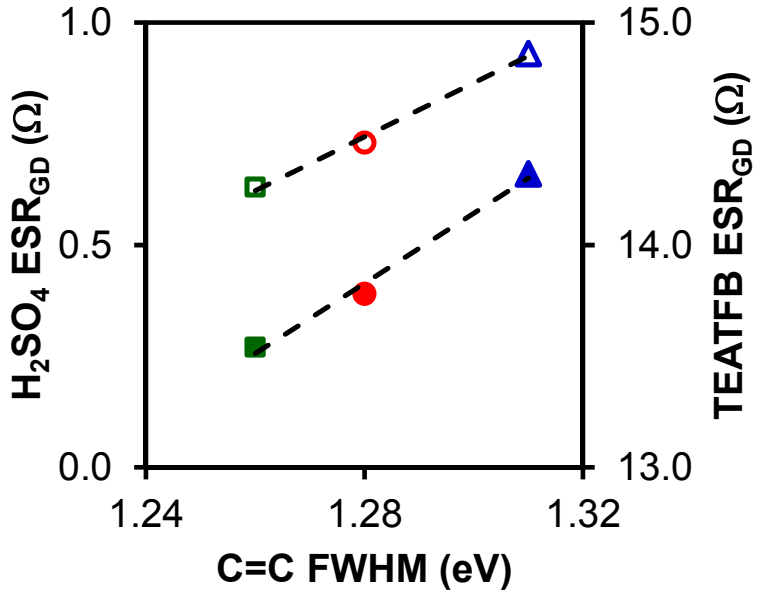

Figure 6.8. Variation of the ESR_{GD} in both electrolytes with the FWHM obtained for the C=C from XPS. Carbon aerogels: △, ANi1; ○, ANi4; □, ANi6. Open symbols H_2SO_4; closed symbols TEATFB.

The results from these curves are compiled in Table 6.3. The values of C_{max} (at 1 mHz) are close to those obtained from the charge-discharge experiments at 0.250 A g^{-1}. The relaxation time constant (τ) can be obtained from the frequency f_0 at the maximum of the plot of the imaginary part of the capacitance (C') against the frequency by the equation $\tau = 1/2\pi f_0$. The relaxation time constant is a

quantitative measure of the speed with which the device can be discharged [20]. Results compiled in Table 6.3 show that the discharge in acidic media is faster than that in the non-aqueous electrolyte due to the different intrinsic resistance of the carbon aerogel.

CONCLUSIONS

Carbon aerogels prepared with $Ni(CH_3COO)_2$ as catalyst present similar microporosity than that prepared by conventional catalyst, Na_2CO_3. Nevertheless, the mesopore structure is more developed in the former case. Ni particles are embebed in graphitic cluster and the increase in the graphitic order in carbon aerogels produce a decrease in the electrical resistance and an increase in the gravimetric capacitance of the carbon gels when used as supercapacitor electrodes in both acidic and non-aqueous aprotic electrolytes.

BIBLIOGRAPHY

[1] Gamby, J.; Taberna, P.L.; Simon, P.; Fauvarque, J.F.; Chesneau, M. Studies and characterisations of various activated carbons used for carbon/carbon supercapacitors. *J. Power Sources* **2001**, *101*, 109-116.

[2] Bonnefoi, L.; Simon, P.; Fauvarque, J.F.; Sarrazin, C.; Sarrau, J.F.; Dugast, A. Electrode compositions for carbon power supercapacitors. *J. Power Sources*, **1999,** *80*, 149-155.

[3] Zhang, L.L.; Zhao, X.S. Carbon-based materials as supercapacitor electrodes, *Chem. Soc. Rev*. **2009**, *38*, 2520-2531.

[4] Hulicova-Jurcakova, D.; Seredych, M.; Lu, G.Q.; Bandosz, T.J. Combined Effect of Nitrogen- and Oxygen-Containing Functional Groups of Microporous Activated Carbon on its Electrochemical Performance in Supercapacitors, *Adv. Funct. Mater.* **2009**, *19*, 438-447.

[5] Taberna, P.L.; Simon, P.; Fauvarque, J.F. Electrochemical Characteristics and Impedance Spectroscopy Studies of Carbon-Carbon Supercapacitors, *J. Electrochem. Soc.* **2003**, *150*, A292-A300.

[6] Sing, K.S.W.; Everett, D.H.; Haul, R.A.W.; Moscou, L.; Pierotti, R.A.; Rouquerol, J.; Siemieniewska, T. Reporting physisorption data for gas/solid systems with special reference to the determination of surface area and porosity, *Pure Appl. Chem.* **1985**, *57*, 603-619.

[7] Zapata-Benabihe, Z.; Moreno-Castilla, C.; Carrasco-Marín, F. Influence of the Boron Precursor and Drying Method on Surface Properties and Electrochemical Behavior of Boron-Doped Carbon Gels. *Langmuir* **2014**, *30*, 1716−1722

[8] Elmouwahidi, A.; Bailón-García, E.; Pérez-Cadenas, A.F.; Maldonado-Hódar, F.J.; Carrasco-Marín, F. Activated carbons from KOH and H3PO4-activation of olive residues and its application as supercapacitor electrodes. *Electrochimica Acta* **2017**, *229*, 219–228.

[9] Fairén-Jiménez, D.; Carrasco-Marín, F.; Moreno-Castilla, C. Adsorption of Benzene, Toluene, and Xylenes on Monolithic Carbon Aerogels from Dry Air Flows. *Langmuir* **2008**, *24*, 2820-2825

[10] Maldonado-Hodar, F.J.; Moreno-Castilla, C.; Rivera-Utrilla, J.; Hanzawa, Y.; Yamada, Y. Catalytic Graphitization of Carbon Aerogels by Transition Metals, *Langmuir*, **2000**, *16*, 4367-4373.

[11] Schwan, J.; Ulrich, S.; Batori, V.; Ehrhardt, H.; Silva, S.R.P. Raman spectroscopy on amorphous carbon films, *J. Appl. Phys.* **1996**, *80*, 440-447.

[12] Yang, D.Q.; Sacher, E. Ar^+-induced surface defects on HOPG and their effect on the nucleation, coalescence and growth of evaporated copper. *Surface Science*, **2002**, *516*, 43-45.

[13] Estrade-Szwarckopf, H. XPS photoemission in carbonaceous materials: A "defect" peak beside the graphitic asymmetric peak. *Carbon*, **2004**, *42*, 1713–1721

[14] Mysyk, R.; Raymundo-Piñero, E.; Pernak, J.; Béguin, F. Confinement of Symmetric Tetraalkylammonium Ions in Nanoporous Carbon Electrodes of Electric Double-Layer Capacitors. *Journal of Physical Chemistry C*, **2009**, *113*, 13443- 13449.

[15] Elmouwahidi, A.; Zapata-Benabithe, Z.; Carrasco-Marín, F.; Moreno-Castilla, C. Activated carbons from KOH-activation of argan (Argania spinosa) seed shells as supercapacitor electrodes, *Bioresource Technol.* **2012**, *111*, 185-190.

[16] Hulicova-Jurcakova, D.; Kodama, M.; Hatori, H. Electrochemical performance of nitrogen-enriched carbons in aqueous and nonaqueous supercapacitors. *Chem Mater* **2006**, *18*, 2318–2326

[17] Ue. M. Mobility and ionic association of lithium and quaternary ammonium-salts in propylene carbonate and gammabutyrolactone, *J Electrochem Soc*, **1994**, *141*, 3336–3342.

[18] Eliad, L.; Salitra, G.; Soffer, A.; Aurbach, D. Ion sieving effects in the electrical double layer of porous carbon electrodes: estimating effective ion size in electrolytic solutions. *J. Phys. Chem. B*, **2001**, *105*, 6880–6887.

[19] Endo, M.; Maeda, T.; Takeda, T.; Kim, Y. J.; Koshiba, K.; Hara, H.; Dresselhaus, M.S. Capacitance and pore-size distribution in aqueous and nonaqueous electrolytes using various activated carbon electrodes. *J. Electrochem. Soc.* **2001**, *148*, A910–A914

[20] Batalla García, B.; Feaver, A.M.; Zhang, Q.; Champion, R.D.; Cao, G.; Fister, T.T.; Nagle, K.P.; Seidler, G.T. Effect of pore morphology on the electrochemical properties of electric double layer carbon cryogel supercapacitors. *J Appl Phys.* **2008**, *104*, 0143051–0143059